U.PORTO

FEUP FACULDADE DE ENGENHARIA
UNIVERSIDADE DO PORTO

TENSILE BEHAVIOUR CHARACTERIZATION OF A HIGH PERFORMANCE FIBER REINFORCED CONCRETE

JOÃO PAULO FERNANDES SEQUEIRA DO VALE PEIXOTO

Dissertação submetida para satisfação parcial dos requisitos do grau de
MESTRE EM ENGENHARIA CIVIL — ESPECIALIZAÇÃO EM ESTRUTURAS

Professora Doutora Sandra da Conceição Barbosa Nunes

Doutor Amin Abrishambaf

JUNHO DE 2020

Ao meu avô

ACKNOWLEDGEMENT

To Professor Sandra Nunes and to Doctor Amin Abrishambaf for all the availability, support, patience showed and for all contributions to the work and to my personal knowledge.

To Paula and Cláudio from the Laboratório de Estruturas da FEUP for all the help and dedication in the performance of all the necessary tests and respective procedures.

To the rest of the Laboratório de Estruturas da FEUP and all the involving parts for all the different types of material and equipment provided

To all my professors from previous years for the knowledge transmitted during the journey that culminated in making off this work.

To my girlfriend, Joana, for the given incentive and encouragement.

To my mother for all the advices and recommendations regarding in this work.

To all my colleagues from FEUP for the help and all the moments lived in my academic progress.

To all my friends and family forgiven me all the support I needed to complete this task.

Resumo

O betão é o material de construção mais utilizado no mundo apresentando, entre outras característicus, uma elevada resistência à compressão. Contudo, tem um comportamento à tração e à flexão mais fraco, influenciando negativamente a sua durabilidade. O reforço com barras de aço tem sido, ao longo dos anos, a solução encontrada pelos projetistas para resolver estes problemas. Mais recentemente, fibras de vários materiais, como o aço, têm sido adicionadas ao betão de forma a complementar e, em alguns casos, substituir completamente as barras de aço, criando assim o betão reforçado com fibras de aço. Face ao anterior, o betão de alta performance reforçado com fibras de aço apresenta como principal diferença uma matriz com uma maior resistência à compressão e um maior volume de fibras.

Neste estudo é feita uma revisão da literatura relacionada com este material para compreender melhor como funciona, que variantes têm efeito no seu desempenho, como é que o seu comportamento pode ser avaliado e qual o seu papel e utilidade na comunidade científica ao longo dos anos e nos dias que correm.

Foi testado o comportamento deste compósito em ensaios de arrancamento de uma única fibra com gancho (as fibras Dramix® 4D). Com o objetivo de perceber a influência do comprimento de embebimento e da inclinação da fibra neste processo, foram feitas seis combinações diferentes na betonagem dos provetes: três com um comprimento de embebedamento igual a metade do comprimento da fibra e três com um quarto do comprimento da fibra; para cada comprimento foram utilizadas três diferentes orientações iguais a 0º, 30º e 60º.

Além disso, de forma a tentar entender melhor a influência direta que as fibras têm no comportamento à tração do material, foram também realizados ensaios WST em betões com 1% de volume de fibras usando três tipos de fibras: as já mencionadas fibras 4D, as fibras Dramix® 5D e fibras curtas sem gancho.

Outra importante questão é a definição de uma lei constitutiva do material: foi discutido e aplicado o método de análise inversa usando os resultados dos ensaios WST.

Com o trabalho experimental realizado, percebeu-se que o comprimento de embebimento tem pouca influência na carga máxima e no respetivo deslocamento da fibra comparado com a inclinação da fibra: a máxima força diminui e o seu deslocamento cresceu com o aumento da inclinação. Apenas três fibras foram arrancadas (as restantes romperam) pelo que é concluído que para matrizes de alta resistência são necessárias fibras mais fortes ou com uma geometria do gancho diferente. Os ensaios WST mostraram que as fibras influenciam apenas o comportamento após a fissuração: a adição das fibras curtas permitiu uma rotura mais dúctil do betão; as fibras 4D e 5D permitiram obter um comportamento "*strain-hardening*" apesar das fibras 4D terem resultado numa rotura mais brusca. Os resultados da análise inversa mostraram que o modelo é mais adequado ao betão corrente ou a betões com fibras que criem um comportamento "*strain-softening*" (as fibras curtas) do que a betões que mostrem um "*strain-hardening*" (as fibras 4D e 5D).

Palavras-Chave: betão de elevado desempenho reforçado com fibras ensaios de arrancamento, análise inversa, comportamento à tração, fibras de aço.

ABSTRACT

Concrete is the most used material around the world, namely due to its high compressive strength. However, its flexural and uniaxial tensile behaviour are much weaker, negatively affecting its durability. Reinforcement with steel rebars has been, throughout the years, the solution found by designers to solve these weaknesses. More recently, fibres of different types of materials, like steel, have been added to concrete in order to complement or, in some cases, completely replace the traditional reinforcement, creating the fibre reinforced concrete. High performance fibre reinforced concrete can be distinguished by its matrix with higher compressive strength and higher fibre content.

In this study, a literature review related to this material is presented in order to try to better understand how it works, to identify the main factors which affect its performance, how its behaviour can be evaluated and what is its role and utility in the scientific community throughout the years and nowadays.

The behaviour of the composite was tested in single fibre pull-out tests (the 4D Dramix® fibres). In order to understand the influence of the embedded length and the fibre's inclination angle, six different combinations were studied: three with embedded length equal to half of the fibre's length and three with one quarter of the fibre's length; for each embedded length, three different inclinations equal to 0º, 30º and 60º were tested.

Also, in order to better observed the direct influence of the fibre on the tensile response of the material, Wedge Splitting Tests were performed with 1% fibre content using three different fibre types: the Dramix® 4D fibres, and 5D fibres and smooth short fibres.

Other important issue is the definition of a constitutive law of the material: the inverse analysis method was discussed and applied using the results of WST's.

With the experimental work performed it was understood that the embedded length has little influence in the maximum pull-out load and respective slip when compared to the fibre's inclination: the maximum force is lower and its displacement is higher for higher inclinations. Only three fibres were pulled-out (the others ruptured) and so, stronger fibres or fibres with a different hook geometry are more adequate for high strength matrixes. The WST showed that the fibres only influence the post-peak behaviour of plain-concrete: the addition of short fibres allowed a more ductile failure; the 4D and 5D fibres allowed a strain-hardening behaviour even though the rupture of the samples with 4D fibres showed a more brittle failure. The results of the inverse analysis showed that the model is more adequate for plain concrete or for materials with fibres that create a strain-softening behaviour (the short fibres) than to materials that show a strain-hardening behaviour (the 4D and 5D fibres).

KEYWORDS: high performance fibre reinforced concrete, pull-out tests, inverse analysis, tensional behaviour, steel fibres.

Índice Geral

LIST OF FIGURES

LIST OF TABLES

SYMBOLS, ACRONYMS AND ABBREVIATIONS

Symbols

l_f – Fibre's length

d_f – Fibre's cross-sectional diameter

V_f – Fibre volume or content

A_f – Area of the fibre's cross-section

σ_{cc} – Stress at the first crack

σ_{pc} – Post cracking stress

σ_{fu} – Tensile strength of the fibre

σ_{mu} – Tensile strength of the matrix

E – Young's Modulus

T – Bond strength

ε_{cc} – Elongation at the stress of first crack

ε_{pc} – Elongation at the post-cracking stress

D_{max} – Maximum aggregate size

D_{ave} – Average aggregate size

S – Fibre's spacing

$f_{cm,28d}$ – Compression strength tested at the age of 28 days

n – Number of fibres in a cross-section

α – Fibre orientation factor

b – Width of the mould's section

h – Length of the mould's section

z – Fibre's centroid distance to the crack plane

η_b – Average fibre's efficiency factor

δ_c – Deflection at the first crack's load

δ_u – Deflection at the post-crack load

f_{cc} – Load of the first crack

f_r – Post-crack load

σ_{f1} – Equivalent bending stress of the first crack

σ_{f2} – Post-crack equivalent bending stress

ψ – Fibre's perimeter

$f_{c,cube}$ – Compressive strength of a cubic specimen

$f_{cm,cube}$ – Average compressive strength of the cubic specimens

$f_{ct,sp}$ – Tensile splitting force of cylindrical specimens

$f_{cm,tsp}$ - Average tensile splitting force of cylindrical specimens

$f_{ck,cube}$ – Characteristic value of the compressive strength of cubic specimens

A_n – Notched cross-section's area

$\bar{\delta}$ – Recorded displacement in the uniaxial tensile test

$\bar{\delta}_p$ – Average displacement at the peak-stress in the uniaxial tensile test

w- Crack width

L – Specimen's length in the three-point bending test

y – Distance between the bottom of the specimen and the line of measurement in the three-point bending test

h_{sp} – Distance between the top of the notch and the top face of the specimen in the three-point bending test

δ – Deflection

F_L – Load at the limit of proportionality

f_L – Tension stress at the load at the limit of proportionality

F_j (j=1,2,3,4) - Load applied for CMOD values of 0.5, 1.5, 2.5 and 3.5 mm

$f_{r,j}$ – Residual flexural tensile stresses correspondent to each F_j

F_{sp} – Splitting force in the wedge splitting test

F_v – Vertical force applied in the wedge splitting test

μ – Coefficient of friction

f_{R1k} – Strength correspondent to CMOD1 (=0.5) in the three-point bending test

f_{R3k} – Strength correspondent to CMOD1 (=2.5) in the three-point bending test

f_{Lk} – Load at the limit of proportionality

l_{sc} – Characteristic length

w_u – Ultimate crack strength

ε_{cu} – Ultimate compression strain in FRC

ε_{su} – Ultimate tensile strain in the steel

ε_{Fu} – Ultimate tensile strength in FRC

γ_F – Safety factor

K – Fibre orientation factor in the fib Model code 2010

f_t – tensile strength of concrete

a_1 – slope of the first branch in the bilinear stress-crack width relationship

G_f - Area beneath the force-CMOD curve resultant of the WST

m - Mass

a_0 - Initial notch length

a_m - Mean width of groove

b - Distance from bottom of specimen to line of CMOD-measurements

b_m - Mean width of specimen on each side of groove

d_1 - Horizontal coordinate of the load point measured from line of symmetry

d_2 - Vertical coordinate of the load point measured from bottom of specimen

h - Height of ligament

L - Outer horizontal and vertical dimensions

Acronyms/ Abbreviations

NSC – Normal Strength Concrete

MSC – Medium Strength Concrete

HSC – High Strength Concrete

FRC – Fibre Reinforced Concrete

HPFRC – High Performance Fibre Reinforced Concrete

UHPFRC – Ultra High Performance Reinforced Concrete

UHPM – Ultra-High Performance Mortar

FEUP – Faculdade de Engenharia da Universidade do Porto

MIEC – Mestrado Integrado em Engenharia Civil

DEC – Departamento de Engenharia Civil

WST – Wedge Splitting Test

Ref – Reference

SLS – Service Limit State

ULS – Ultimate Limit State

FIER – Fibre Intrinsic Efficiency Ratio

CMOD – Crack Mouth Opening Displacement

Fig. – Figure

Tab. – Table

Eq. - Equation

1
INTRODUCTION

1.1 Motivation

All around the world it is possible to view that concrete is the most common material used in all types of constructions. It is estimated that $1m^3$ of concrete is produced per person per year in the entire planet Earth (Coutinho, 2011). This makes it the second most used material in world, after water. Its usage has been growing since the nineteenth century (Kirby e Laurson, 1932).

Concrete, when applied with no reinforcement, has well-known weaknesses such as its low tensile strength and limited ductility. Finding a solution to these problems is of highly importance. The addition of fibres as a mean to reinforce a weaker matrix goes back to the early-age construction methods where natural fibres were added to clay to produce bricks. However, the first study using steel fibres as a reinforcement of a cementitious matrix was in the early 60's by Romauldi and Batson (Htut, 2010). In their work, the advantages of fibres were clearly noted in the ductility and tensile response when a good volume and distribution were accomplished.

Fibre Reinforced Concrete (FRC) is a mixture of concrete with randomly distributed and orientated fibres mixed in the bulk that can be made of different types of materials and have different lengths and shapes. Although the compressive strength is practically not affected, the addition of fibres enhances other mechanical properties of the matrix such as the tensile/ flexural strength, its ductility and resolves the brittle failure, which is characteristic of the concrete and increases the fracture energy contributing to the material's durability.

FRC are mainly used to complement the traditional reinforcement. It is seen as a solution to non-structural elements or to control early thermal cracking, and plastic or drying shrinkage cracking. However, more recently, high performance fibre reinforced concrete (HPFRC), which has enhanced mechanical properties compared no normal FRC has been seen as good way to give a structural role to the fibres, combining them with steel rebars or, in some cases, to fully replace them. In this case, it would reduce the man-labour costs related to placement of steel rebars (Abrishambaf, 2015).

This work aims to discuss the behaviour of HPFRC, focusing mainly on the influence of steel fibres parameters on the bending/tensile behaviour of HPFRC. Pull-out tests were carried out to better understand the pull out mechanism that develops when the fibres are bridging the cracks. The wedge splitting test was selected to assess the influence of different types of fibres in the tensile behaviour of

plain concrete. Finally, an inverse analysis was carried out to find a constitutive law that can characterize the material.

In Figure 1 we can see some examples of modern structures in which steel fibres were adopted as a solution to complement steel rebars.

a)

b)
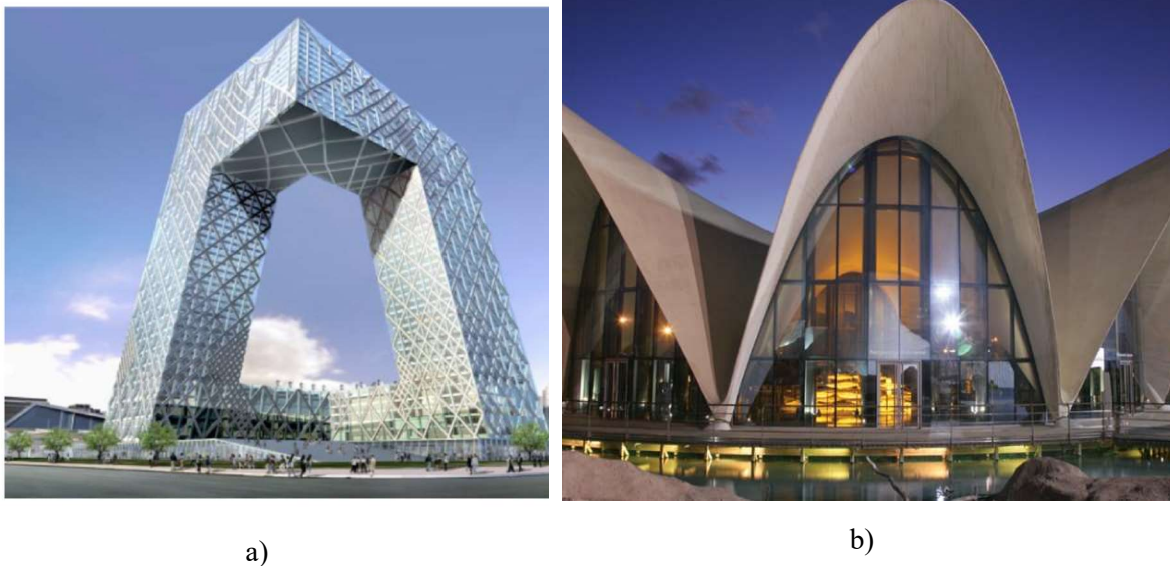
Figure 1 - Examples of structures with FRC
a) CCTV Tower, Beijing, China; b) Oceanographic Park, Valencia, Spain

1.2 Experimental work and objectives

The biggest contribution of the fibres is in the cracked state. Instead of a sudden downfall in the load supporting capacity, a much smoother reduction occurs. This is due to the bridging effect of the fibres in the cracks. The efficiency of this process depends on the fibre's resistance to the pull-out mechanism in the cracks. The pull-out resistance of the matrix depends on various factors. In the experimental programme carried out in this work, the influence of the fibre's embedded length and inclination angle will be studied in single fibre pull-out tests using the Dramix® 4D fibres in plain concrete. Two embedded lengths were use: $l_f/2$ and $l_f/4$, where l_f is the fibre's length. Each embedded length was tested with three different inclination: 0º, 30º and 60º. For each combination 6 tests were made. At the same age, eight cubes were tested in compression tests and three splitting tensile tests were performed in cylindrical specimens. Both had short fibres added to the mixture.

Moreover, WST tests were performed in order to understand the influence of different types of fibres (short smooth fibres and the Dramix® 4D and 5D hooked-end fibres) in the tensile response of plain concrete. 1% of each type were added to separate mixtures creating three different types of samples.

The different tests and their details are shown in Table 1.

Table 1 - Laboratory tests performed

Test	Fibres added to the mixture	Embedded length	Inclination angle (º)	Number of specimens
Pull-out test	No fibres were added	l$_f$/4	0	6
			30	6
			60	6
		l$_f$/2	0	6
			30	6
			60	6
Compression test	Short fibres	-	-	8
Splitting tensile test	Short fibres	-	-	3
Wedge Splitting Test	Short fibres	-	-	7
	4D fibres	-	-	4
	5D fibres	-	-	5

1.3 Organization of the thesis

In this dissertation, in Chapter 2, a literature review is presented, with reference to HPFRC mix-design, properties, testing methods and main applications , providing theoretical background on the various subjects discussed in the following chapters.

Chapter 3 is dedicated to the pull-out behaviour of the steel fibres in a cementitious matrix. After an initial part consisting of a dedicated literature review, the experimental program developed under the current MSc is presented and the corresponding results are presented and compared to previous studies.

In Chapter 4, some direct and indirect tests used to characterize the tensile behaviour of HPFRC are presented and its procedures are described. Finally, the behaviour of three HPFRC mixtures is compared in the current study, using the wedge splitting test.

Finally, Chapter 5 presents the inverse analysis of the WST results with reference to the three HPFRC mixtures analysed in Chapter 4.

Chapter 6 presents the main conclusions regarding the acquired knowledge throughout the execution of this work and recommendations for future research.

2

HIGH PERFORMANCE FIBRE REINFORCED CONCRETE

2.1 Introduction

Concrete is one of the most common structural materials used in today's construction but, even though its compressive strength is high, its ductility is low meaning that after the first crack appears, the crack widen and propagate very fast resulting in a brittle failure, proportional to the compressive strength applied. Also, its tensile strength is low resulting in the appearance of cracks and affecting its durability. Because of that, concrete is commonly reinforced with, for example, steel rebars. In recent years, steel fibres, which in the past have been used mainly to improve the ductility and to control shrinkage's cracking, are being used for structural issues as well.

In this chapter, some literature review about the High Performance Fibre Reinforced Concrete will be presented. Its advantages and composition will be explained as well as its response to different types of solicitations. Some important precautions to guarantee the best possible performance and which factors influence it are also studied and presented here.

2.2. Definition

The fibre reinforced concrete (FRC) is a mixture of concrete, which mainly consists of cement paste (matrix) and aggregates, reinforced by randomly distributed fibres (Fig 2). The fibres are able to turn the brittle concrete into a cementitious composite with improved mechanical properties. The most significant advantages are related with tensile and flexural behaviour (Ruano et al., 2014).
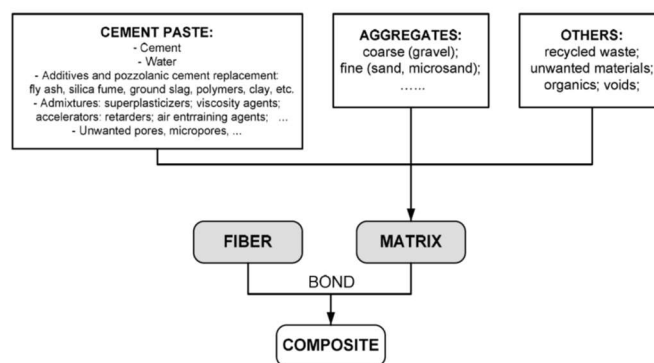
Figure 2 - FRC Composition (Naaman, 2008)

The relation between the fibre volume, the compressive strength of the concrete and the classification of the different types of fibre reinforced concrete is shown in Figure 3. When the fibre volume is between 1 and 2% and the compressive strength goes from around 100 to 200 MPa, the fibre reinforced concrete is classified as High Performance Fibre Reinforced Concrete (HPFRC) which is the focus of this study.
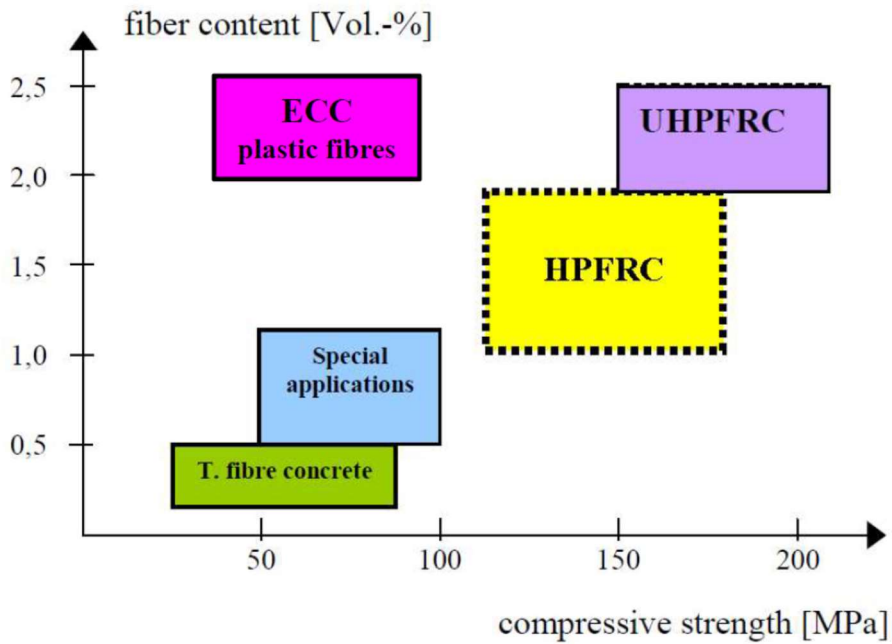
Figure 3 - Different types of fibre reinforced concretes (Blazy et al, 2020)

The main objective of adding fibres to concrete is to control the crack propagation and to create a more stable crack spreading by a bridging mechanism: the load applied in the composite is transmitted to the fibre by the matrix through a bond connection which then redistributes the load back into the matrix and the process repeats itself. This allows the composite to support the load, instead of the concrete alone, creating a more ductile response (Li and Wu, 1992).

In conventional concrete, when loading is applied a linear elastic branch develops until the critical tensile stress is reached. Here, a brittle failure is experienced due to drastic reduction in the concrete's resistance as seen in Figure 4.
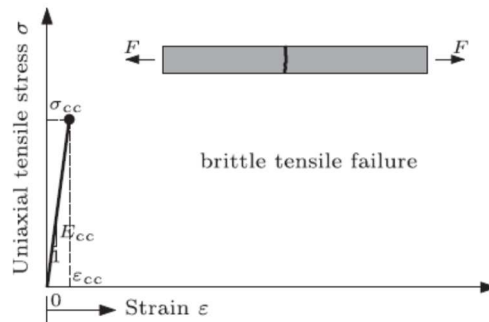
Figure 4 - Tensile response of conventional plain concrete (Wille, El-Tawil and Naaman, 2014)

Depending on the fibre volume fraction, HPFRC can show strain-hardening or strain-softening behaviour in the post-peak response after the linear elastic branch. Strain-softening behaviour means that when subjected to loading (Fig. 5a Phase I) after the concrete's tensile strength is reached and the first crack appears (Fig 5a, Point A), the stress-strain curve shows a smooth softening branch with a loading reduction corresponding to the pull-out of the fibres from the matrix. (Fig 5a, Phase III). This allows a higher energy absorption and a more ductile behaviour than normal concrete.

If the fibre volume is high enough, the post-crack strength is higher than first-crack strength. This characterizes the strain-hardening response, a desirable characteristic for HPFRC. When the first crack appears in the concrete (Fig 5b, Point A), instead of the smoothing branch described before, a multi-cracking process develops in the concrete where the fibres bridges the macro-cracks (Fig 5b, Phase II) increasing the tensile strength of the concrete (Naaman and Reinhardt, 2006). In the end of the strain-hardening branch, one crack becomes critical (Fig 5b, Point B), no more cracks develop, and only the critical one will continue to open. Then, other cracks start to unload – this corresponds to the softening branch (Fig 5b, Phase III) (Naaman, 2008). At this point, the fibres are pulled out – if the bond strength is overcome – or rupture – if the tensile strength of the fibre's steel is reached - or usually a combination of both failure modes (Abdallah and Fan, 2017) .
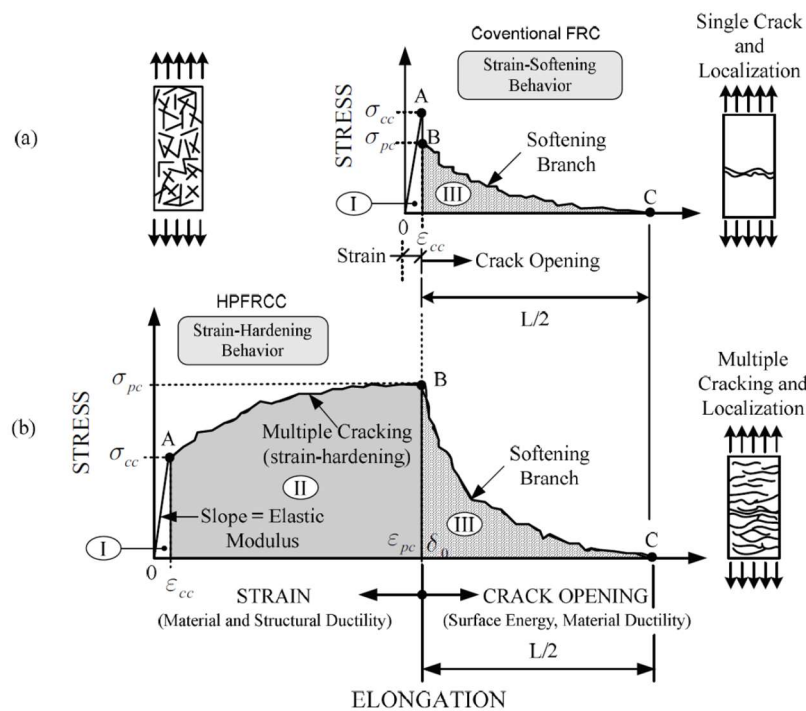
Figure 5 -Tensile responses of fibre reinforced concrete: a) strain-softening behaviour; b) strain-hardening behaviour (Naaman, 2008)

Besides the improvement of the tensile and the flexural behaviour of the concrete, the application of fibres in concrete improves ductility, durability and toughness. Also has economic advantages compared to typical reinforcement, mainly because the execution is much simpler and requires less workmanship (Naaman and Reinhardt, 2003). The compressive behaviour also improves but not as significantly when compared to tensile behaviour (Hamiruddin et al., 2018). On the other hand, the workability of the concrete decreases with the increase of the fibre content (Abbass, Khan and Mourad, 2018). The influence of the fibres in the concrete will be discussed in the next sections

7

2.3 Mix design

A composite material is usually made of one continuous and one, or more, additional discontinuous material, fixed or randomly distributed in order to improve the properties of the continuous material. HPFRC is composed by concrete (a continuous material resultant of other materials but that it will be assumed as one part) and randomly distributed fibres (discontinuous material).

The properties which mainly influence the efficiency and performance of the composite are the physical/chemical properties of both matrix and fibres, fibre content/orientation and the bond connection between fibre and matrix (Löfgren, 2005).

2.3.1 Cementitious Matrix

Some studies on HPFRC mixtures are shown in Table 2. For most of the cases, the fibre volume fraction goes from 0,5% to 1,5% which is the most common in HPFRC. Also, most of them uses hooked end fibres because they show an improvement in the pull-out behaviour which leads to an increased fracture energy in the composite.

Table 2 - Different HPFRC compositions adapted from (Blazy et al, 2020)

Ref.	Binder	w/b	D_{max} (mm)	V_f	l_f,d_r;geometry	$f_{cm,28d}$ (MPa)
(Abbass, Khan and Mourad, 2018)	ASTM Type 1 cement	0,25 (w/c)	10	0,5%;1%,1,5% 0,5%;1%,1,5% 0,5%;1%,1,5%	40/0,62; 1HE 50/0,62; 1HE 60/0,75 1HE	88;90;93 87;91;93 87;92;94
(Okeh et al., 2019)	CEM I 52.5 R	0,27 (w/c)	10a	0,75%(HE) + 0%(S) 0,562%(HE)+0,188%(S) 0,375%(HE)+0,375%(S) 0,188%(HE)+0,562%(S) 0%(HE)+0,75%(S) 1%(HE)+0%(S) 0,75%(HE)+0,25%(S) 0,5%(HE)+0,5%(S) 0,25%(HE)+0,75%(S) 0%(HE)+1%(S)	60/0,9;1HE+13/0,2;S 60/0,9;2HE+13/0,2;S	88 84 83 88 98 89 89 87 91 98
(Jang, Jeong and Yun, 2018)	PC+SF+FA	0,25	13	1,25%	30/0,5;1HE	94
(Ruano et al., 2014)	Cement CPN50	0,3 (w/c)	10	0,76%	-;-	95
(Mousavi, Ranjbar and Madandoust, 2019)	PC 42.5 Type I + SF	0,24 (w/c)	12,5b	0,2% 0,4% 0,6% 1%	28/0,4;1HE	102 100 102 103
(Gholampour and Ozbakkaloglu, 2018)	OPC+SF	0,295	10c	1% 2%	13/0,18;S	103 114
(Deeb, Karihaloo and Kulasegaram, 2014)	CEM+mS+LP	0,24	10b	0,5%	30/0,55;C	100
(Yoo and Shin, 2018)	OPC+Zsf+FA	0,195	10d	0,5% 1%	30/0,5;1HE	93 108
(Kazemi et al., 2017)	PC Type II+LP	0,4 (w/c)	12,7	1,6%	36/0,7;1HE	91

(Skazlić, Serdar and Bjegović, 2008)	CEMII/B-M (S-V) 42,5 N +SF	0,2 0,18 0,18	11e 8e 11e	1%+0,5% 3% (total) 0,5%+0,5%+0,5%	13/0,2 + 30/0,6 13/0,2+30/0,6+50/0,1 13/0,2+30/0,6+50/0,1	109 122 95
(Piérard, Dooms and Cauberg, 2013)	CEM I 42,4 R HSR LA+SF	0,32 (w/c)	8c	0,7%+0,3%	6/- 30/-	130-140
(Li, Yu and Brouwers, 2018)	CEM I 42,5 R+mS+LP	0,2 (w/p)	8c	2%	13/0,2;S	164

(O)PC: (ordinary) Portland cement; (z)SF: (zirconium) silica fume; mS: micro silica; FA: fly ash; LP: limestone powder; w/b: water to binder weight ratio; w/c: water to cement weight ratio; w/p: water to powder weight ratio; D_{max}: maximum diameter of coarse aggregate; V_f: fibre content; lf fibre length; df: fibre diameter fcm,28d: mean compressive strength at 28 days; 1HE: simple hooked-end; 2HE: double hooked-end; S: straight; C: crimped ends; nature of coarse aggregate: (a) flint, (b) limestone, (c) basalt, (d) granite, (e) diabase

Kooiman (2000) considered that adding fibres to the concrete without making the proper adjustments and alterations in the matrix results in the decrease of the workability, making it impossible to fully profit from the fibres benefits. Therefore, some issues and some precautions should be considered.

If the matrix structure around the fibres is not homogeneous, the bond connection between the two constituents is not well made. Therefore, the mixture should show a proper workability. A better solution is self-compacting concrete. Self-compacting is flowable and needs no extra compaction after casting like in conventional concrete (Marković, 2006). It has a proper and improved granular composition with a higher amount of small aggregate, which results in less porosity and better workability. This makes it possible to achieve an appropriate fibre orientation and uniform distribution through the concrete and, therefore, to increase the efficiency of fibres in the mixture (Grünewald and Walraven, 2000). The ductility and flexural stress are, as so, enhanced (Grünewald and Walraven, 2002).

It is also essential to avoid segregation as the water next to the fibre can create voids after it is evaporated, thereby compromising the good function of the bond between the fibre and the aggregates.

Another important factor which affects the well-functioning of the fibres is their distribution and orientation. Marković (2006) described the perfect fibre's arrangement as a triangular or a square array with equal spacing, *S*, and with the fibres aligned with the principal stresses. Both cases are represented in Figure 6.
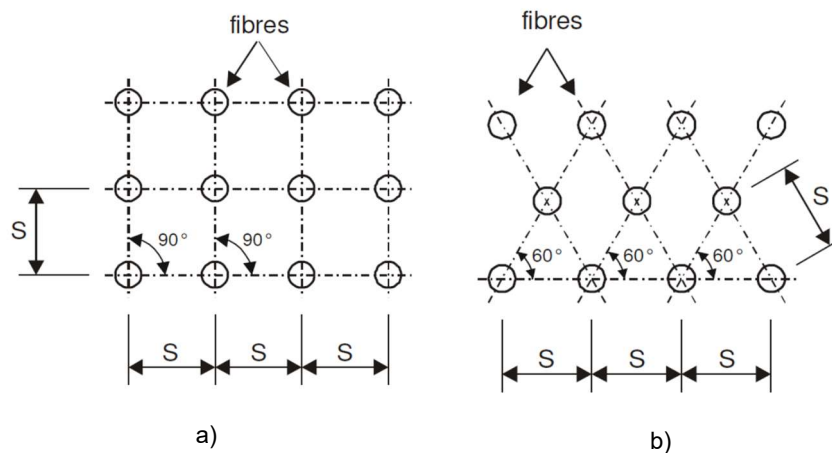
Figure 6 - Perfect fibre's arrangements a) Square array; b) Triangular array (Marković, 2006)

To achieve this scenario, the author established two conditions should be satisfied:

- The grains with maximum aggregate size (D_{max}) should fit between the fibres (Fig 7a);
- The grains with average size (D_{ave}) must be arranged in order to be in contact with each other (Fig 7b).
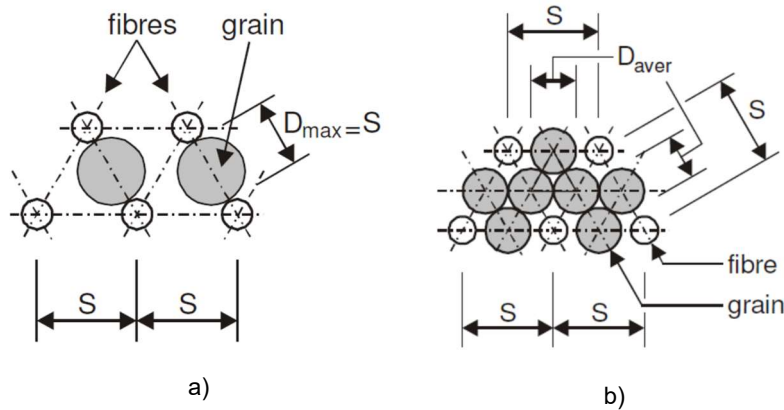
Figure 7 - Conditions to achieve ideal fibre arrangement: a) D_{max} based on S; b) D_{aver} based on S (Marković, 2006)

The spacing between the fibres is a factor which cannot be controlled due to the fibre's random distribution and orientation. Therefore, D_{max} should be chosen based on the intended spacing. Many authors studied this subject (Mckee, 1969; Romualdi and Mandel, 1964; Kobayashi and Cho, 1976).

2.3.2 Fibre Reinforcement

Fibres can be classified according to four parameters (Naaman, 2003):

- Material: natural organic, natural mineral, or man-made;
- Physical/chemical properties: density, roughness, reactivity, chemical stability;
- Mechanical properties: stiffness, ductility, elastic modules, tensile strength;
- Geometry and shape (Fig 8):
  - Diameter;
  - Length;
  - Perimeter;
  - Cross-section: circular, triangular, rectangular…;
  - Shape: flat, straight, twisted, hooked, etc. (Fig 8)
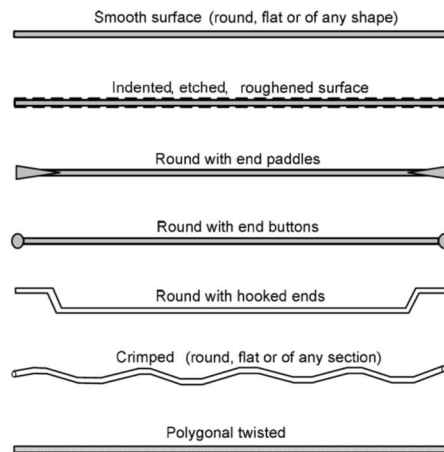
Figure 8 - Various Fibre's shapes (Naaman, 2008)

Table 3 shows some examples of fibre's materials and its properties. The most common one widely used in the production of HPFRC is steel and, therefore, will be the focus of this research.

Table 3 - Fibre's materials and some of its properties adapted from (Löfgren, 2005)

Type of fiber	Diameter (μm)	Specific Gravity (g/cm^3)	Tensile Strength (MPa)	Elastic Modulus (GPa)	Ultimate elongation (%)
Metalic					
Steel	5-1000	7.85	200-2600	195-210	0.5-5
Glass					
E glass	8-15	2.54	2000-4000	72	3-4.8
AR glass	8-20	2.7	1500-3700	80	2.5-3.6
Synthetic					
Acrylic (Chupanit)	5-17	1.18	200-1000	14.6-19.6	7.5-50
Carbon (high modulus)	7-18	1.7-1,9	1500-4000	200-800	1.3-1.8
Nylon (polyamide)	20-25	1.16	965	5.17	20
Polyester (PET)	10.8	1.34-1.39	280-1200	10-18	10-50
Natural Organic					
Cellulose (wood)	15-125	1.5	300-2000	10-50	20
Coconut	100-400	1.12-1.15	120-2000	19-25	10-25
Bamboo	50-400	1.5	350-500	33-40	-
Natural Inorganic					
Asbestos	0.02-25	2.55	200-1800	164	2-3
Wollastonite	25-40	2.87-3.09	2700-4100	303-530	-

Naaman (2003) defined some conditions for an effective fibre reinforcement, as seen in Figure 9: (i) the tensile strength of the fibre should be significantly higher than the tensile strength of the matrix; (ii) the elastic modulus of the fibre should be higher than the elastic modulus of the matrix; (iii) a bond strength between the matrix and the fibres should be at least within the same order as the tensile strength of the matrix; and (iv) the Poisson's ratio and the coefficient of thermal expansion of the matrix and the fibres should be within the same order.
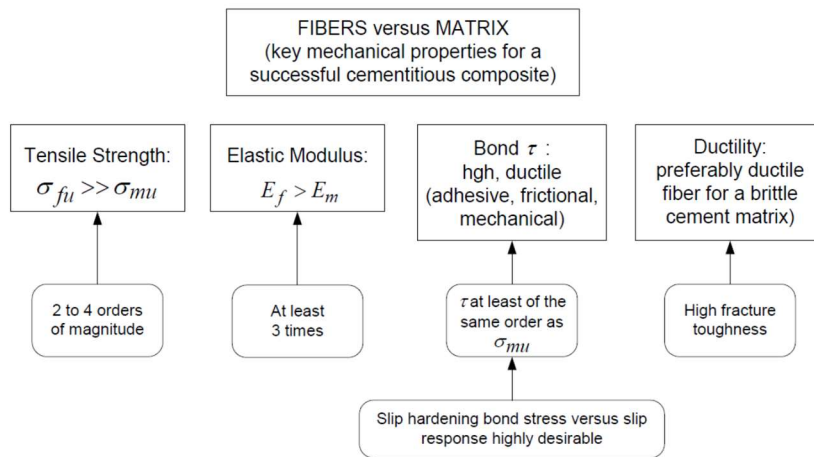
Figure 9 - Conditions for an effective fibre reinforcement (Naaman, 2003)

2.3.2.1 Fibre's length

Usually, fibres' length varies from 6 to 60mm. Löfgren (2005) divides them in two groups:

- The micro fibres: The fibres that have the length smaller than the maximum aggregate size and have its cross-section's diameter of the same order as the diameter of the aggregate's grains. These can bridge the micro cracks;
- The macro fibres: The fibres which have a length bigger than the maximum aggregate size, and a cross-section diameter bigger than the aggregate grain's diameter and an aspect ratio (the ratio between the fibre's length and the fibre's diameter) below 100. These fibres can bridge the macro cracks.

Each group has a different role and Rossi, Acker and Malier (1987) were the firsts to come up with a clarification: the first cracks that start to appear in the concrete are the micro-cracks and the short fibres are the most adequate to bridge them (Fig 10). The reason is that there are much more small fibres than larger fibres in the same volume fraction as they are smaller and weight much less. In the case of using high volume fraction, these fibres will improve the tensile strength of the composite and will also increase matrix cracking strength. When the micro-cracks start to agglomerate and to form a macro crack, the smaller fibres start to be pulled out from the matrix or ruptured. Then the macro-fibres will be activated, to not only improve the tensile response, but also to increase the ductility and fracture energy of the concrete.
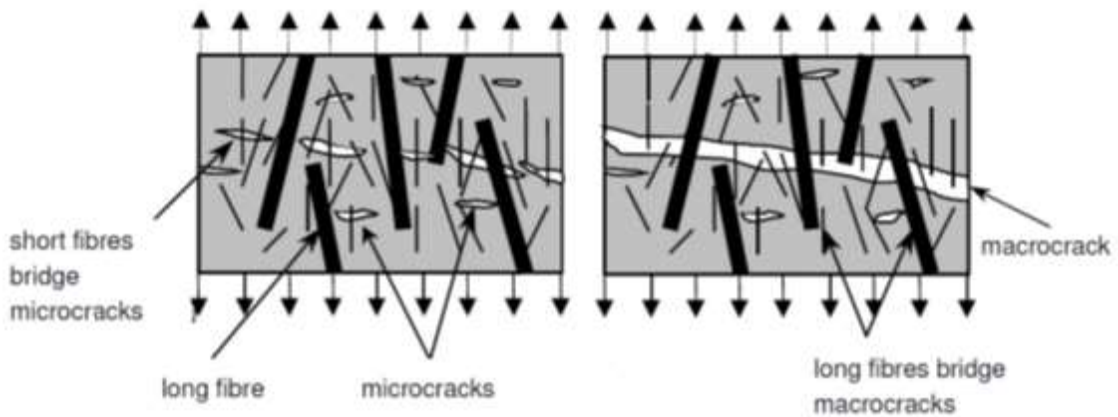
Figure 10 - Role of short and long fibres (Marković, 2006)

2.3.2.2 Fibre's shape

In order to enhance and strengthen the mechanical connection of the fibre to the matrix, it is usual to transform the classic straight fibre. Recently, Dramix® company developed hooked end steel fibres with different lengths and geometries. These fibres can be of three types: 3D, 4D or 5D. Their nomenclature is related to the number of segments that compose the hook, as seen in Figure 11.

Figure 11 - Hooks of the 3D, 4D and 5D Dramix® fibres (Bekaert, 2012)

The mechanical properties increase accordingly to the hook type, as seen in Figure 12.
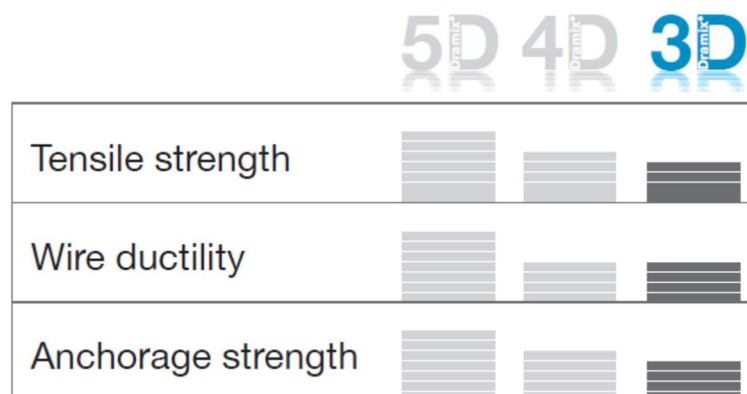
Figure 12 - Characteristics of Dramix® fibres (Bekaert, 2012)

According to the Bekaert catalogue:

- 3D fibres can have an aspect ratio of 45, 65 or 80, length of 35 or 60 mm and a tensile strength between 1160 and 1550 N/mm². They are mainly used in flooring, tunnel applications, precast and residential applications;
- The 4D and 5D fibres have an aspect ratio of 65, length of 60 mm and a tensile strength of 1500 and 2300 N/mm² respectively. 4D fibres can solve service limit state (SLS) issues while 5D fibres can be used for structural applications in ultimate limit state (ULS) problems.

The hook allows to raise the amount of absorbed energy because of the anchorage mechanism: in order to pull out the fibre, not only the connection between the matrix and the fibre needs to be ruptured (the chemical debonding), but also the anchorage mechanism needs to be overcome (the mechanical debonding) by straightening the hook. Moreover, the steel which composes the fibres has high ductility and strength, and so the resistance to fibre rupture and the ductility are also enhanced (Fig 13).
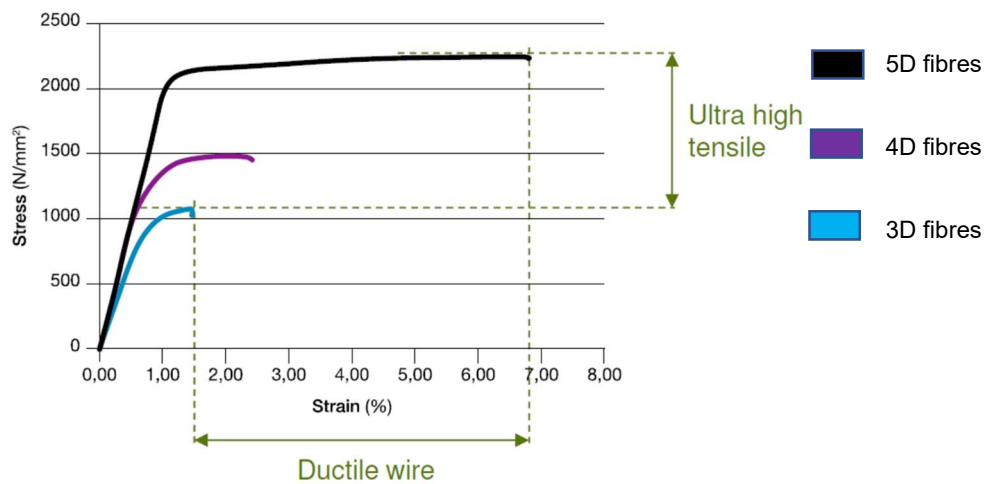
Figure 13 - Tensile strength of Dramix's fibres (Bekaert, 2012)

2.3.2.3 Fibre's orientation and distribution

The bridging mechanism (that characterizes the effect of the fibres on the concrete) is based on a homogeneous redistribution of stresses. Therefore, a good distribution and orientation of the fibres is needed (Dupont and Vandewalle, 2005). Van Gysel (2000) has proven a direct proportional relationship between the toughness of the composite and the number of effective fibres counted in a cracked cross-section. Effective fibres are defined as the ones with a straightened hook through the fracture section.

The ideal situation would be to have the fibres aligned with the principal stresses, but that situation cannot be achieved if the fibres are randomly distributed. Krenchel (1975) proposed a relationship between the number of fibres in a cross-section and the total volume of fibres added to the concrete (see Equation 1). n is the number of fibres in a cross section, α is the orientation factor, V_f is the fibre's volume fraction and A_f the cross section area of the fibre:

$$n = \alpha \frac{V_f}{A_f} \tag{1}$$

To obtain the value of the orientation factor, Dupont and Vandewalle (2005) suggest that three different zones in mould should be identified as showed in Fig 14:

- zone 1: when there are no boundary conditions so the fibre can rotate freely (bulk zone);
- zone 2: when there is one boundary condition (wall effect) affecting the orientation of the fibre;
- zone 3: when there are two boundary conditions (wall effects) affecting the orientation of the fibre.
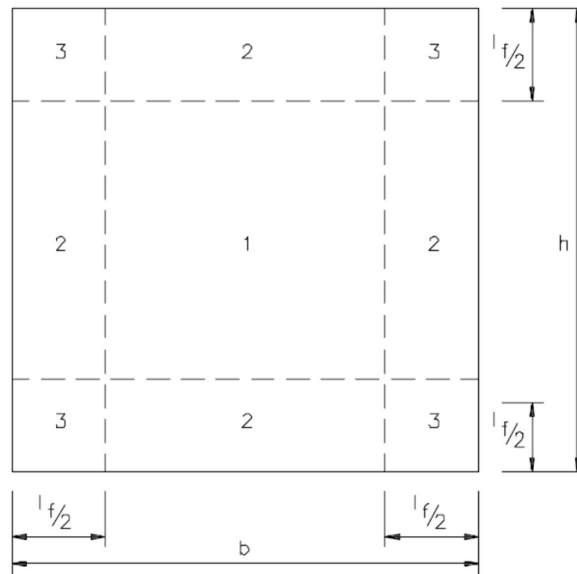
Figure 14 - Different zones in the mould (Dupont and Vandewalle, 2005)

The overall orientation factor will then be calculated using the orientation factor in the three zones (Dupont and Vandewalle, 2005) as explained in Equation 2:

$$\alpha = \frac{\alpha_1 * (b - l_f)(h - l_f) + \alpha_2 [(b - l_f) l_f + (h - l_f) l_f] + \alpha_3 * l_f^2}{b * h} \tag{2}$$

where b and h are the dimensions of the mould, l_f is the fibre's length, α_1 is the orientation factor in zone 1, α_2 is the orientation factor in zone 2 and α_3 is the orientation factor in zone 3. α_1=0,5 and α_2=0,6 and α_3=0,84. They are independent of the fibre's length.

Seven assumptions were made:

- The orientation factor is not influenced if the fibre is hooked. The fibres are all considered straight;
- When there is a long vibration time or the concrete has high workability, the fibres will align in a horizontal plane (Grünewald and Walraven, 2002). Barragán et al. (2000) stated

15

that, in order to simplify the effects previously mentioned, these should not be considered if the vibration time is less than 1 or 2 minutes and the concrete has low workability;

- Each fibre is represented by its gravity centre. Each point of the concrete specimen's cross section is considered to have an equal probability of being the fibre's centre of gravity;
- In zone 1, the boundary conditions do not affect the orientation of the fibre;
- In zone 2, only one side of the cross-section influence the orientation of the fibre;
- In zone 3, two sides of the cross section influence the orientation of the fibre;
- The top of the section is assumed to have the same boundary conditions as the sides of the mould. After casting, this surface is levelled so there are no fibres sticking out which could lead to a higher number of fibres. This effect is not considered here;
- The embedment length is $l_f/2$.

More details about the equation's derivations can be found in Dupont and Vandewalle (2005).

(Dupont e Vandewalle, 2005) proposed this method in order to determine the orientation factor of the fibre based on the assumption that the fibre's embedded length is $l_f/2$ to simplify calculations. However, this assumption is not always true.
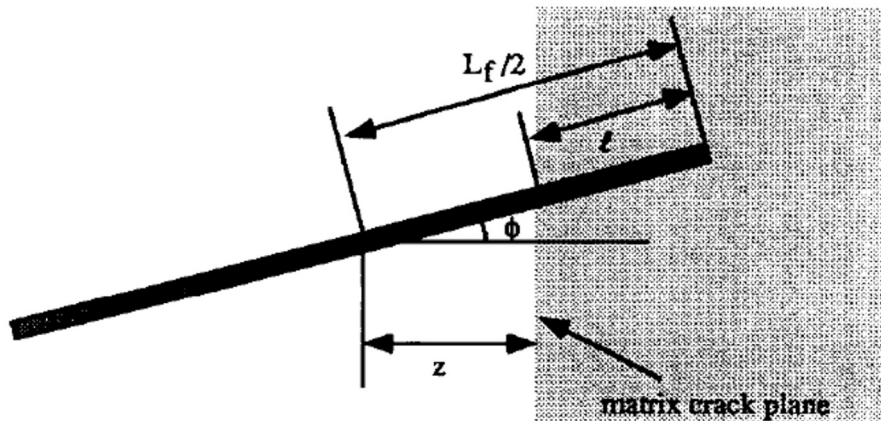
Figure 15 - Fibre in crack plane (Li, Wang and Backer, 1991)

Li, Wang and Backer (1991) also studied the case where the embedded length is not fixed as $l_f/2$. Instead, the centroidal distance, z, (shown in Figure 15) is also a variable.

Kooiman (2000) determined that if the dimensions of the mould exceed five times the fibre's length, the effect of the boundary conditions is reduced. Therefore, Soroushian and Lee (1990) suggested a calculation of an average fibre efficiency factor, η_b, based on the dimensions of the mould, fibre's length and the boundary conditions in case of a 2D distribution. Their results for fibres with a length of 35mm are showed in Figure 16.
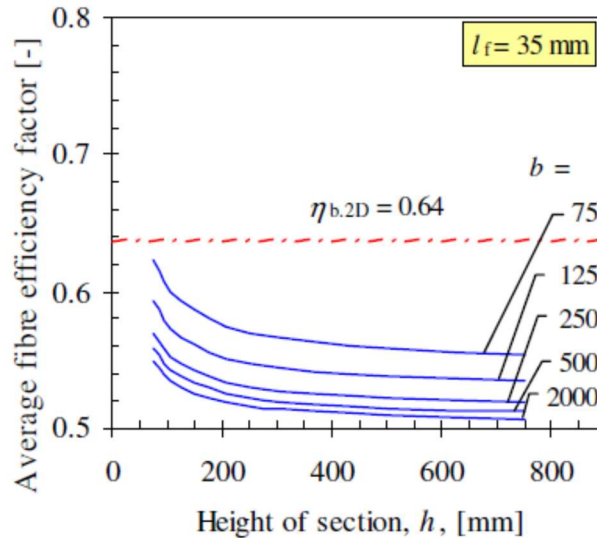
Figure 16 - Values of η_b for l_f=35mm (Soroushian and Lee, 1990)

Where h and b are the dimensions of the moulds.

In order to determine the real fibre orientation and distribution in a hardened concrete, other methods can be used. Mainly, they are divided into two categories: destructive and non-destructive methods (Barnett et al., 2010)

Some examples of destructive methods are the washout test which is performed when the concrete is in the fresh state, and for composites with metallic fibres: it consists in collecting a sample of the mixture and separate the fibres from the concrete using a magnet. The ratio between the number of fibres and the volume of concrete gives the average fibre concentration (Vandewalle and Dupont, 2003). In the hardened state, another current method is to count the fibres in a single cross-section of concrete. It can be performed after mechanical tests (Barros et al., 2005). Other destructive methods are the CT-scan (computerized tomography scan) (Stähli, Custer and van Mier, 2008), image analysis (Ferrara, Ozyurt and Di Prisco, 2011) and the x-ray method (Barnett et al., 2010).

As for non-destructive methods, the most common are the electrical resistivity method (Barnett et al., 2010), ultrasounds, quantitative acoustic emission technique (Reinhardt, Grosse e Weiler, 2001) and the magnetic approach method (Faifer et al., 2010; (Nunes, Pimentel e Carvalho, 2016; Nunes et al., 2015; Pimentel et al., 2015)).

2.4 Workability

The addition of fibres to a concrete matrix enhances its tensile response by controlling the cracking process and resolving the brittle failure and lack of ductility. The higher the fibre's volume fraction, the more improvement in the concrete mechanical properties can be achieved (Figueiredo and Ceccato, 2015). However, the increase in fibre content is also proportional to the reduction in the workability in the fresh state. This can compromise the fibre distribution and the bond to the matrix (due to the inadequate quality of matrix around the fibres) and, therefore, reducing fibre efficiency in the composite. One explanation is that, compared to the same aggregate volume, fibres have a much higher specific

surface and require more paste to lubricate. Also, the fibres constrain the mobility of coarse aggregate particles.

This contradiction creates the need to solve the loss in workability without reducing fibre content. Johnston (2004) concluded that by decreasing the aggregate in the mixture, higher volume fibres could be added without a big loss in workability. Also, the author reported that the strong presence of fine aggregates in the composite had a positive effect on the workability and allowed more fibres to be added.

Other measure that has been answering this need is Self-Compacting Concrete with the use of strong superplasticizers. This type of concrete has high flowability and cohesiveness (Sahmaran, Yurtseven and Ozgur Yaman, 2005) and also contributes to the improvement of the fibre's distribution, making it more uniform.

Okeh et al. (2019) concluded from slump-flow testing that the decrease of the ratio of macro/micro fibres reflects negatively on the workability. The author explained the negative effect of micro-fibres in the workability: the interfacial zone of cement and aggregates in wet state is altered due to the presence of high amount of micro-fibres and its high aspect ratio. This alteration is due to the large surface area of the micro-fibres which increases the bond and adhesion between particles and, this way, compromising the spread.

2.5 Mechanical properties
2.5.1 Compression behaviour

The compression behaviour of plain concrete is characterized by a linear elastic branch followed by a non-linear behaviour until the first crack appears. This is followed by a sudden loss of strength, as seen in Figure 17, resulting in a brittle failure. Vonk (1992) studied the reasons for this behaviour and concluded that the sliding friction in pre-existing flaws in the aggregate-paste interface leads to tensile cracks which start to align in the direction of principal stresses. In normal strength concrete, aggregate is much stronger than the paste, and therefore the cracks can be formed in the paste or in the interface between the aggregate and paste. Conversely, in the high strength concrete, the weakness is the aggregate's resistance itself. This allows a higher compression resistance but leads to a much more brittle failure (Darwin et al., 2001).

The fibres are able to solve this brittle failure, allowing a much smoother strain softening behaviour after the peak load (Glavind, 1992). The pre-peak behaviour and the compressive strength are not affected, only the response of the composite after the first crack is improved as seen in Figure 17.
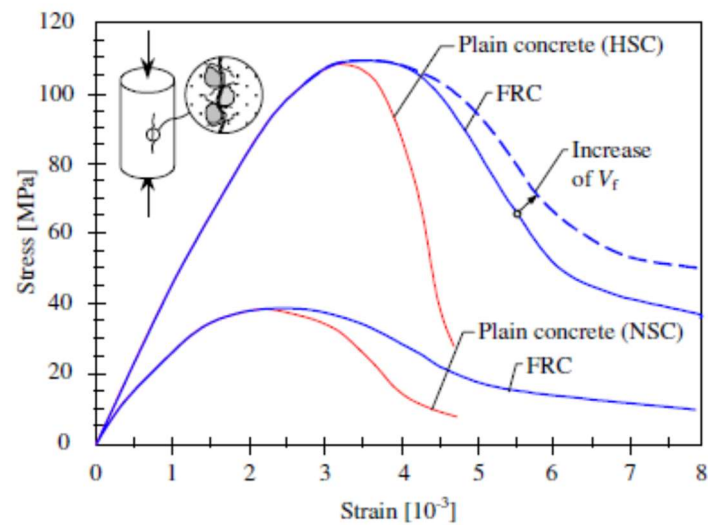
Figure 17 - Strain-stress curve of different types of concrete under compression (Löfgren, 2005)

2.5.2 Elastic Modulus

Although in many studies about the elastic modulus it has been observed that the addition of fibres to the concrete has real small influence on the elastic modulus (Lee, Oh and Cho, 2015; Mansur, Chin and Wee, 1999; Rossi and Harrouche, 1990) a slight decrease when the fibre volume is increased was observed. (Almeida and Neves, 2005) explained this phenomenon by stating that the fibre's which aligned parallel to the principle stresses act like voids. Also, the fibres difficult the consolidation of concrete negatively affecting the elastic modulus (Suksawang, Wtaife and Alsabbagh, 2018). In Noushini, Vessalas and Samali (2014) study, it was observed that long fibres have a more notorious effect than short fibres.

2.5.3 Behaviour in bending/tension

Naaman and Reinhardt (2006) stated that the tensile behaviour of composite can be classified as strain-hardening or strain softening and the bending behaviour as deflection-hardening or deflection-softening. If a strain-hardening behaviour is observed in tension, the composite will show a deflection-hardening behaviour when subjected to bending. On the other hand, if the FRC demonstrates a strain-softening response with tension loads, then both deflection-hardening or deflection-softening can be observed in bending tests, as explained in Figure 18.
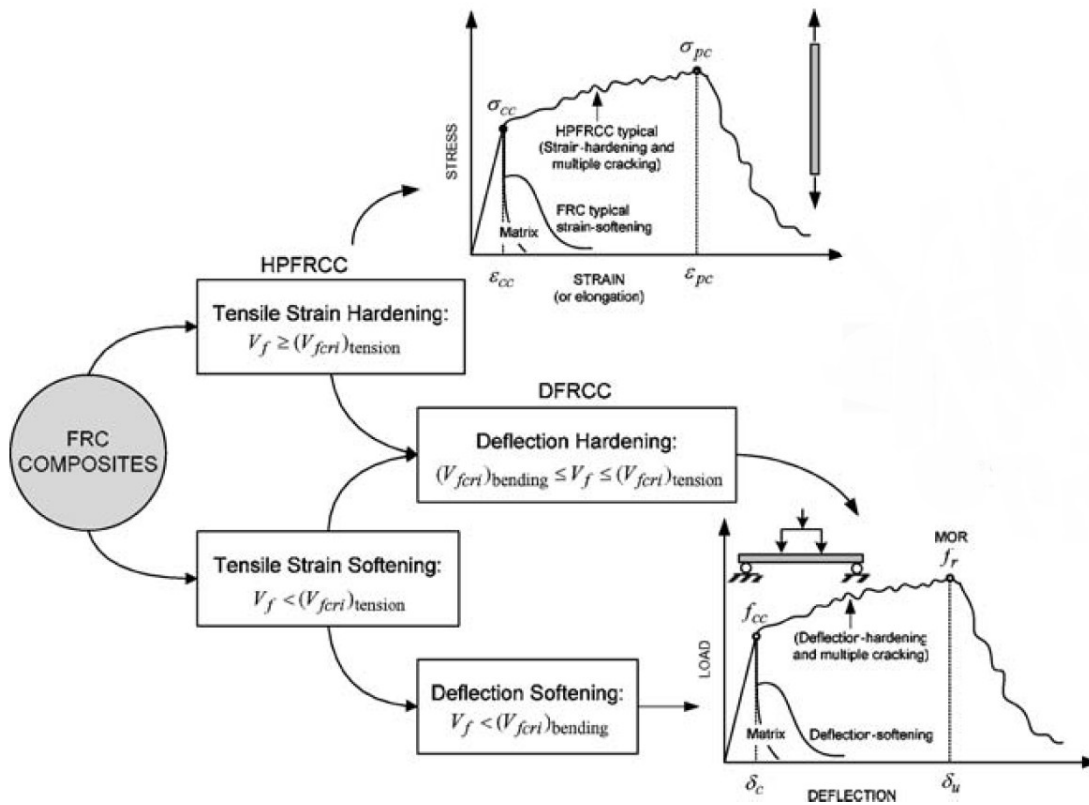
Figure 18 - Tensile and flexural responses of FRC (Naaman and Reinhardt, 2006)

As can been seen in Figure 19, the stress-strain curve starts with a linear elastic branch until it reaches the point concrete's tensile strength (σ_{cc} ε_{cc}) and the first crack appears (this depends mainly on the matrix tensile strength). Note that, until this point, the concrete's behaviour is not significantly influence by the fibres. The main advantage of the fibre's addition comes after the peak load when, instead of a sudden downfall of the curve and a brittle failure, a much smoother softening branch and a ductile failure are observed. Here, the fibres are supporting the load while are being gradually pulled out of the concrete. (Naaman e Reinhardt, 2006). This strain-softening behaviour is characteristic of the HPFRC.
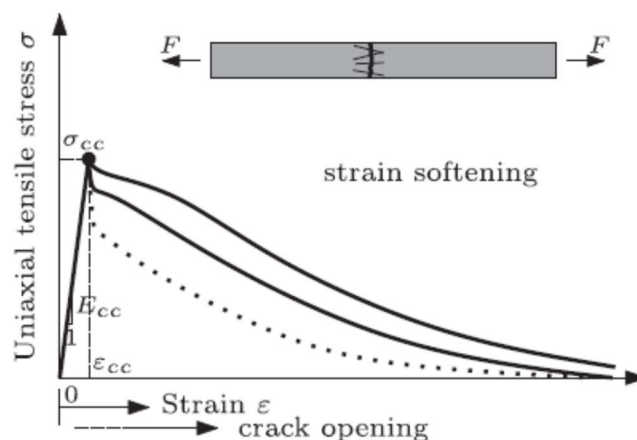
Figure 19 - Strain softening behaviour (Wille, El-Tawil and Naaman, 2014)

For high fibre volumes, HPFRC can present a strain-hardening behaviour. This means that when subjected to tension and the tensile limit is reached, its resistance not only does not decrease but increases to a post cracking strength, σ_{pc}, higher than the matrix tensile strength, σ_{cc}. The addition of a sufficient number of fibres allow the development of multi-cracking process where the fibres bridge several cracks, supporting the load that is being applied in the concrete and distributing the stresses in the crack to uncracked zones enhancing its ductility. At the peak, a critical crack forms and no more cracks will develop. In the softening branch that follows, this crack will increase its width and then other cracks, in which the fibres are being pulled out, will start to unload as well.
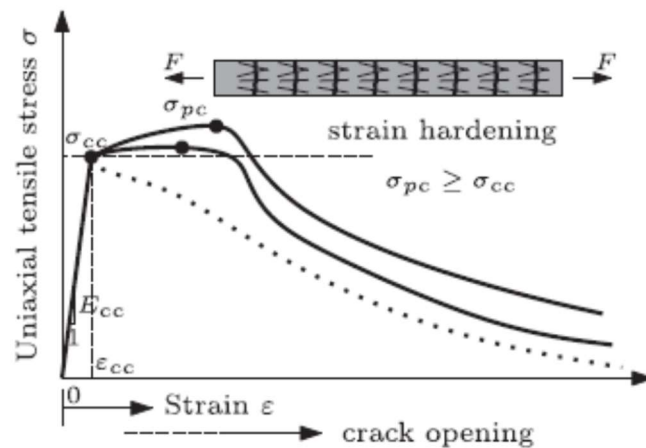
Figure 20 - Strain-hardening behaviour (Wille, El-Tawil and Naaman, 2014)

When plain concrete is being subjected to bending and the critical load is reached, the part in tension will crack and there's a drastic reduction in the load carrying capacity. According to Yoo, Yoon and Banthia (2015), for low fibre volumes (<0,5%), deflection-softening can be observed where, even though the flexural strength is not influenced, the post-peak ductility is higher. After the peak load, the fibres bridge the appearing crack controlling the propagation of other cracks. This results in a smother reduction of the load carrying capacity of the concrete. (Fig 21) The post-peak ductility increases with the increase in fibre content.
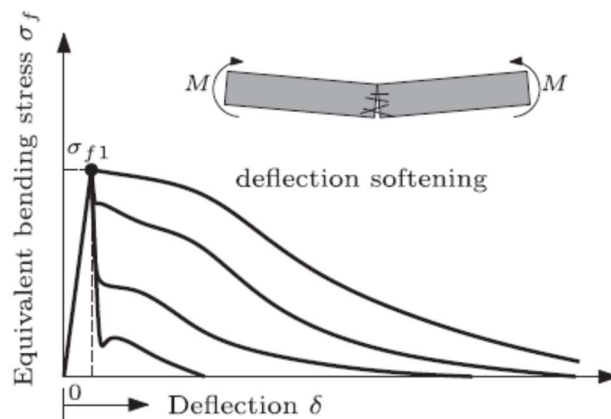
Figure 21 - Deflection-softening behaviour (Wille, El-Tawil and Naaman, 2014)

Also according to Yoo, Yoon and Banthia (2015), for a higher fibre content (>1%), deflection-hardening behaviour can be observed (Fig 22). After the peak load is reached, the fibres allow a multi-cracking process to happen (similar to strain-hardening) and increasing the flexural strength to a post-cracking peak (σ_{f2}). This ascending branch is then followed by a descending branch where all the cracks start to slowly unload.
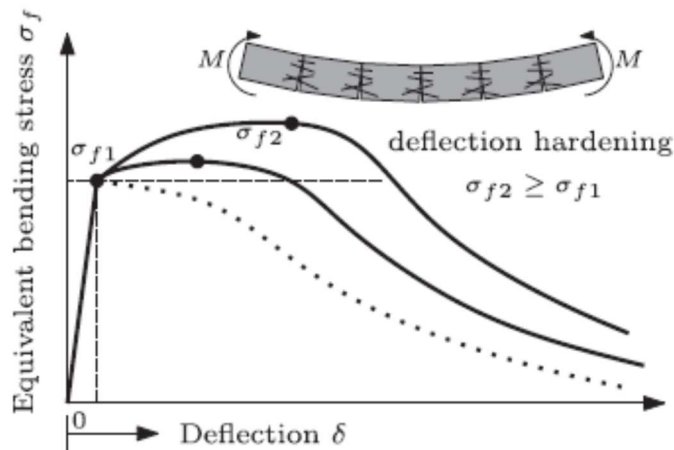
Figure 22 - Deflection hardening behaviour (Wille, El-Tawil and Naaman, 2014)

2.6 Applications of HPFRC

Fibres have been used in construction for almost three millenniums, but they were only combined with cement matrices around 1874. The last four decades mark the growth in its popularity, market penetration and modern investigation worldwide. Such a success is due, in part, to significant evolution in the fibre reinforcement, the characteristics of the cementitious matrix, the bond connection between fibre and matrix, more studies about the mechanics of the composite and improved cost-effectiveness (Naaman, 2007a). The developments that are related to the increase of this type of materials in construction today, according to the same author, are:

- The increasing offer of different types of fibres with different characteristics which can add strength, ductility and toughness;
- The introduction to new types of superplasticizers which allows to improve the mechanical properties of concrete without loss of workability;
- The use and better understanding of the effect of different types of micro-fillers such as silica fume and fly ash on the matrix porosity, strength and durability;
- The more efficient bond between the fibre and matrix provided by the addition of polymer;
- The innovation in production processes such as self-compacting mixtures which allow to mix high fibre volumes with small effects in the porosity of the matrix.

The main range of applications for steel fibres is shown in Figure 23. They can be used in stand-alone applications in light structural elements such as cladding, cement boards or slabs on grade and pavements. Also, they can be combined with other types of supporting materials of reinforcement and be used in impact seismic resistant structures, jacketing for repair and strengthening of beams and columns, and, in the case of steel, encased beams and trusses to improve ductility and fire resistance. They have also been used in repair and rehabilitation works (Naaman, 2007b).
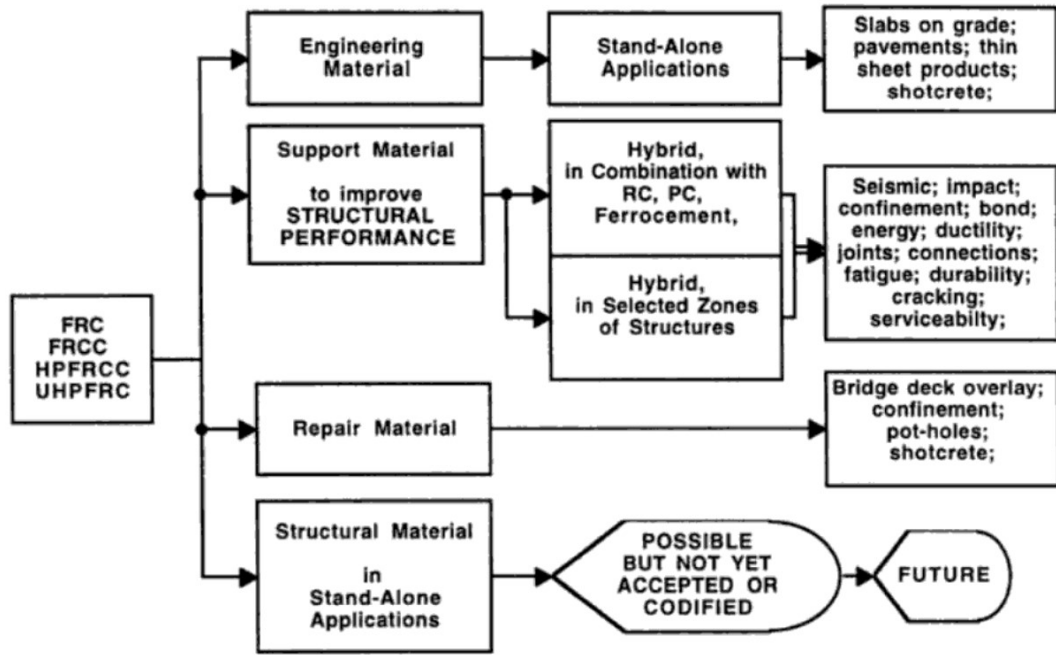
Figure 23 - Applications for FRC (Naaman, 2000)

Due to economic reasons, fibres are not used in the whole structure of a building. In fact, they are most commonly applied only in specific zones (Figure 24). Examples include punching shear zone around columns in two-ways slab systems, end blocks and anchorage zones in prestressed concrete beams, beam to column connections in seismic resistant frames, beam to shear wall connections, coupling beams for seismic-cyclic resistance, out-rigger beams; in-fill damping structural elements, lower end of shear walls, tension zone of RC and PC beams to reduce crack widths and improve durability, compression zone of beams and columns to improve ductility (Naaman, 2007a).
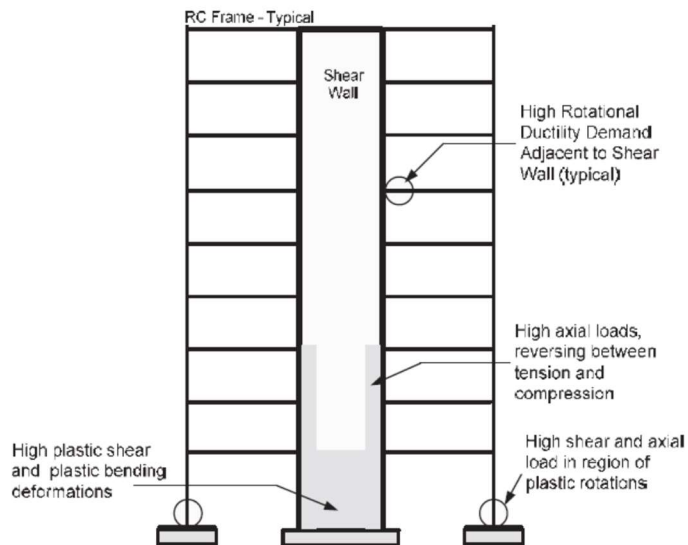
Figure 24 - Applications of FRC in specific zones of a building (Naaman, 2007a)

The main purpose of adding fibres to the concrete is to control the cracking and micro-cracking progress, improve the tensile and bending post-peak response and ductility. However, they are also a solution to improve the structural functioning. They enhance the bond and the bond versus slip response between reinforcing bars and concrete under monotonic and cyclic loading preserving the cover of concrete under large deformations, This helps to maintain the integrity of the structure by keeping reinforcing bars from buckling in columns (Naaman, 2007a).

As stated in EC EN1998, concrete buildings which use flat slab frames as primary seismic elements are not completely covered. This comes from the lack of knowledge of the stiffness of the slab-column connection, the behaviour of flat slabs under seismic actions, the resistance under cyclic and dynamic loading as well as the brittleness of the punching failure. High and ultra-high performance fibre reinforced concrete (HPFRC, UHPFRC), compared to normal strength concrete (NSC), have enhanced mechanical resistance and durability and allow to create slender and lighter structures. However, the lack of legislation and design rules regarding these materials makes it harder to use them as a structural solution. Being more costly materials, one of the objectives of the HiperSlab project is to apply these materials in localized areas of slab-column connections while the rest of structure is designed with NSC. This allows the designer to take advantage of the improved properties of HPFRC and UHPFRC in a rationalized way in order to lower their economic impact. This project has two different phases: first, some punching tests under monotonic loading will be performed to study different structures layouts with localized used of both material which will then be followed by tests with cyclic horizontal actions performed until failure to better understand the structure's behaviour under earthquake induced deformations. This project aims to improve the information about these materials and to create design recommendations for including the two materials in structures under seismic loading.

3
PULL-OUT BEHAVIOUR OF STEEL FIBRES

3.1 Introduction

Among other advantages, fibres improve mainly the tensile response of concrete. Although its mechanical properties in elastic phase can be also improved with the addition of small-fibres to bridge micro-cracks (Stang, Li and Shah, 1990), its effect is much more notable in the post-cracking stage. This is due to the bridging effect performed by fibres in the cracks, redistributing the stresses, supporting the loads and enabling more energy to be absorbed (Naaman et al., 1991). Therefore, it is of highly importance to understand the fibres' pull-out mechanism in order to evaluate their ability to transfer stresses between two laps of a crack.

Although there is no standardized testing method to characterize this aspect (Guerrero and Naaman, 2000), the pull-out test is an usual option. The fibres' pull-out test can be made with a single fibre or with multiple fibres. However, the single-fibre pull out test has a good degree of precision and it's much easier to be performed (Abrishambaf, 2015). Some examples of its configurations are presented in Figure 25.
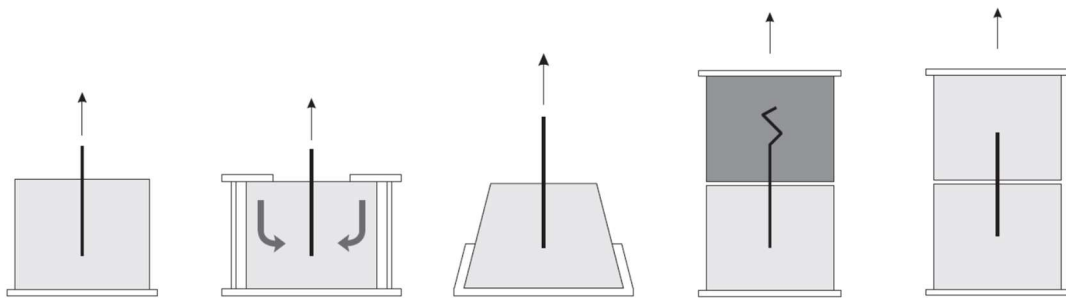
Figure 25 - Various configurations of single fibre pull-out test (Cunha, Barros and Sena-Cruz, 2007)

The transmission of stresses between the fibres and the matrix is made through a bond connection (Fig 26) where three mechanisms can be distinguished (Marković, 2006):
- Debonding of the fibre from matrix, when the chemical bond (the adhesion between the fibre and matrix) is destroyed;
- Mechanical debonding, when the deformed part of the fibre (if it exists) starts to be straighten;
- Pull-out of the fibre, when the fibre moves in its matrix channel.
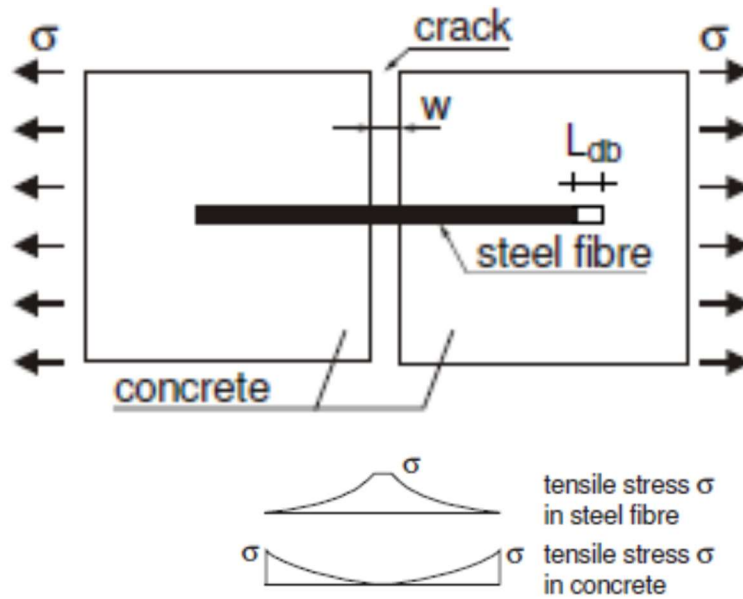
Figure 26 - Stress distribution in a crack (Marković, 2006)

The first to be mobilized is the adhesion/chemical bond, which is the bond between the fibre and the concrete that surrounds it. Bentur and Mindess (2006) describe the debonding process as micro-fractures occurring in the interface zone of the fibre and the matrix. The interface zone is a more porous zone due to an insufficient particles' packing and to water accumulation around the fibre (an inhomogeneous component of the composite). This zone is represented in Figure 27.
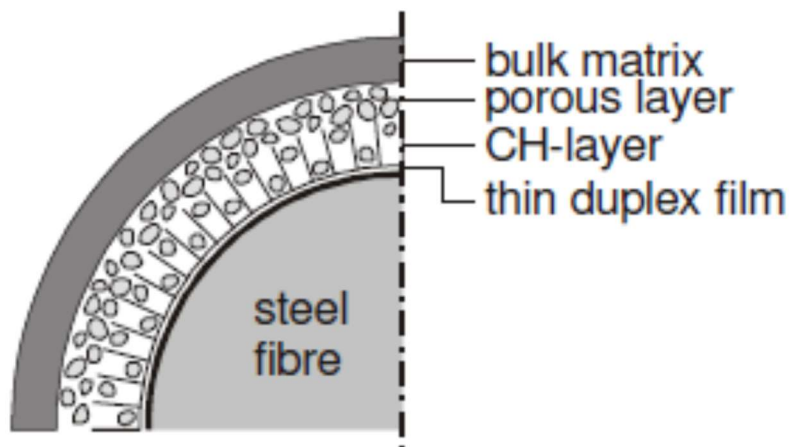
Figure 27- Interface zone (Marković, 2006)

When the chemical bond is destroyed, the mechanical bond can be mobilized by fibre's mechanical deformations. Afterwards, friction stresses are generated as the fibre is sliding along its length in the matrix channel (Homrich and Naaman, 1987).

3.2 Factors which influence the fibre's pull-out behaviour
3.2.1 Fibre geometry

The geometry of the fibre has great influence on its pull-out behaviour. Although there are many different types of shapes, in this work only straight and hooked-end fibres will be compared.

The pull-out response of the fibre can be represented in a load-slip curve. Cunha, Barros and Sena-Cruz (2007) studied this curve and concluded that, for straight fibres, there are only two bond mechanisms: the adhesion and friction. The pull-out process starts with the linear increase of the slip with the load. This corresponds to the elastic behaviour of bond (Fig 28, Phase 1). Then, a non-linear branch develops, which corresponds to the formation of micro-crack in the interface zone and, consequently, the debonding of the fibre (Fig 28, Phase 2) until the peak load (critical crack length). After the peak, the stage of fully debonding of the fibres occurs (Fig 28, Phase 3): a sharp reduction in the load is observed, until the fibre is completely debonded and starts to slide. The fibre will then start to slide. This stage is mainly governed by the friction resistance. The load continues to decrease because the frictional resistance is decreasing as well: the sliding of the fibre results in gradually less surface area in contact with the concrete (Fig 28, Phase 4). The energy absorbed by the system (or pull-out work) corresponds to the area beneath the curve. Note that, during the loading process, if the tensile strength of the fibre is reached before the bond's strength, the fibre will rupture; the strength will decrease drastically and less energy will be dissipated. This phenomenon won't allow to take full advantage of the bridging process. As such, it is very important to choose a suitable fibre (considering geometry and tensile strength) according to the concrete compressive strength to increase the its effectiveness in the composite.
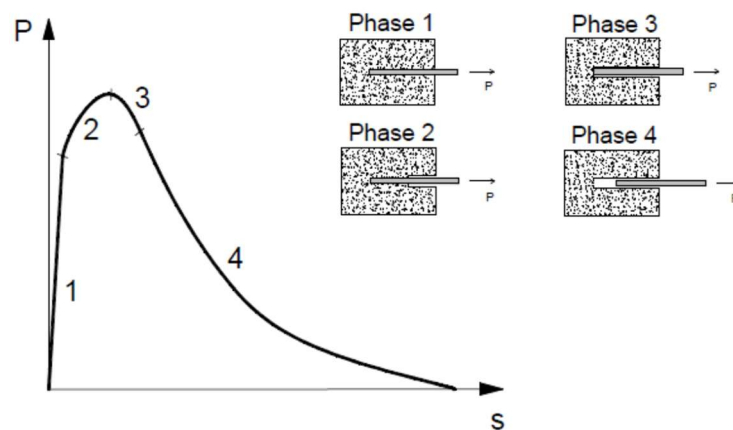
Figure 28 - Pull-out mechanism of smooth fibres (Abrishambaf, 2015)

For hooked-end fibres, the bond has three mechanisms (instead of two like straight fibres): the adhesion bond, the mechanical bond and the friction bond. Similar to the smooth fibres, the load-slip curve also starts with a linear ascending branch (Fig 29, Branch OA) corresponding to the elastic deformation of the bond, followed by a non-linear branch corresponding to the debonding process (Fig 29, Branch AB) until the fibre is completely debonded (Fig 29, Point B). At this point, the mechanical resistance, corresponding to the deformation of the hook, is mobilized originating an ascending branch (Fig 29, Branch BC). This resistance is highly dependent on the fibre's geometry as more energy is needed to deform the fibre if the cross-section has a larger diameter. When the first hook is straightened, the sliding of the fibre occurs, mobilizing the friction resistance (Fig 29, Branch CD). The second curvature corresponds to the deformation of the second hook (Fig 29, Branch DE) until the fibre is completely

straighten and the final sliding occurs also with the resistance of the residual friction stresses. Due to the hooked end, the fibre will not be completely straightened so the friction stresses will increase in comparison to the smooth fibres originating more resistance also in the final phase of the process. As shown in Figure 29, with the hooked-end fibres, there is a larger area beneath the curve.
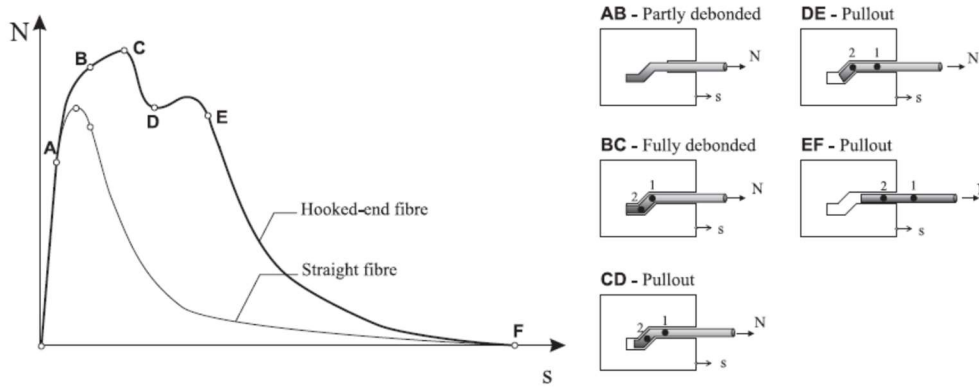
Figure 29 - Pull-out mechanism of hooked-end fibres (Abrishambaf, 2015)

Naaman (2003) studied a new technology in order to improve the adhesion, the bond and the frictional resistance. First, the author concluded that the post cracking strength of the fibre is dependent on the Fibre Intrinsic Efficiency Ratio (FIER):

$$FIER = \frac{\psi * l_f}{A} \qquad (3)$$

Where, ψ is the fibre's perimeter, l_f is the fibre's length and A is the cross-sectional area.

So in order to improve the post-cracking strength, he followed the line of thinking showed in Figure 30:
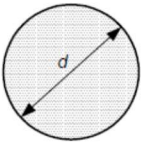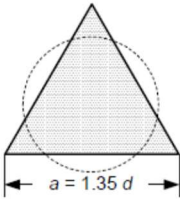
Figure 30 - Improvement of original round cross-section: A) Circular; B) Triangular; C) Substantially Triangular Fibre (Naaman, 2003)

These modifications improve the adhesion and the friction bond of the fibre to the matrix.
Naaman (2003) also proposed that, in order to improve the mechanical bond, twisted fibres creating ribs along its length were the best solution. The pull-out response of the new Torex fibres (twisted fibres with polygonal cross-section) compared to smooth and hooked-end fibres is presented in Figure 31.
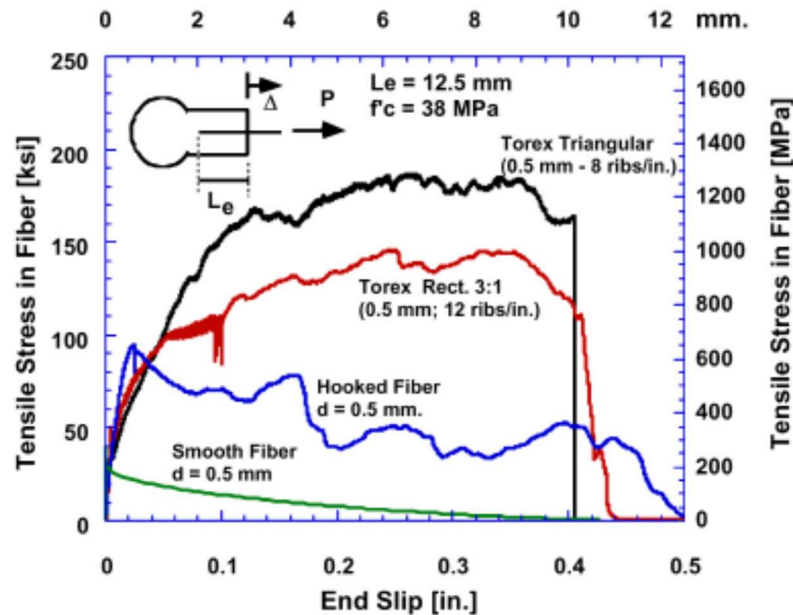
Figure 31 - Pull-out response of straight, hooked and Torex fibres (Naaman, 2003)

As proved by experimental results, the use of new Torex fibres allow higher stresses in the fibre with wider cracks and a higher absorption of energy than hooked fibres. It is important to note that when the maximum pull-out load is reached, it can remain high for big slips. In order to support these high stresses, the fibres are made with high strength steel.

3.2.2 Fibre material

The fibre material is very important in the pull-out response of the fibres because the tensile strength of steel needs to be adequately chosen according to the stresses that the composite will have to support. The steel needs to endure high stresses without rupture, always within economic viability.

3.2.3 Cementitious matrix

The quality and characteristics of the cementitious matrix also has high influence on the pull-out response of fibres.

Wei, Mandel and Said (1986) determined that for low values of water/binder (w/b) ratio, the matrix has higher density and higher microhardness in the fibre-matrix interface zone. Therefore, a better response is expected.

The presence of fine filler materials (e.g., silica fume, fly ash, limestone filler, metakaolin or polymer additions) allows the empty spaces between the cement particles and the fibre in the interface to be filled as their particles are much smaller than the cement particles. This results in a higher packing density in the interfacial zone between fibre/matrix (Cunha, Barros and Sena-Cruz, 2007). Also, the addition of silica fume enhances the concrete's shrinkage, resulting in higher clamping pressure of the fibre, which improves the debonding and the frictional resistance (Li e Stang, 1997).

Abdallah and Fan (2017) studied the influence of the matrix compressive strength in the fibre's pull-out response with 3 different types of fibres (Dramix®, 3D, 4D and 5D) using Normal Strength Concrete (NSC), Medium Strength Concrete (MSC), High Strength Concrete (HSC) and Ultra-high Performance Mortar (UHPM) with compressive strengths of 33MPa, 52 MPa, 71 MPa and 148 MPa, respectively. The results are presented in Figure 32.
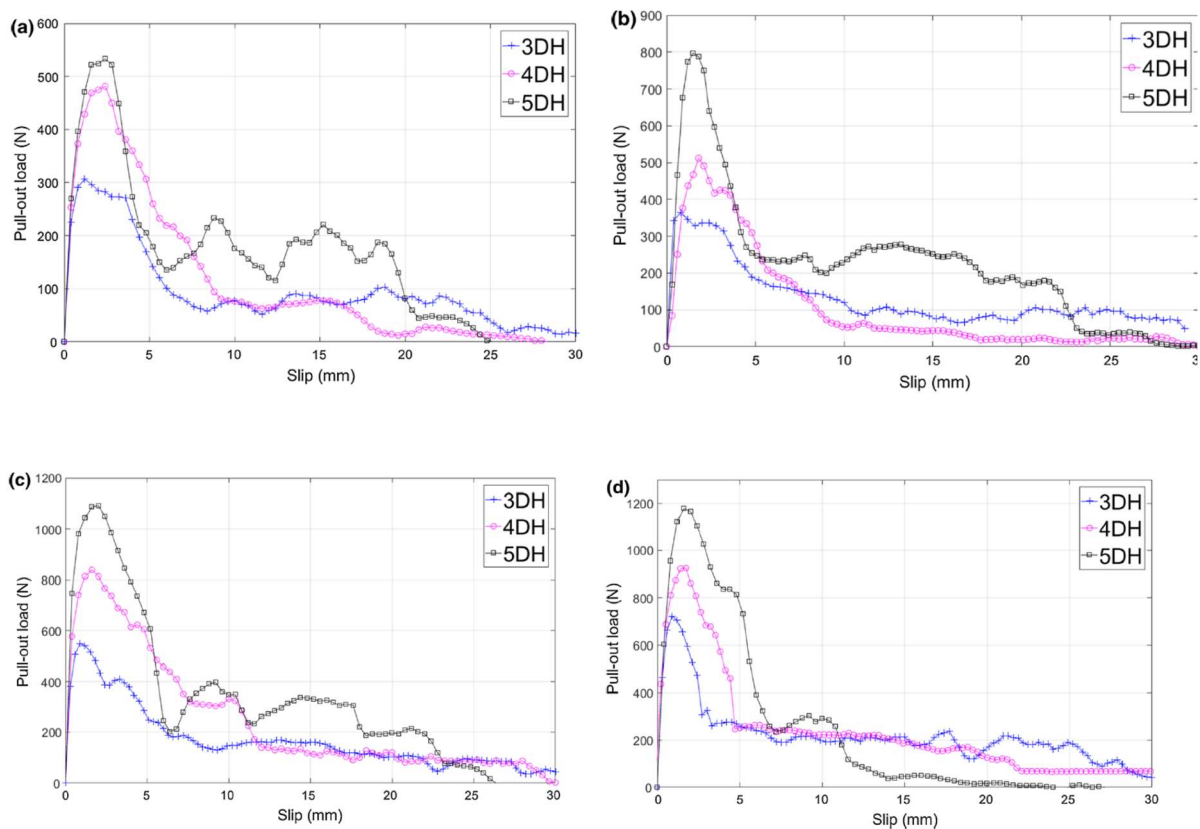
Figure 32 - Pull-out response of 3D, 4D and 5D Dramix fibres a) NSC (33MPa) b) MSC (52 MPa) c) HSC (71MPa) d) UHPM (148MPa) (Abdallah and Fan, 2017)

As expected, the maximum pull-out load and pull-out work (energy absorption which corresponds to the area beneath the curve) increases from 3D to 4D and from 4D to 5D fibres (Fig 32). This is due to

the higher mechanical resistance provided by the better anchorage mechanism of the hooks and to the more resistant steel, which requires more energy to be deformed and can support higher stresses without rupture.

For all fibres, the maximum pull-out load and the pull-out work are expected to increase with the compressive strength of the matrix due to the higher deformation of the hook. This is due to the better matrix properties which makes the bonding between the fibre and the matrix more resistant. However, the pull-out work is higher for HSC than for UHPM for 4D and 5D fibres. This relates to the fact that only for higher tensile strengths it is possible to fully straight the 5D fibres and in lower strength concrete, there are still deformations and irregularities in this type of fibres, which creates more friction stresses when they are sliding.

In the HSC and UHPM, both the 3D and 4D fibres are fully straight. However, in UHPM fibre rupture is experienced (Fig 33). This can be seen in Figure 32d in the sudden reduction of strength in both curves. Also, even after the fibre's rupture, stresses continued to be supported by the fibres until they are completely pulled out: their hooks are not completely straightened in NSC and MSC even though the deformation is clearly higher for MSC (Fig 33).
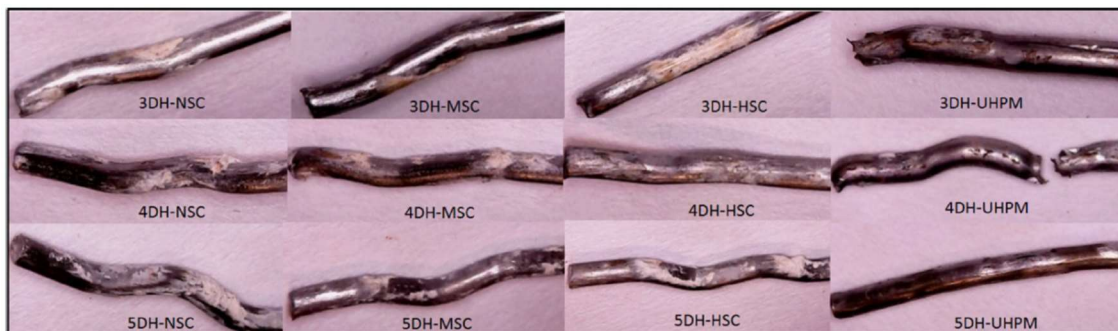
Figure 33 - Pulled out fibres (Abdallah and Fan, 2017)

For 5D fibres, the hook deformation also grows with the compressive strength of the matrix and it's only fully deformed in the UHPM (Fig 33). This is also visible in Figure 32d as the residual energy corresponding to the frictional stresses is much smaller than in the other concretes because the hook is completely straighten: 5D fibres can only be completely efficiently in UHPM reinforcement, as they can only take full advantage of their total mechanical deformation of the hooks in this type of matrixes .This fibre did not experience rupture in any of the matrixes due to its ultra-high tensile strength.

3.2.4 Fibre Orientation

Fibres are, commonly, randomly distributed in the concrete. In a certain crack, although few fibres may be aligned with the principal stresses, they usually form an inclination angle which influences their pull-out behaviour (Robins, Austin and Jones, 2002).

When a fibre that forms a certain angle different from 0º with the plane parallel to the crack is being pulled-out, it tends to align perpendicularly to the cracks plane (as a consequence of the increasing of the crack's width). This causes the fibre to bend and to require more load in the pull-out process due to a snubbing effect (Fig 34) (Dupont, 2003).
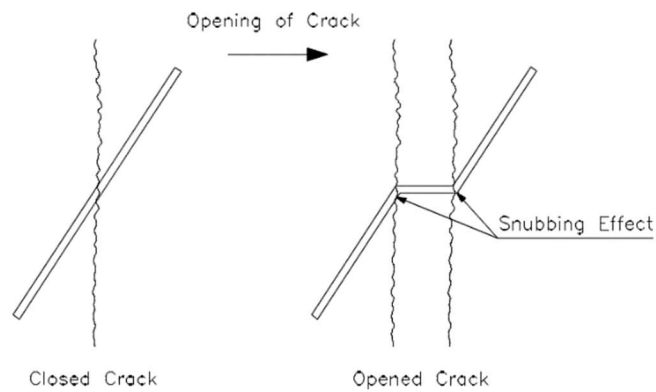
Figure 34 - Snubbing effect (Dupont, 2003)

Van Gysel (2000) concluded that the maximum pull-out load increased with inclinations up to 10º due to the snubbing effect. For larger angles, it decreases due to the spalling effect (Fig 35). The influence of those two parameters is showed in Figure 36.
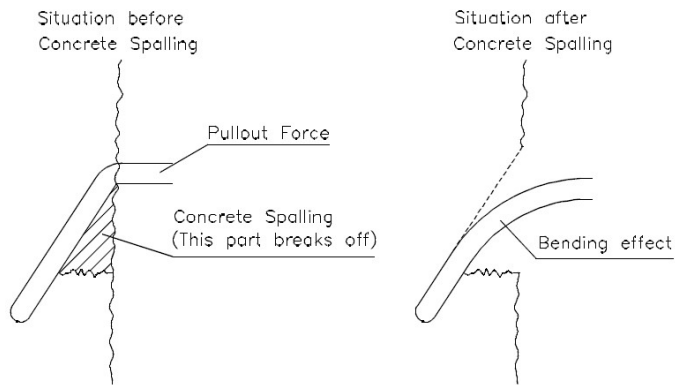
Figure 35 - Concrete spalling (Dupont, 2003)
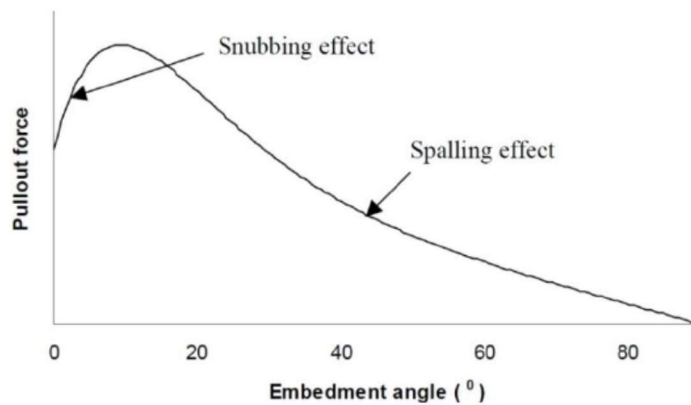
Figure 36 - Effect of snubbing and spalling in the maximum pull-out load (Van Gysel, 2000)

Naaman and Shar (1976) determined that the pull-out load increased with inclination angles up to 45º. For angles of 45º and 60º, both Van Gysel (2000) and Banthia and Trottier (1994) witnessed fibre rupture caused by the high stresses in the fibre's exit point.

Robins, Austin and Jones (2002) also studied the effects of the fibre's inclination on the pull-out load with an embedded length of 15mm (Fig 37).
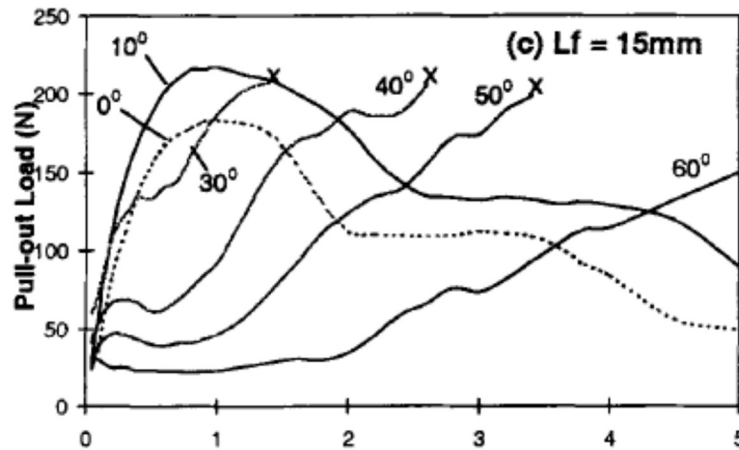
Figure 37 - Fibre's orientation influence in the pull-out response of a single fibre with embedment length of 15mm (Robins, Austin and Jones, 2002)

It was experienced that the maximum pull-out load increases up to the inclination of 10º. For higher inclinations there is no significant alteration.

In all the cases, the slip at maximum load increases with the orientation angles because of the concrete spalling at fibre exit point, as already explained.

For a 60º angle, the fibre was completely pulled-out. Here, the concrete spalling is so drastic reducing snubbing effect making the slide of the fibre much easier. In fact, the slip correspondent to the maximum pull-out load is so big that it becomes irrelevant.

For angles of 30º, 40º and 50º fibre's rupture was experienced because of the high concentrated stresses in the point that the fibre exits the matrix.

The different conclusions and test results discussed in previous studies are justify with the variance in other parameters like the matrix strength, the fibre's strength, cross-section, embedment length and anchorage mechanism (Cunha, Barros and Sena-Cruz, 2007). In conclusion, the optimal range of fibre's inclination is between 0 and 20º degrees. For larger angles, the pull-out load usually decreases.

3.2.5 Embedment length

Robins, Austin an Jones (2002) determined that, in order to fully mobilize the anchorage of the hook, the embedment length must be enough to cover all the fibre's hook. If not, the potential fibre's pull-out

strength cannot be fully mobilized. Fibres with deformations along its length are even largely influenced by the embedment length: the friction resistance caused by the mechanical deformations is the most significant bond to the matrix in this fibres and its influence grows with the contact area between the two constituents.

Increasing the fibre's embedment length almost always increases the pull-out resistance due to the increase of the surface area of the fibre in contact with the matrix enhancing its frictional stresses. This is mainly observed for straight fibre (Li and Stang, 1997). However, in the pull-out mechanism of hooked-end fibres, the dominant bond is the mechanical bond provided by the anchorage mechanism of the hook. Because of this, there is a decrease of the influence of larger embedment lengths in the pull-out resistance since they mainly influence the adhesion and friction bond (Naaman and Najm, 1991).

Figure 3.14 shows the influence of fibre's embedded length in both maximum pull-out force and slip at the maximum load for hooked-end and smoothed fibres. The maximum pull-out force grew with the embedded length for both fibre's types in all inclination. However, its effect was stronger in the smooth fibres. Regarding the slip correspondent to the maximum pull-out force, only for align fibres it was possible to establish a connection: for both smooth and hooked-end fibres, the slip increased for the larger embedded length.
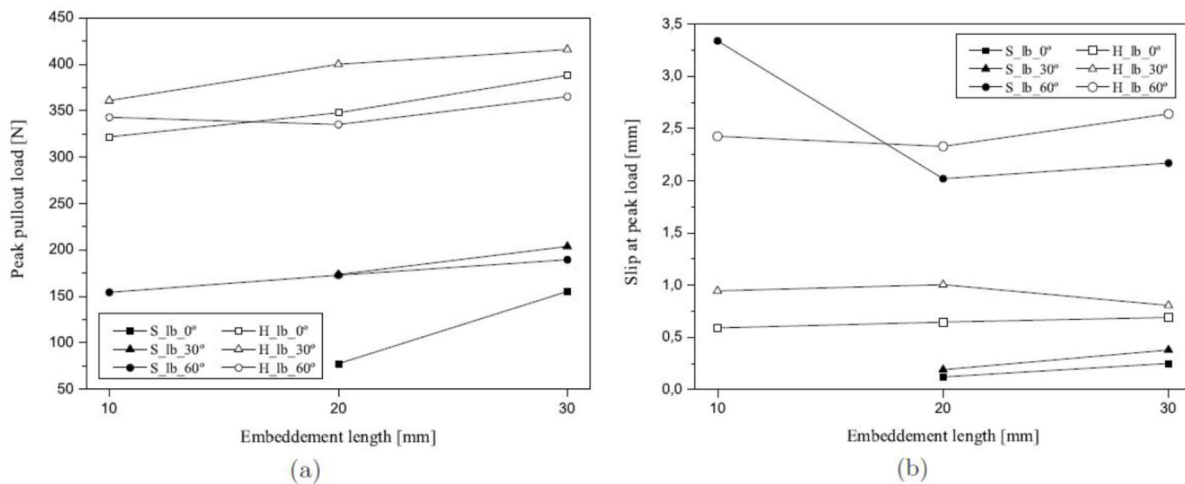
Figure 38 Influence of fibre's embedded length in a) Maximum pull-out load; b) Slip at maximum load (Cunha, 2010)

3.3 Pull-out tests on single fibres: test set-up and parameters
3.3.1 Matrix composition

In the pull-out tests, one matrix composition was made (Mix A) and is presented in Table 4. No fibres were added to this mixture used in the casting of the pull-out specimens since the only parameter that is being studied in these pull-out tests is the bond between fibre and concrete. However, in order to characterise the mechanical properties of the mixture, 1% fibre volume fraction was added to the specimens used in the mechanical tests to prevent the explosive failure of the specimens during testing.

Table 4 - Mix A composition

Mix A (kg/m^3)	
Cement (kg)	531.86
Limestone powder (kg)	203.72
Superplasticizer (Viscocrete 20HE) (kg)	12.548
Sand (kg)	811.82
Coarse aggregate (kg)	721.43
Silica-fume (kg)	53.19
Water (kg)	147.85
Short fibres 13/0.2 (%)	78.50

The mixing procedure is presented in Figure 39. First, sand, one quarter of the water and coarse aggregate where mixed for 150 seconds. After a waiting period for absorption of 150 seconds, cement, limestone powder, silica fume, the remaining water and superplasticizer were added and mixed with cement paste for 300 seconds. The resulting concrete was scraped off the material and mixed again for 180 seconds. There was no need for vibration or compaction in both processes because the concrete is self-compacting.
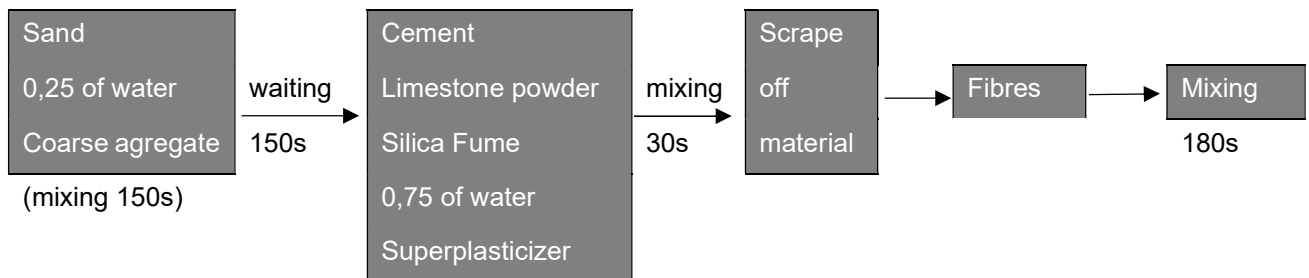
Figure 39 - Mixing procedure of Mix A

3.3.2 Fibre characteristics

The fibres used in this study were the Dramix® 4D 65/35BG. The nomenclature tells us the hook type, followed by the aspect ratio/length. B stands for Bright and refers to the finishing, while G stands for glued and refers to the way that the fibres are packed when sold. The main mechanical and geometrical characteristics of the fibres are presented in Table 5.

Table 5 - 4D Dramix® fibre's characteristics

Characteristics	4D 65/35BG
Aspect Ratio (l_f/d_f)	65
Length (mm) (l_f)	36
Diameter (mm) (d_f)	0,55
Hook	4D
Tensile Strength (N/mm^2)	1850
Young Modulus (MPa)	200

3.3.3 Specimens

Using Mix A with the addition of the fibres, eight cubes of 100*100*100 mm^3 (Fig 40a) and three cylinders with 100mm of diameter and 200 mm of height (Fig 40b) were casted to be tested at the age of the pull-out tests to characterise the compressive strength and the tensile strength.

a)   b)
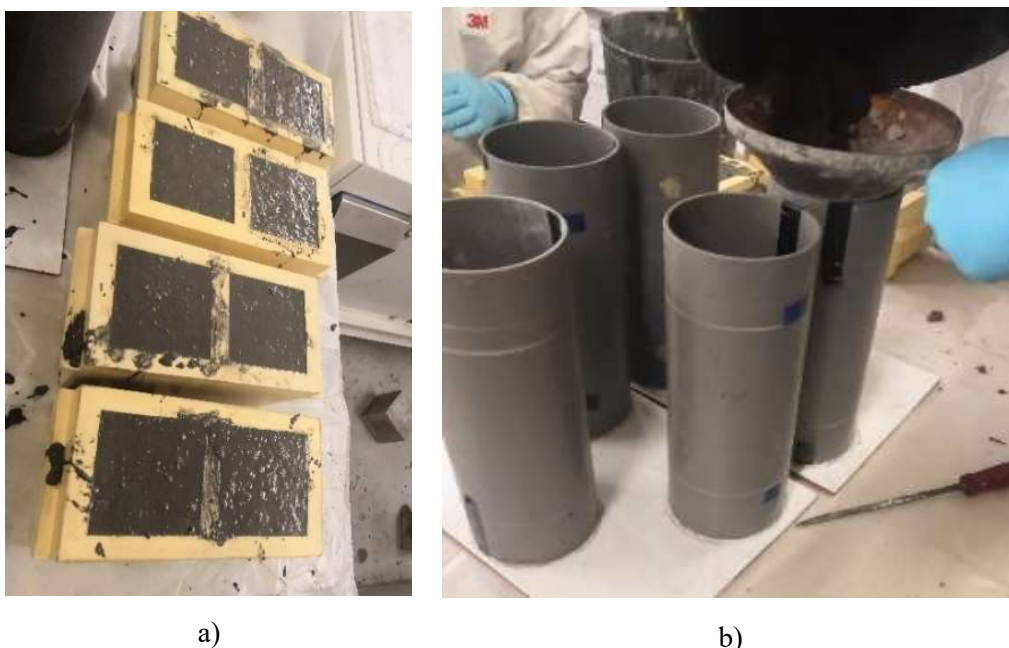
Figure 40 - Casting of the specimens for the mechanical tests: a) cubic specimens; b) Cylindrical specimens

The specimens used in the pull-out tests were cast without the addition of short fibres to the matrix since the parameter which is being studied in those tests is the bond to plain concrete. Tests were carried out after 81 days of wet curing, in a chamber with controlled temperature (20 ºC). The moulds for the pull-out test specimens were made using PVC tubes sliced into smaller tubes with 70 mm of diameter and 70 mm of height. Before casting, the fibres were embedded into a polystyrene foam plate with the desired orientation angle, θ, and different embedded lengths, l_e. Table 3.3 shows every combination of those

parameters used. Then, the moulds were glued to the polystyrene foam with hot glue with the fibre located in its centre (Fig 41).

a)

b)
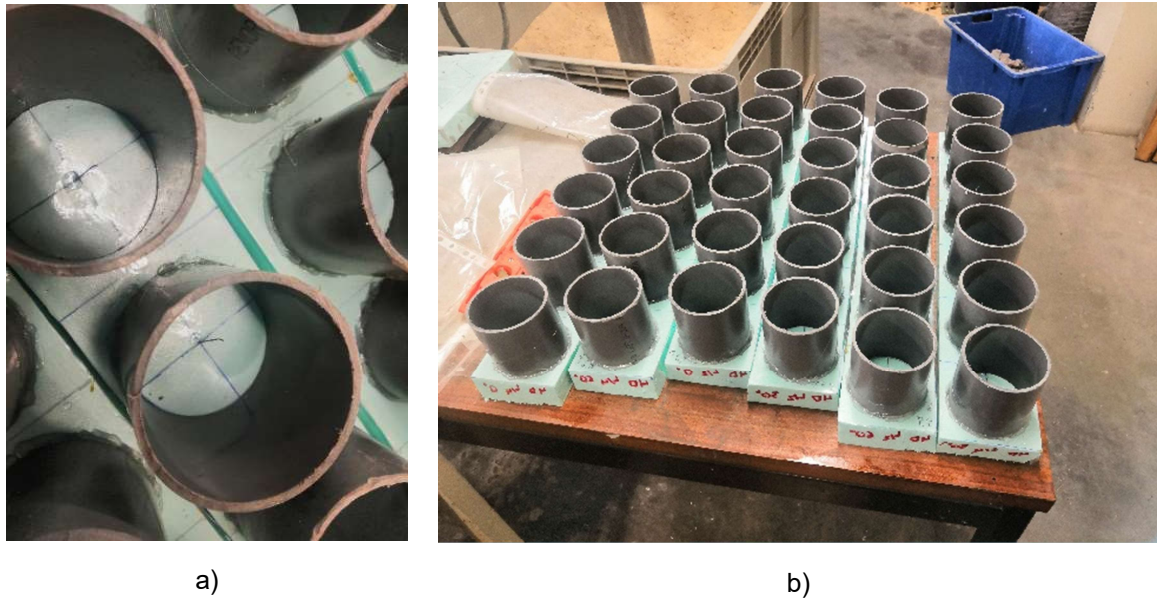
Figure 41 - Preparation of the moulds for the casting of the pull-out specimens: a) PVC tubes glued to the Styrofoam board with the fibres fixed in the centre of the moulds b) Moulds prepared for casting

Table 6 - Specimens produced for the pull-out tests

Fibre type	l_f (mm)	d_f (mm)	Matrix	Embedded length (mm)	Inclination angle (º)	Number of specimens
4D 65/35BG	36	0,55	Mix A	$l_f/2$ (17,5)	0	6
					30	6
					60	6
				$l_f/4$ (8,75)	0	6
					30	6
					60	6

After the glue dried out, each mould was lubricated with oil using a brush. Special care was taken in this stage as the fibres must not be oiled because it would compromise their adherence to the concrete. When casting the specimens, special care was taken to not pour concrete on the fibre, which can disturb its embedded orientation angle: a spoon was used until the fibres were fully covered by concrete (Fig 42a). Afterwards, the rest of each mould was filled (Fig 42b)

<div align="center">a)   b)</div>
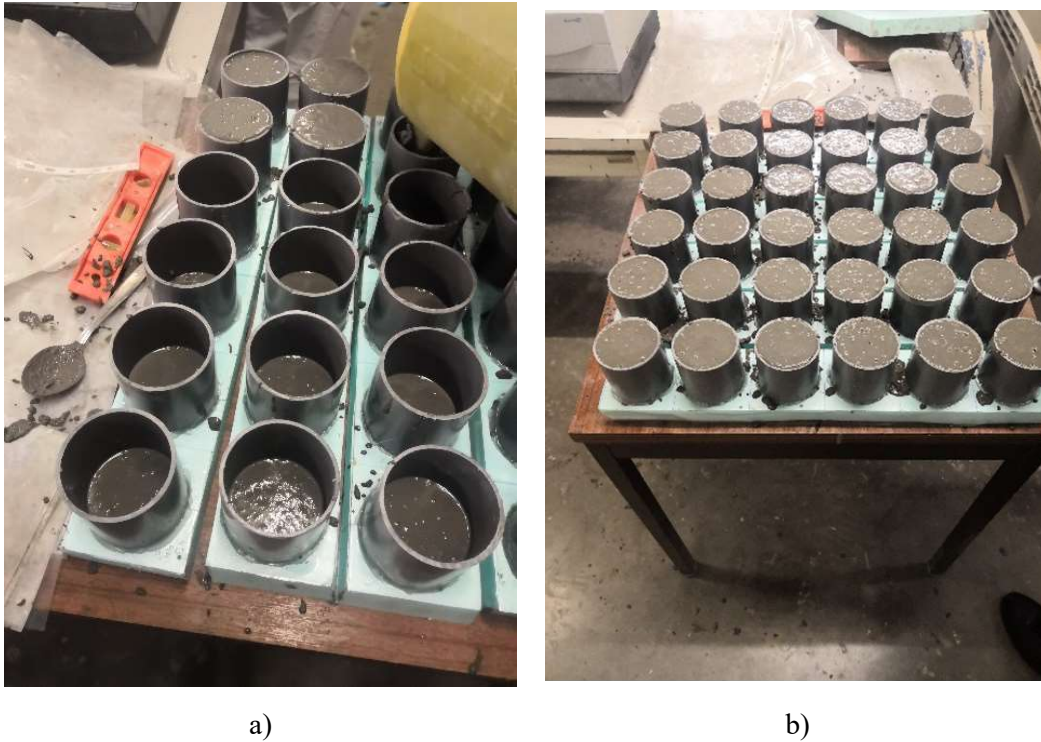
Figure 42 - Casting of the specimens for the pull-out tests: a) Carefully covering the fibre with concrete using a spoon; b) moulds completely filled

3.3.4 Test set-up

The pull-out test isn't standardized and therefore many set-ups can be adopted. In Figure 43, the test set-up used in this work is presented. The test consists in pulling a fibre out of an immobilized concrete specimen through a direct tensile force. The specimen is fixed to the machine through a metallic plate attached to the machine by screws and the fibre is hold by a clamp. The load was measured by installing an external load cell on the top plate of the machine with the maximum load capacity of 50 kN. In order to record slip during the test, an LVDT was installed on the back side of the grip. The free end of the fibre was clamped in the grip as near as possible to the fibre exit point to neglect the fibre's elastic deformation contribution to the slip measurement. The test was performed under a close-loop displacement control with a displacement increment of 0,003mm/s up to 1,5mm; and then it increases to 0,06mm/s till the end of the test (Table 7). The test is terminated when the fibre is completely pulled-out or ruptured.

<div align="center">Table 7 - Pull-out test's velocity</div>

Velocity (mm/s)	Displacement (mm)
0,003	0-1,5
0,06	1,5-40
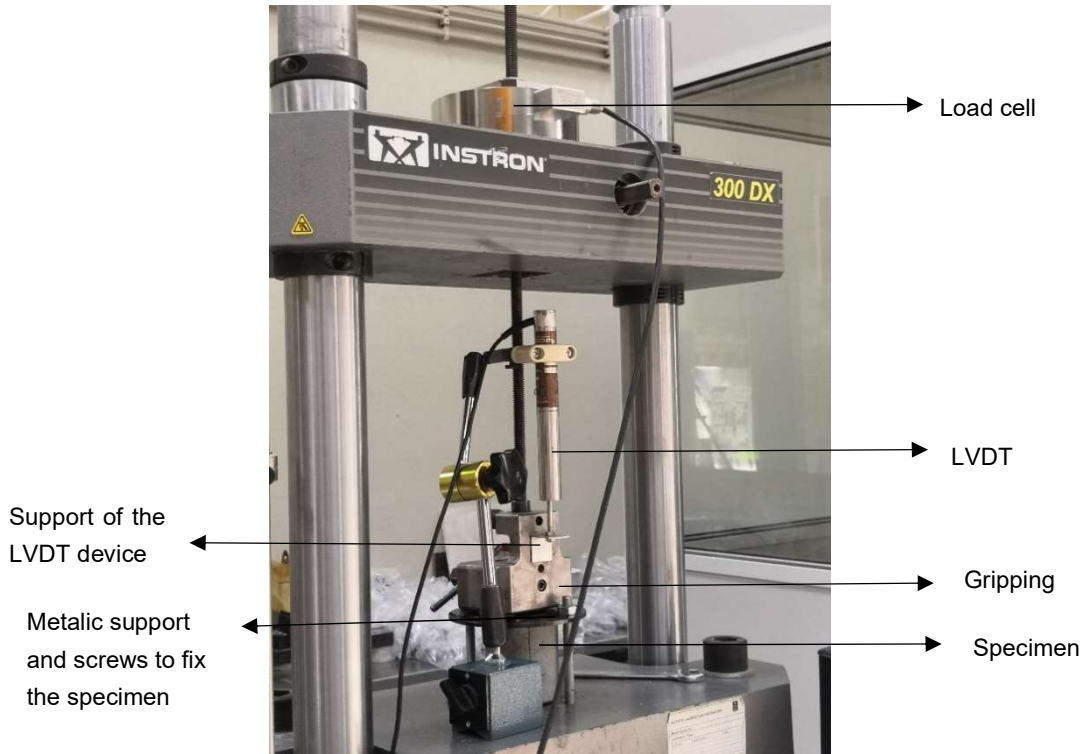
Figure 43 - Pull-out test set-up

3.4 Results and discussion
3.4.1 Concrete mechanical properties

Mechanical tests were made to characterize the compressive strength and tensile splitting strength of the matrix. The tests and their respective age are shown in Table 8.

Table 8 - Normative and age of the mechanical tests

Test	Normative	Age of the test (days)
Tensile splitting test	NP EN 12390-6:2011	81
Compressive test	NP EN 12390-3:2011	81

A compressive test was performed on the eight cubes with the same matrix of the fibre pull-out tests with the addition of a small percentage of the steel fibres in order to avoid the explosive failure mode of the specimens. The results are presented in Figure 44 and Table 9. An average compressive strength, $f_{cm,cube}$, of 143.4 MPa was recorded for the proposed mixture.
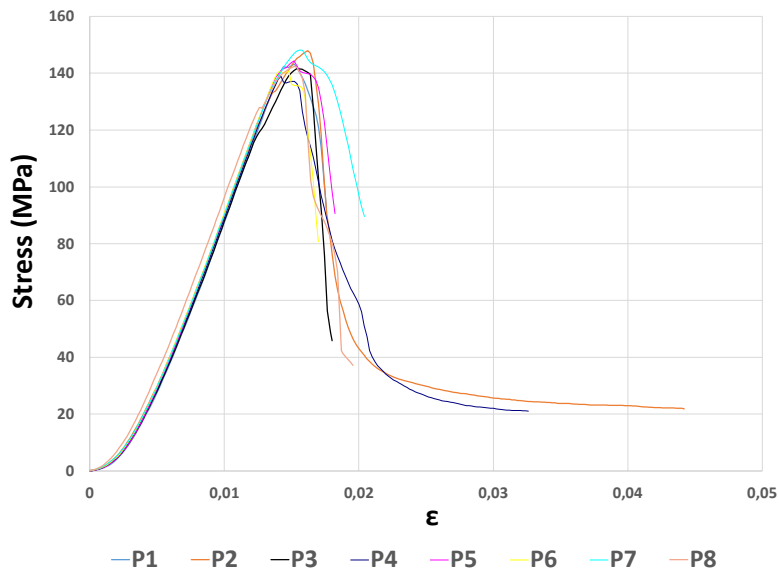
Figure 44 - Results of the cubes compressive tests

Table 9 - Results of the cubes' compressive tests

Specimen	Maximum force (kN)	Cross-Section (mm²)	$f_{c,cube}$ (MPa)	$f_{cm,cube}$ (MPa)	Standard desviation (MPa)	Mass (g)	Density (kg/m³)
P1	1432,18		143,2			2551	2551
P2	1478,65		147,9			2540	2540
P3	1415,74		141,6			2539	2539
P4	1389,04	10000	138,9	143,4	3,3	2545	2545
P5	1442,98		144,3			2557	2557
P6	1406,99		140,7			2519	2519
P7	1481,75		148,2			2557	2557
P8	1424,23		142,4			2579	2579

Furthermore, using the same mixture for the compressive strength test, three cylinders, were also tested to determine splitting tensile strength. The results are shown in Table 10. An average splitting tensile strength, $f_{ctm,sp}$, of 8.8 MPa was obtained for this mixture.

Table 10 - Results of the cylinders' splitting tensile test

Specimen	Height (mm)	Diameter (mm)	Maximum force (kN)	$f_{ct, sp}$ (MPa)	$f_{ct,sp}$ (MPa)	Standard Desviation (MPa)	Mass (g)	Density (kg/m³)
C1	236	103	349,1	9,1			5055	2571
C2	235	103,5	324,2	8,5	8,8	0,3	4994	2526
C3	225	102,5	319,6	8,8			4788	2579

The fib Model Code 2010 proposes a classification of the concrete based on the characteristic value of its compressive strength in cubical specimens Equation 4 (adapted from fib Model Code 2010) gives the characteristic value, $f_{ck,cube}$, based on its mean value, $f_{cm,cube}$. Both values are in MPa.

$$f_{ck,cube} = f_{cm,cube} - 8 \qquad (4)$$

Using $f_{cm,cube}$=143.4 MPa, $f_{ck,cube}$=135.4 MPa.

According to the mentioned classification, this concrete belongs to class C110, the second highest. For this class, a splitting tensile force, $f_{ct,sp}$=5.4 MPa is expected. When comparing this value with the obtained value in this work (8.8 MPa), it is possible to see that the second is higher. This happens because of the introduction of short steel fibres in the mixture.

3.4.2 Pull-out tests

3.4.2.1 Overview of the results

The results of the pull-out tests are shown in Figure 46 in the form of load-displacement curves. The maximum force and respective slip of each specimen are presented in Table 12. Moreover, the fibres after the tests are shown in Figure 45. Table 11 shows the validation of the specimens after the fibre pull-out test. In some cases, the fibres were either ruptured inside the grip or slipped from the grip. These series of the specimens were considered as invalid specimens and were excluded. This is common in performing fibre pull-out test specially if the griping system is based on the clamping system (which is the case of this study) instead of the wedge type griping system which is more suitable to perform pull-out tests on hooked end fibres. In a few specimens, LVDT was not connected properly, therefore, it was not able to measure slip in the elastic phase (e.g. l_f/4-0°-6 and l_f/4-30°-5 specimens), in which the slip values were negligible. These specimens were considered as the valid specimens, however, for these specimens, only the maximum force was considered.

In all curves, the ascending branch can be divided in a linear branch and a non-linear branch. The linear branch corresponds to the elastic phase of the bond. Then, the non-linear branch corresponds to the permanent rupture of the adhesion between the fibre and the surrounding matrix. When the curve is close to the peak, the hook starts to be mobilized. After the peak, a smooth decay of the load is registered until the hook is fully mobilized. In the next phase, the fibre pull-out behaviour is mainly governed by the friction in which the fibre starts to move inside its matrix channel. By increasing slip, fibre pull out from the matrix and a gradual reduction in the load was observed.

Across all specimens, the main fibre failure mechanism was fibre rupturing. The only exception were the specimens with aligned fibres and embedded length of l_f/2 where three fibres were pulled-out (Specimen 2, 5 and 6). In these fibres, the hooked part was fully mobilized. However, for the same orientation angle but with less fibre embedded length l_f/4, no fibre pullout was observed. The only reason can be due to different quality of the matrix and to difference in the grip's force. The rupture of the majority of the fibres is related to the high strength of the matrix, in which the fibre tensile strength is not enough to pull-out the fibre from the matrix. It should be mentioned that the tests were performed after 81 days of curing, which resulted in an even stronger matrix. Therefore, for this type of matrixes,

steel fibres with higher tensile strength are recommended which lead to a better performance in the composite level.

4D
L/4

0°		30°		60°	
1.		1.		1.	
2.		2.		2.	
3.		3.		3.	
4.		4.		4.	
5.		5.		5.	
6.		6.		6.	

a)

4D
L/2

0°		30°		60°	
1.		1.		1.	
2.		2.		2.	
3.		3.		3.	
4.		4.		4.	
5.		5.		5.	
6.		6.		6.	
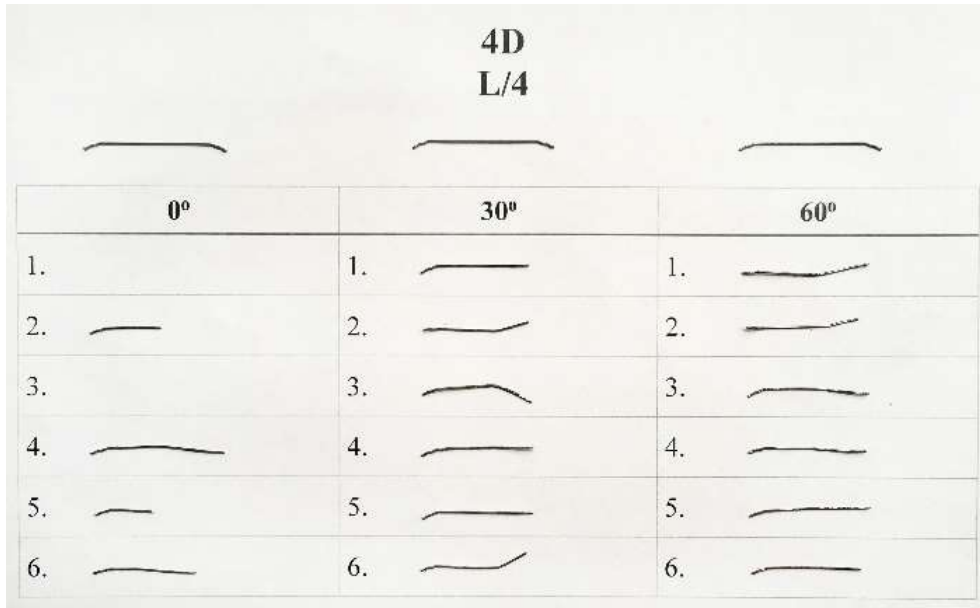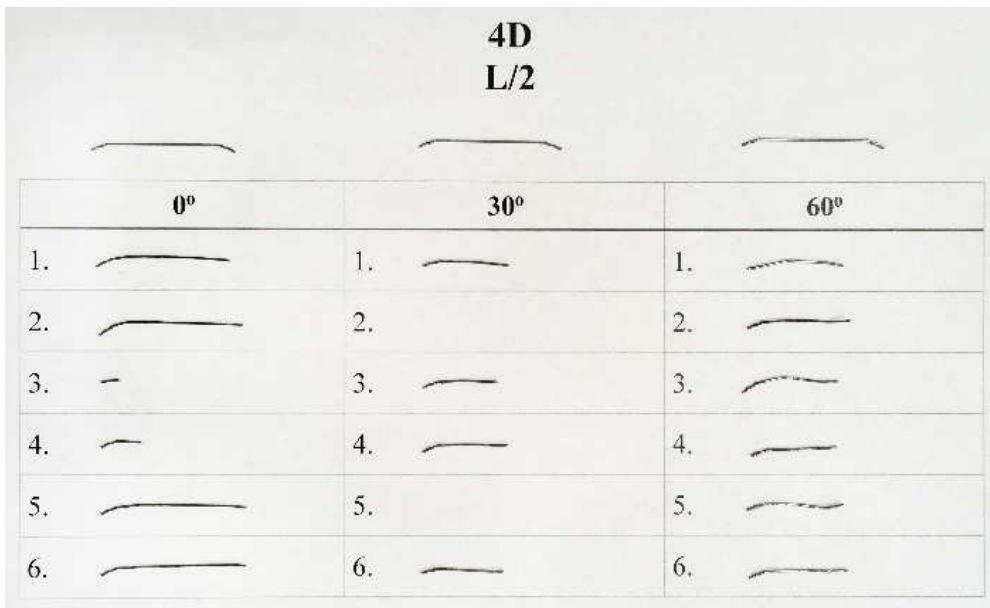
b)

Figure 45 - Fibres after testing

Table 11 - Fibre's failure mechanisms

	$l_f/4$			$l_f/2$		
	0º	30º	60º	0º	30º	60º
1	Valid	Valid	Valid	Valid	Valid *	Invalid
2	Invalid	Valid	Invalid	Valid	Invalid	Valid
3	Invalid	Valid	Valid	Invalid	Invalid	Valid
4	Valid	Valid	Valid	Invalid	Valid *	Valid
5	Invalid	Valid *	Valid	Valid	Invalid	Valid
6	Valid *	Valid	Valid	Valid	Valid	Valid

* There is a problem in LVDT connection.

a)

b)

c)

d)

e)

f)
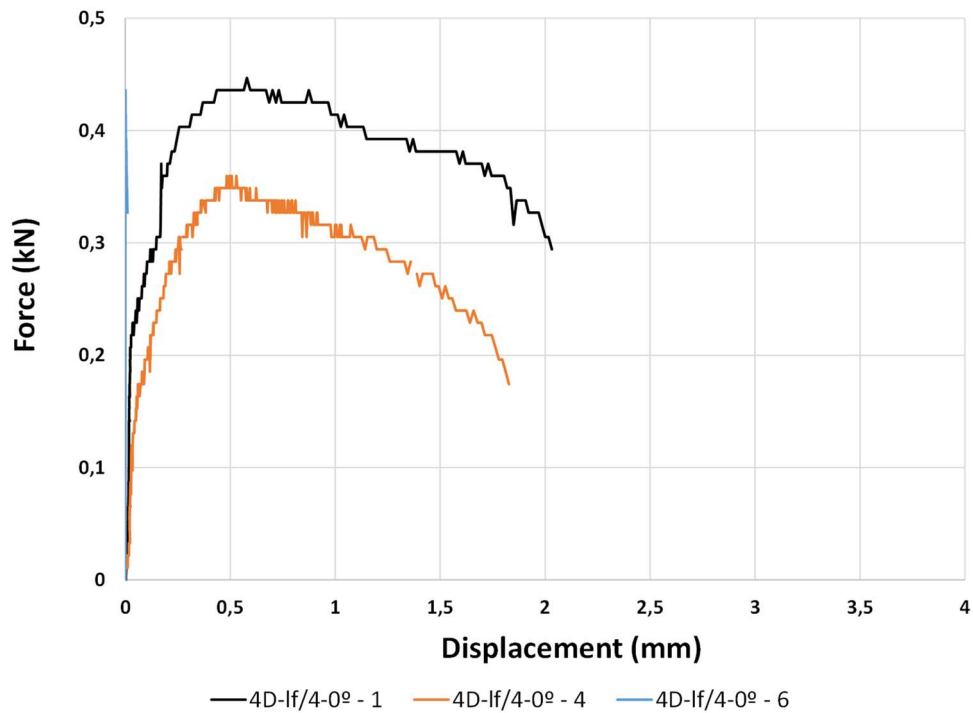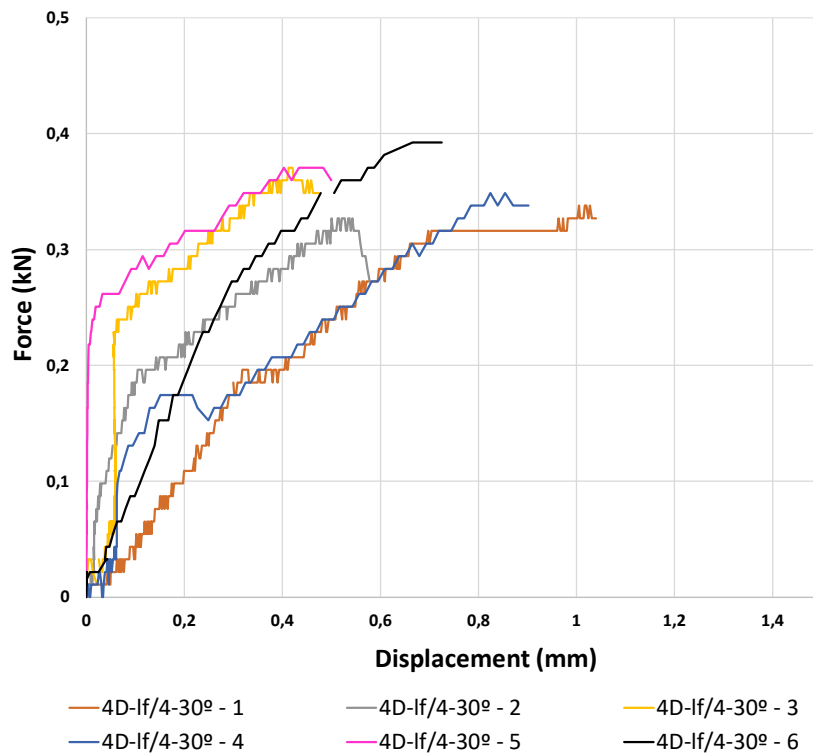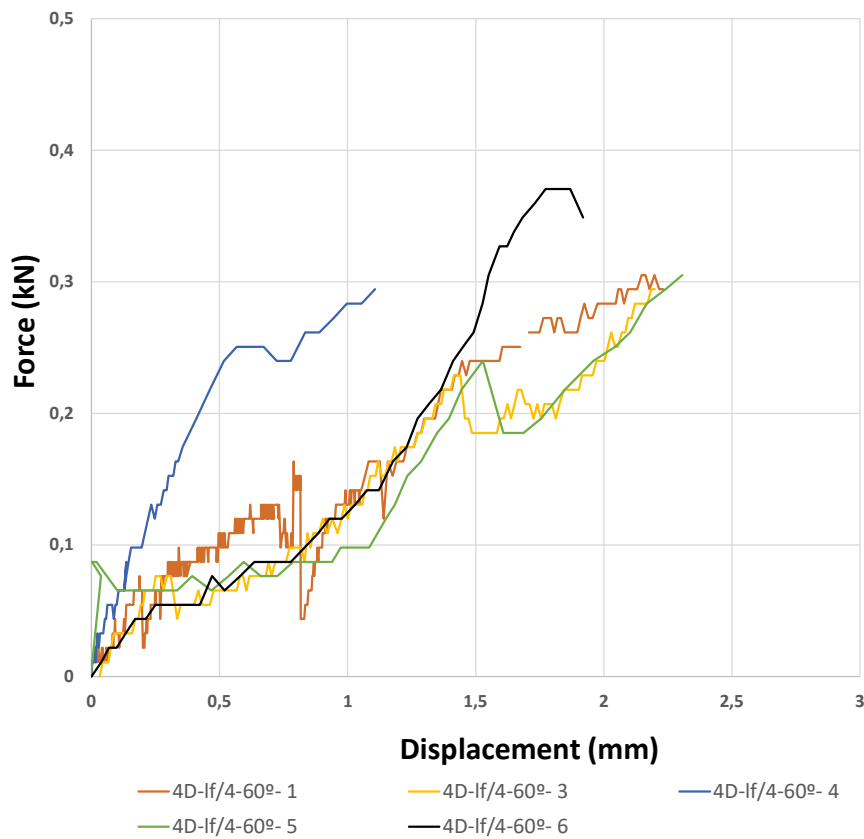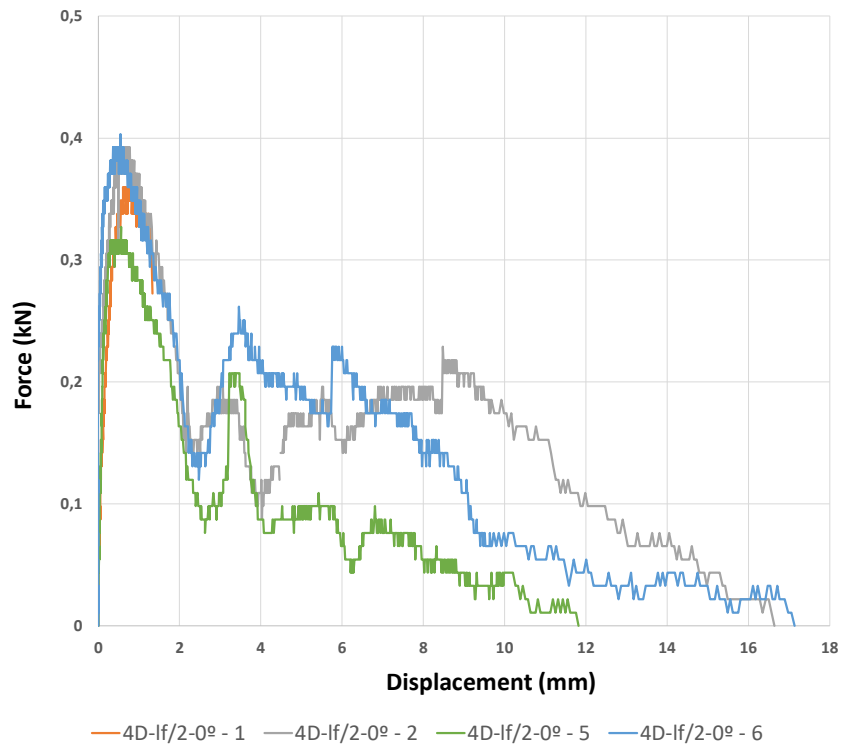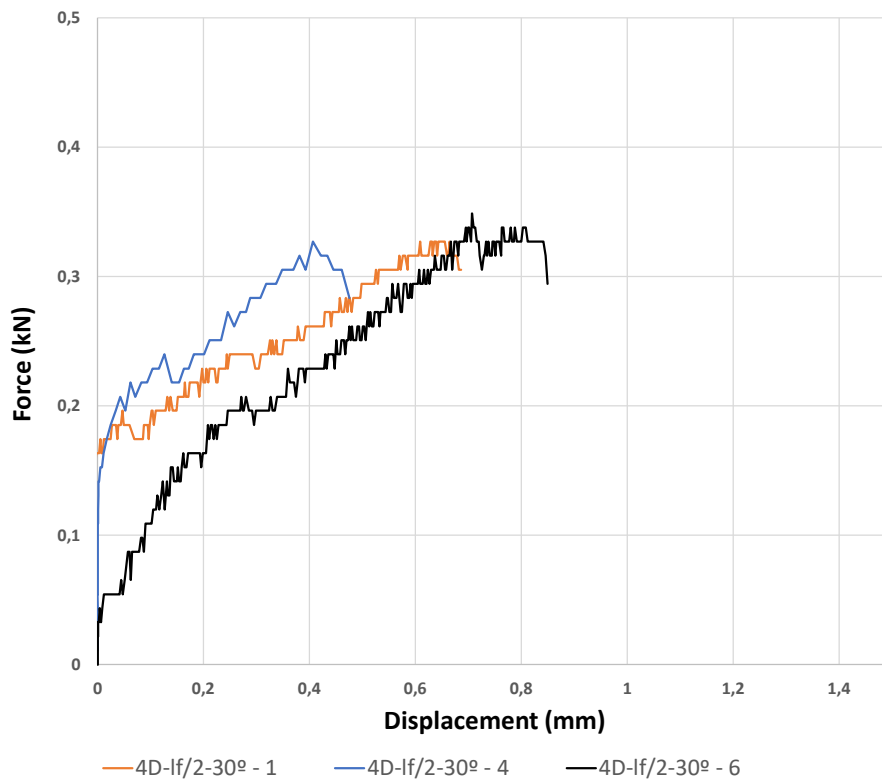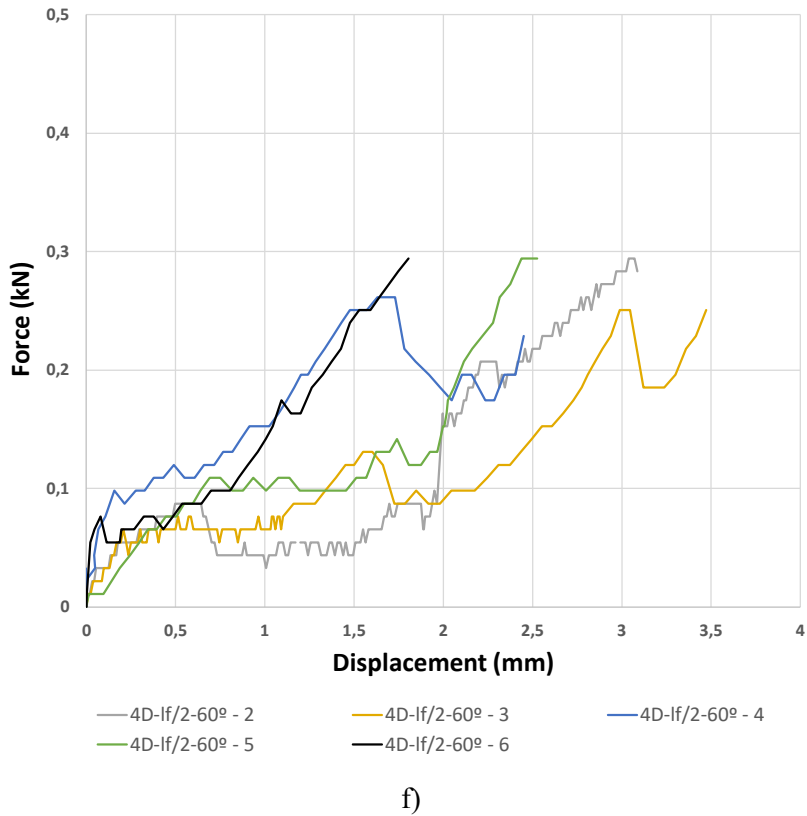
Figure 46 - Pull-out load vs slip curve: a) lf/4 and 0º; b) lf/4 and 30º; c) lf/4 and 60º; d) lf/2 and 0º; e) lf/2 and 30º; f) lf/4 and 60º

Table 12 Pull-out tests results for maximum force and respective slip

Embedded length	Inclination angle (º)	Specimen	Maximum force (kN)	Slip at the maximum force (mm)	Average maximum force (kN)	Average slip at the maximum force (mm)
$l_{f/4}$	0	1	0,45	0,48	0,41	0,49
		4	0,36	0,50		
		6	0,44	---		
	30	1	0,34	1,01	0,36	0,67
		2	0,33	0,5		
		3	0,37	0,41		
		4	0,35	0,76		
		5	0,37	---		
		6	0,39	0,67		
	60	1	0,31	2,15	0,31	1,9
		3	0,29	2,18		

		4	0,29	1,11		
		5	0,31	2,31		
		6	0,37	1,77		
		1	0,36	0,61		
	0	2	0,39	0,56	0,37	0,57
		5	0,327	0,56		
		6	0,40	0,54		
l$_f$/2		1	0,327	---		
	30	4	0,327	---	0,35	0,71
		6	0,3488	0,71		
		2	0,29	3,04		
		3	0,25	2,99		
	60	4	0,26	1,63	0,28	2,38
		5	0,29	2,44		
		6	0,29	1,80		

3.4.2.2 Influence of the embedded length

a)

b)
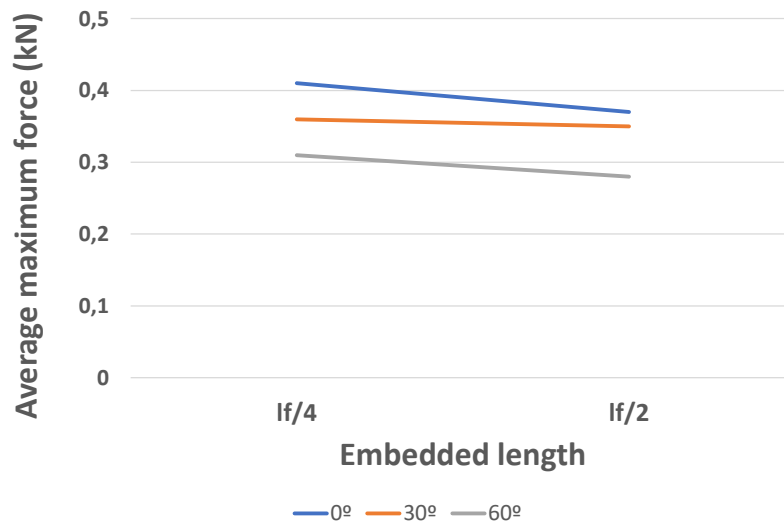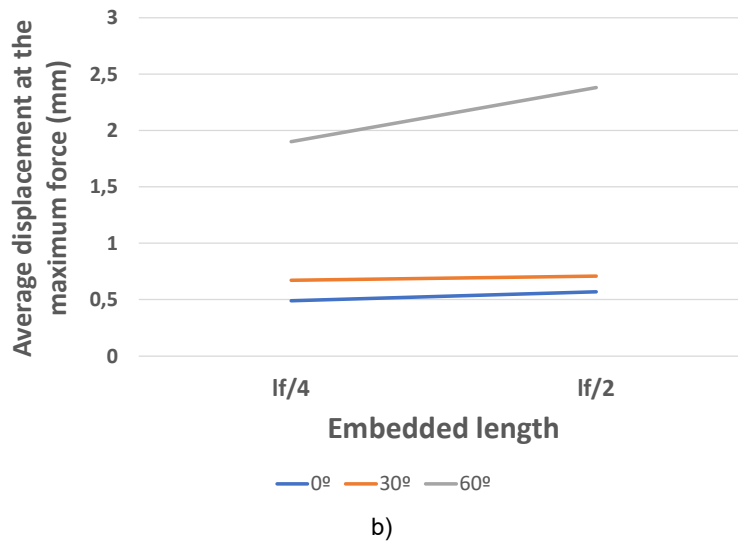
Figure 47 - Influence of fibre's embedded length for 0º, 30º and 60º inclinations angle in: a) maximum force; b) slip at the maximum force

In all inclination angles, the maximum pull-out force is not influenced significantly by the fibre embedded length as seen in Figure 47a. Unlike what is expected, the maximum force slightly increases by increasing the fibre embedded length. This is expected since the fibre rupturing was the main failure mode in the pull-out tests performed in this study rather than fibre pull out which make it difficult to derive out a clear conclusion. In general, for the hooked end fibre types, the mechanical debonding (hook mobilization) component has a more significant contribution on the maximum pull-out load than the chemical debonding which is affected by the fibre embedded length. However, from the previous results, it was reported that, in the case of the hooked end fibres, the maximum pull-out load slightly improved by increasing the fibre embedded length. (Abrishambaf, 2015) .

As seen in Figure 47b, the slip at the maximum force increases by raising the fibre embedded length from $l_f/4$ to $l_f/2$. This influence maximizes for the fibres with 60° inclination angle. As expected, by increasing the fibre orientation angle, the risk of matrix spalling at the fibre exit point increases which leads to register a larger slip at maximum pull-out load.

3.4.2.3 Influence of the inclination angle

a)

b)
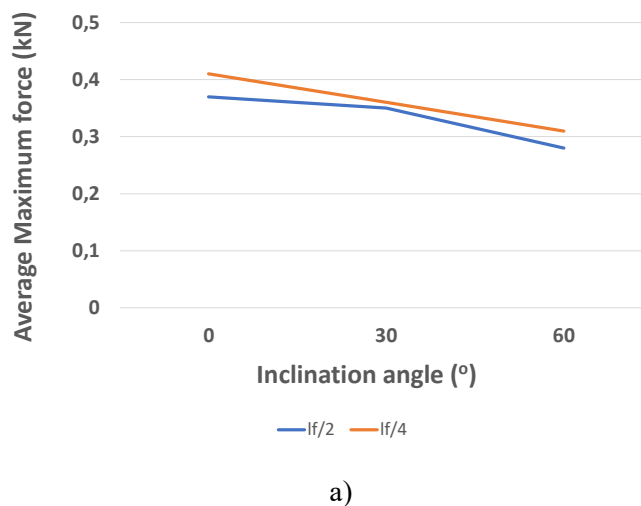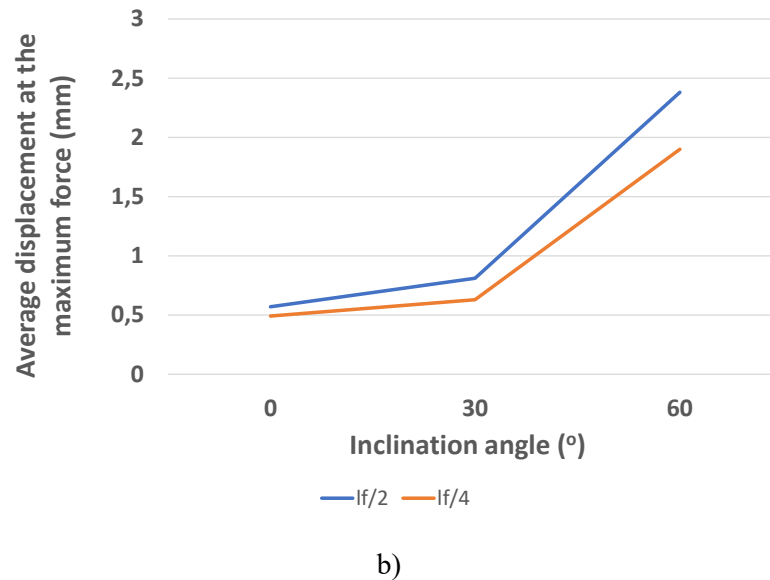
Figure 48 - Average results of the pull-out tests: a) maximum force; b) slip at maximum force

Usually, in the case of hooked end fibres, the maximum pull-out load slightly increases from the aligned to inclined fibres. It is reported that the pull-out load maximizes for the fibres with the orientation angle about 45° (Abrishambaf, 2015). However, in this study, for both embedded lengths, the maximum pull-out force decreases when increasing the inclination angle as seen in Table 12 and, more clearly, in Figure 48a. This is expected since the main failure mode during the pull-out test was fibre rupturing: by increasing the fibre orientation angle, due to the bending effects, the fibres are expected to be ruptured in a load lower than the one corresponded to the fibre tensile strength. For both embedded lengths, the aligned fibre were able to support more load (compared to the inclined fibres) because there is no snubbing effect. The load decreases when the inclination grows to 30º due to the stress concentration at the fibre exit point. The snubbing effect is higher when increasing the inclination angle, which justifies the decrease in maximum load from fibre orientation angle 30º to 60º.

The slip at maximum force is higher for fibres with higher inclinations (Table 12 and Figure 48b). The initial branch of the aligned fibres is steeper compared to other inclination . In other words, for the same load a higher slip is registered. This is due to the concrete spalling in the fibre's exit point. So, the slip at the maximum force is smaller for aligned fibres in both embedded lengths because there was no concrete spalling. The difference in slip between the two embedded lengths increases with the fibre inclination and this growth is even more marked when raising the inclination from 30º to 60º. The higher slip at maximum force is seen in the fibres with 60º of inclination and embedded length of $l_f/2$, which are the specimens where the spalling of the concrete was more evident.

3.4.2.4 Influence of matrix strength

In the work of Poças (2017), pull-out tests with same configuration as the one used in this study were performed on the specimens with the same fibre orientation angles and using an embedded length of $l_f/4$ (15 mm). The matrix shows a lower compressive strength, about 93.2 MPa, compared to the one used in this research. Two types of fibres were used. The comparison between the different specimens are presented in Table 13.

Table 13 - Specimens used in (Poças, 2017) and in this work

1	4D 65/60BG (Poças, 2017)	5D 65/60 BG (Poças, 2017)	4D 65/35 BH (This work)
l_f (mm)	60	60	35
d_f (mm)	0,9	0,9	0,55
Fibre's aspect ratio	65	65	65
Fibre's tensile strength (N/mm²)	1500	2300	1850
Fibre's hook	4D	5D	4D
Embedded length (mm)	15(l_f/4)	15 (l_f/4)	17,5 (l_f/2)
$f_{cm,cube}$ (MPa)	93,2	93,2	143,4

The average force-displacement curves for 4D fibres and each orientation angle is shown in Figure 49. It is shown that the influence of the fibre inclination angle is the same as in this work: the maximum force decreases and the respective slip increases by raising the inclination angle; the ascending branch is steeper in the align fibres compare to the inclined ones.
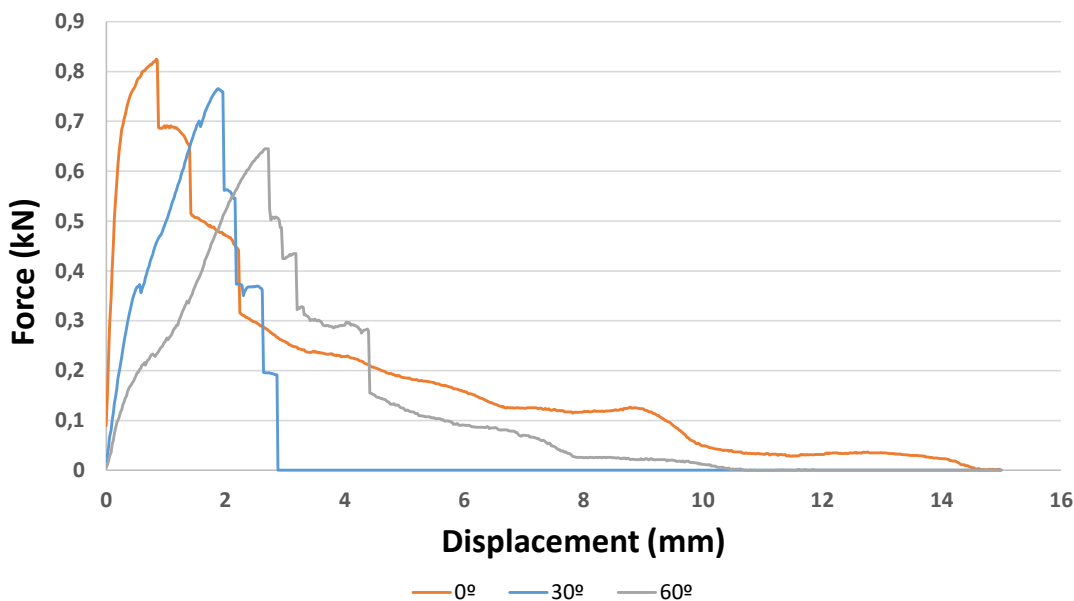
Figure 49 - Average force-displacement curve for 4D fibres and for 0º, 30º and 60º (Poças, 2017)

Since the fibres are different in terms of the diameter and in order to make a fair comparison between the results of this study and the ones reported by Poças (2017), the pull-out load was converted to the fibre tensile stress by dividing it by the fibre´s cross-section area. Figures 50 shows the comparison between the average maximum fibre's tensile stress for both works, respectively. For all fibre orientation

angles, a higher tensile stress was registered in this work. In fact, for a 0º inclination, the fibres in Poças's (2017) work were all pulled-out from the matrix with smaller stresses compared to the tensile strength of the fibres. This is expected since the matrix used in the Poças' work shows a lower compressive strength compared to the matrix of this study. In the work of Poças (2017), some inclined fibres were pulled out from the matrix while in this study all inclined fibres were ruptured. This is due to the lower compressive strength of the matrix used by Poças (2017) which increase the probability of matrix spalling at the fibre exit point to overwhelm the snubbing effect.
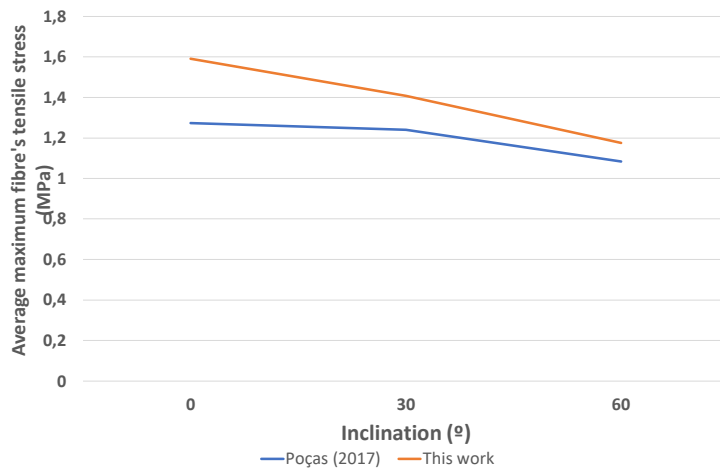
Figure 50 - Comparison between the average fibre's maximum tensile stress of both works (4D fibres) for 0º, 30º and 60º

Due to the different diameters of the fibres used in both works, it is not possible to do a fair comparison between the slip at the maximum force.

3.4.2.5 Influence of fibre type

The average curves for the three different inclinations of both fibre types (4D and 5D) used in Poças' (2017) work are presented in Figure 51.

a)

b)
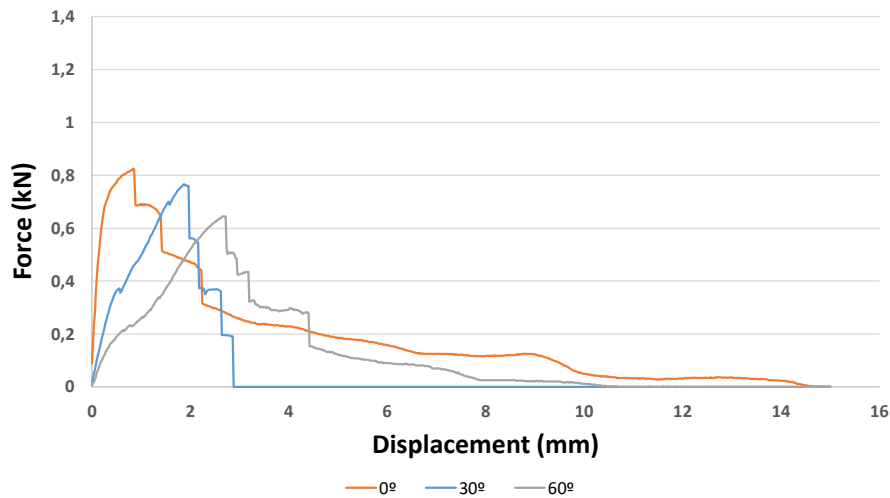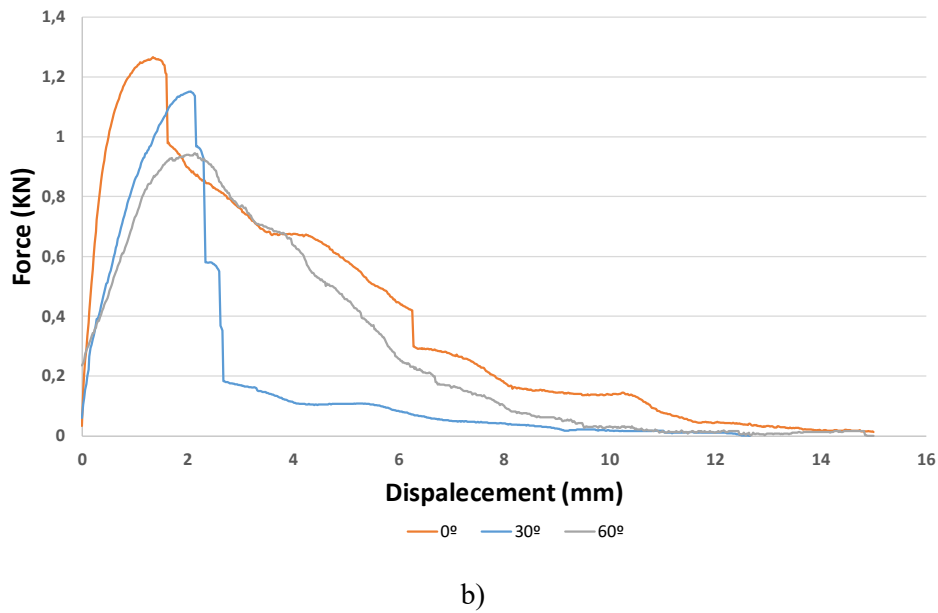
Figure 51 - Comparison between the average curves of the three different inclinations a) 4D fibres; b) 5D fibres
Adapted from (Poças, 2017)

The failure mode of the 5D fibres are approximately the same as the 4D fibres: all the aligned fibres were pulled-out and the 30º fibres ruptured (although one fibre was pulled-out for this inclination). The only difference regarding the failure modes comes in the 60º inclined fibres: the 5D fibres were all pulled-out.
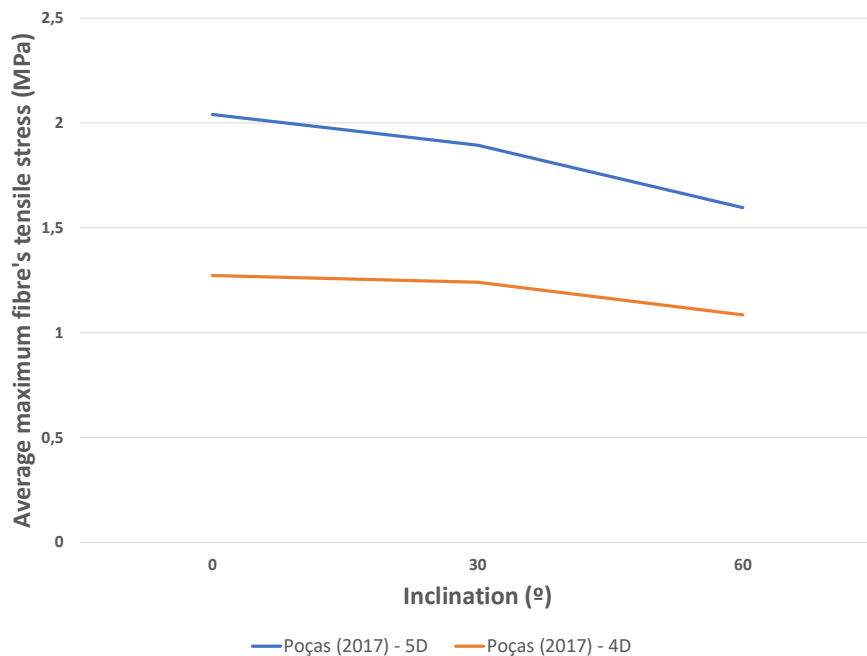
Figure 52 - Comparison between the average fibre's maximum tensile stresses of both fibre types used by Poças
(2017)

Figure 52 shows the average maximum tensile stress in both fibres' types used by Poças (2017). In 5D fibres' testing, it was registered an increase of the average maximum stress in the fibres, compared to the testing of the 4D fibres (which can be seen in all orientations) due to a better anchorage mechanism of their improved hook. This stronger bond (which originated higher stresses in the fibre) was supported with a higher tensile strength steel allowing the aligned fibres to be pulled-out with higher loads, the 30º fibres to absorb more energy until rupturing and all the 60º fibres to be pulled-out.
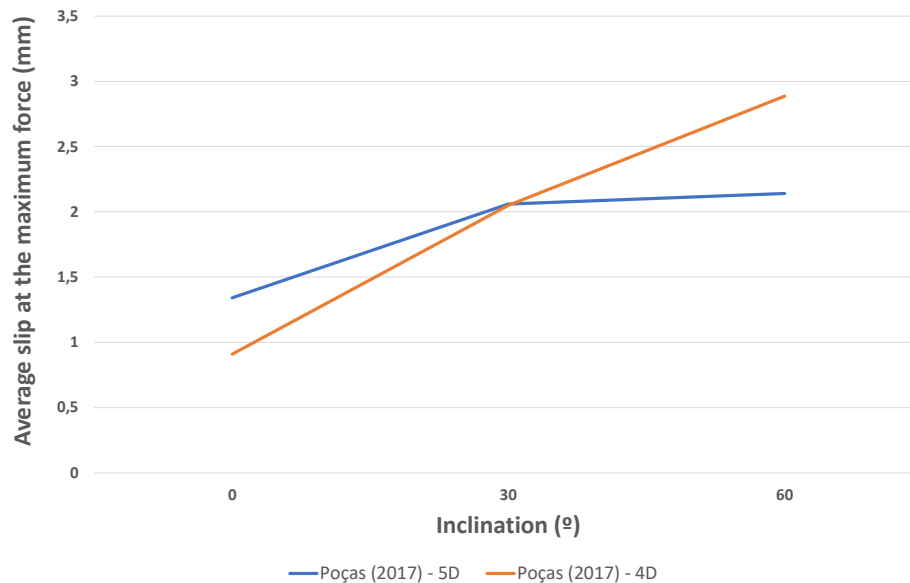
Figure 53 - Comparison between the average slip at maximum force of both fibre types used by Poças (2017)

Figure 53 shows a comparison between the average slip at maximum force for 4D and 5D fibres. As seen, the difference between the slip at the maximum force of both fibre types is small mainly because this parameter is mostly dependent of the spalled concrete which varies with the inclination angle and the matrix strength but not with the fibre type. The slip at the maximum force of the 5D fibres increases when the inclination angle grows from 0º to 30º, similar to the 4D fibres. However, when the inclination raised to 60º, the slip of 5D fibres did not grow like in the 4D fibres because less concrete spalling than expected was observed.

Furthermore, in the case of 5D fibres, the hook was not fully straightened (due to the more resistance steel) which enhanced the frictional stresses between the fibre and the concrete.

3.4.2.6 Final remarks

Concerning the results presented before, it is concluded that:

- The embedded length has very small influence on the maximum pull-out force of hooked-end fibres because the most significant contribution comes from the anchorage mechanism of the hook. In fact, it was expected that the more embedded fibres would have a slightly higher pull-out load but it was not confirmed since the main failure mode was fibre rupturing. Regarding

the influence of embedded length on the slip at the maximum force, specimens with higher embedded lengths presented a higher slip;

- A reduction in the maximum force by increasing the fibre inclination angle is clear in both embedded lengths. This is because of the snubbing effects which cause to the fibre´s rupturing in a tensile stress less than the fibre´s tensile strength. On the other hand, by increasing the fibre orientation angle, a higher portion of the concrete spall at the fibre exit point which leads to an increase in the slip at maximum force resulting in a more steeper branch in the aligned fibres compared to the inclined fibres;

- When comparing the results of this work with the results of Poças (2017), the influence of the matrix strength was clear: in this work, a higher level of stress was applied to the fibres which increase the probability of fibre rupturing. The difference is more noted in the aligned fibres because in the inclined fibres the most common failure mode was fibre rupturing.

- In Poças's (2017) work, the 5D fibres created a stronger anchorage bond in the concrete compared to the 4D ones. Since the 5D fibres show a higher tensile strength, many fibres were pulled-out from the matrix, particularly in the case of the 60º inclined ones. The slip at the maximum force is not significantly influenced by the fibre type since it mainly depends on the concrete spalling which depends mainly on the matrix resistance and fibre inclination. However, when raising the inclination of the 5D fibres from 30º to 60º, the slip only slightly increased. Moreover, the hooked in the 5D fibres were not completed straightened which created higher frictional stresses creating a less inclined post peak branch when compared to the 4D fibres.

4

MECHANICAL TESTING

4.1 Introduction

The addition of fibres to concrete has the main objective of improving its mechanical properties (di Prisco, Iorio and Plizzari, 2003). Even though its compression behaviour can be slightly improved with the presence of steel fibres, the tensile behaviour is the characteristic that is most enhanced (Hamiruddin et al., 2018). In order to analyse the efficiency of the fibres, both the tensile and flexural response must be tested. In this chapter, two major types of methods will be presented for studying the behaviour of the concrete under tension stresses – the direct and indirect methods.

4.2 Characterization of tensile behaviour of HPFRC
4.2.1 Direct methods

The most common test to obtain the relationship between the tensile stress and the crack width (σ-w) is the uniaxial tensile test. However, many difficulties arise with this test. It's of highly importance to perform this test under extremely controlled conditions in order to obtain good results (Østergaard, 2003).

One important factor to take into account is the specimen's geometry. The influence of this parameter was studied in FRC (Barragán, 2002) and in plain concrete (Carpinteri, Chiaia and Cornetti, 2002). Also, among other variables, it is important to underline: the perfect manufacturing and alignment of the concrete specimen with the loading actuator, in order to avoid undesired secondary bending; the adopted attachment between the specimen and loading platens; the performance of the testing control system-(Abrishambaf, 2015).

Also, a key issue of the test is the rotational conditions of the specimen's boundaries. Some studies show that the specimen should be free to rotate (Van Mier, 1996; Van Mier and Van Vliet, 2002) while others suggest that the rotation should be constrained (Hillerborg, 1980; Østergaard, 2003). Although this test in non-standardised, RILEM-TC162-TDF (2001) recommendations suggest that the boundary conditions should be enough to prevent the specimen's rotation.

Regardless of the boundary conditions, the crack propagation starts at one end of the notch tips (introduced in order to create a more stable crack propagation) (Fig 54, Point 1). If the specimen is able to rotate freely (Fig 54a), the crack will develop only from one side (Fig 54a, Points 1, 2, 3 and 4). Therefore, in this case, the cracking process is highly non-symmetric. This is why, according to

Østergaard (2003), the σ-w should not be obtained from the load-displacement curve since the averaging displacement is not representative of the crack opening process in plain concrete. For FRC, due to fibre's bridging effect, the stress in the cracks are much more significant than in plain concrete making the error of the displacement averaging process even higher (Cunha, 2010). Therefore, the rotation should be eliminated. However, it is difficult to do it completely and in some cases the rotation is only partly constrained (Fig 54b). In this case, the rotation also starts from one tip of the notch (Fig 54b, Points 1 and 2). Then, at same stage of the process, since the rotation is constrained, the equilibrium is no longer guaranteed and the crack plane starts to rotate back into the direction perpendicular to the load. So, a second crack starts to develop from the other side of the notched cross-section (Fig 54b, Point 3) coalescing to the first one (Fig 54b, Point 4). This explains the "bump" in the load-deflection curve, since the crack will experience some rotation to attain equilibrium (Hillerborg, 1989). In point 4 of Figure 54b, the cracks will not be aligned perfectly due to the concrete's heterogeneity, resulting in a higher absorbed energy (Van Vliet, 2000). For this reason, it is important to have an efficient gripping which prevents any rotation in order to have more realistic values. If this is the case (Fig 54c), the second crack will start to propagate much sooner (Fig 54c, Points 2 and 3) and both cracks will merge into one crack more rapidly (Fig 54c, Point 4). This crack will experience similar opening through the width, resulting in a correct σ-w relationship (Zhou, 1988).
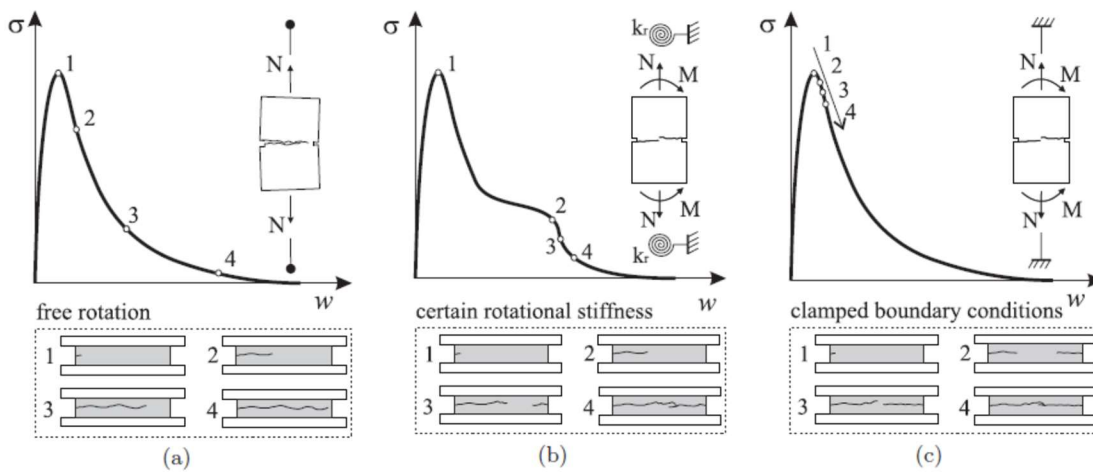
Figure 54 - Load-crack width curve of uniaxial tensile test with different boundary conditions: a) free rotation; b) partly constrained; c) completely constrained (Cunha, 2010)

According to RILEM-TC162-TDF (2001), in uniaxial tension, the σ-w relationship can be obtained by equations 5 and 6.

$$\sigma = \frac{P}{A_n} \tag{5}$$

$$w = \bar{\delta} - \overline{\delta_p} \tag{6}$$

Where P is the load recorded in the test, A_n is the notched cross-section area, $\bar{\delta}$ is the recorded displacement and $\overline{\delta_p}$ is the average displacement at the peak-stress.

4.2.2 Indirect methods

4.2.2.1 Three point bending test (according to EN 14651:2005)

The three point bending test has its nomenclature related to the two points where the beam is supported plus one point where the load is applied (in mid-span). This test analyses the post-cracking behaviour of the FRC. Its objective is to analyse the tensile behaviour under bending through a load-deflection curve or a load-CMOD (Crack Mouth Opening Displacement) curve. The procedure consists of applying a force at the midpoint of a simple supported notched beam imposing a certain deflection (Fig 55).
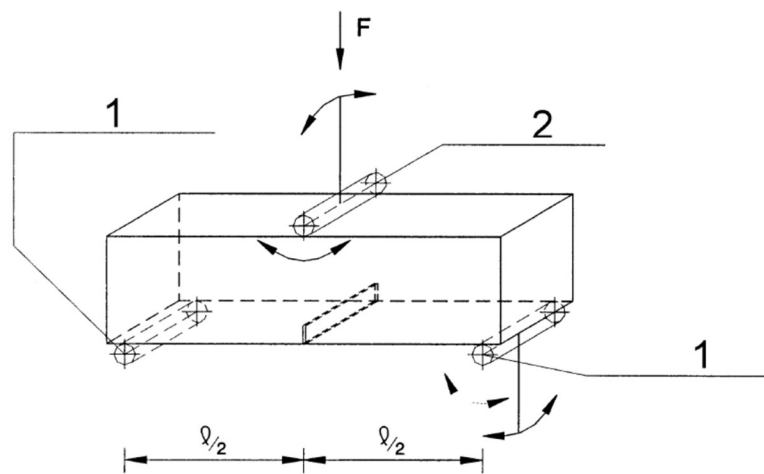
Figure 55 - Test set-up: 1) supporting rollers; 2) loading roller; F) applied force

According to EN 14651:2005, the specimen should be a beam with a cross-section of 150mm×150mm and a length, L, between 550 and 700mm. The mixture, the casting, the used devices, among other specifications about the test can also be found in this standard.

The width of the notch should be of 5mm or less and the distance h_{sp} should be 125±1mm (Figure 56)
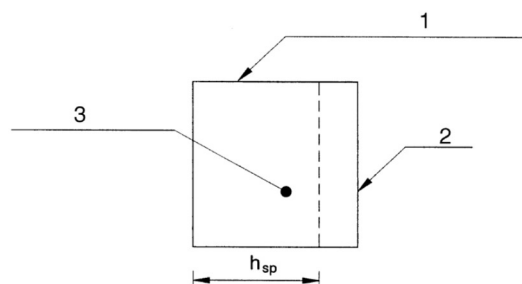
Figure 56 Notch specification: 1) Top surface during casting; 2) Notch; 3) Cross-section of the tested specimen

When the CMOD is measured, the displacement transducer should be installed along the longitudinal axis at the mid-width of the specimen, in a way that the distance, y, between the bottom of the specimen and the line of measurement is 5 mm or less (Fig 57).
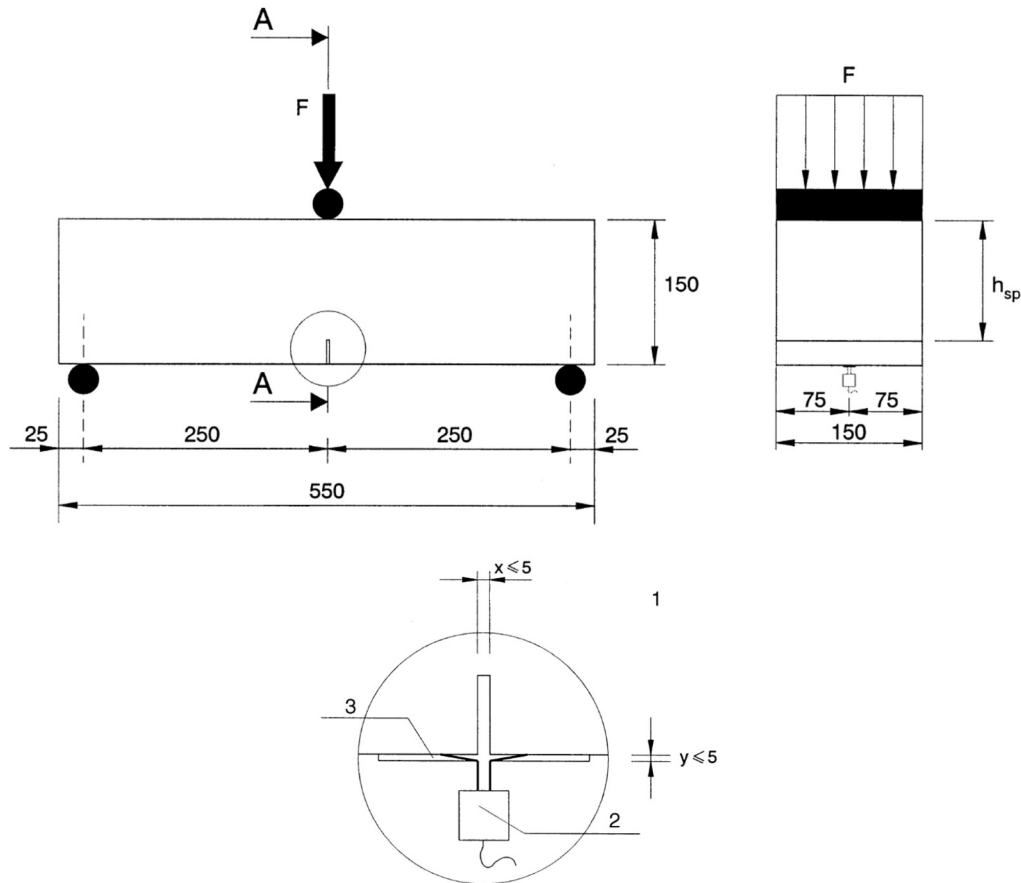
Figure 57 - Test set-up when measuring the CMOD: 1) Cross-section AA; 2) Displacement transducer; 3) Knife edge

When y is different from 0, the following correction should be applied (Eq 7):

$$CMOD = CMOD_y * \frac{h}{h+y}$$

(7)

where $CMOD_y$ is the measured CMOD and h is total height of the specimen. It is also possible to relate the CMOD and the displacement, δ, as follows in Equation 8:

$$\delta = 0{,}85 * CMOD + 0{,}04$$

(8)

When the deflection is measured, a displacement transducer is mounted on a rigid frame that is fixed to the test specimen at mid-height over the supports. One end of the frame should be fixed to the specimen

with a sliding fixture and the other end with a rotating fixture (see Fig 58). Since the transducer should measure the deflection, a thin plate fixed at one end can be placed at mid-width across the notch mouth at the point of measurement, as seen in Figure 59.
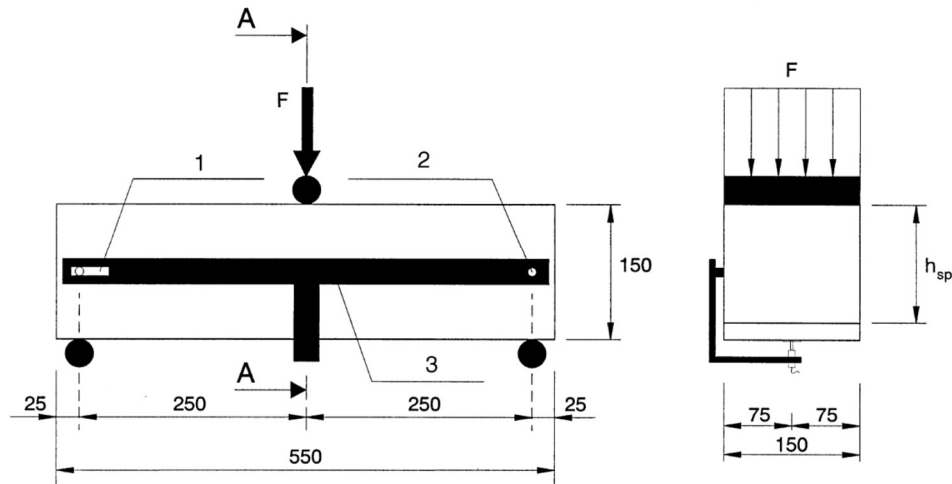
Figure 58 -Test set-up when the displacement is measured: 1) sliding fixture; 2) rotating fixture; 3) rigid frame
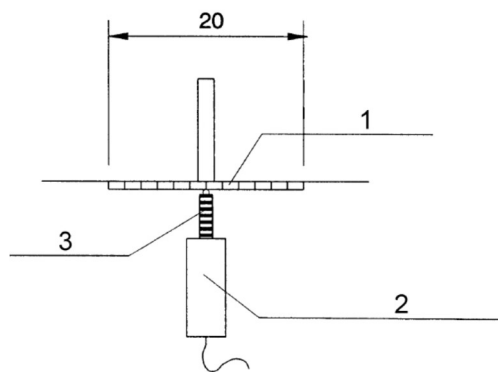
Figure 59 - Cross-section AA: 1) 1mm thick aluminium plate; 2) transducer; 3) spring shaft

There are two tension stress values which can characterize this test, both measured at midspan. One is the maximum tension stress measured in the elastic range during the elastic phase. The second one is the residual flexure tensile stress.

The load at the limit of proportionality, F_L, is the highest load value measured at midspan for a deflection or a CMOD between 0 and 0,05mmm (Fig 60). Then, assuming a linear elastic stress distribution along h_{sp}, the corresponding tension stress can be obtained from Equation 9:

$$f_L = \frac{3*F_L*L}{2*b*h_{sp}{}^2} \tag{9}$$

where L is the span's length, b is the width of the beam.
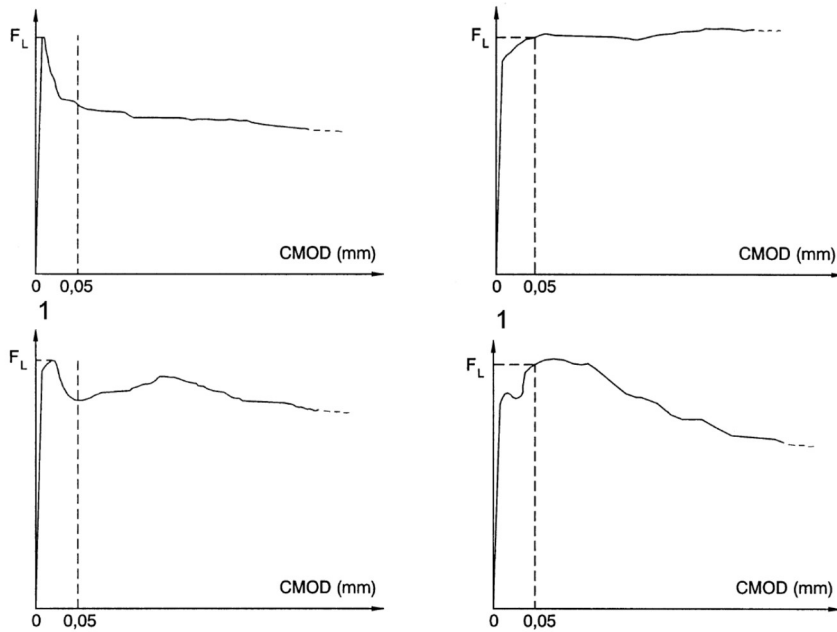
Figure 60 - Value of FL for different load-CMOD curves

The residual flexural tensile stresses, $f_{r,j}$ (with j=1,2,3,4), which correspond to 4 different values for the CMOD where the tension stress is evaluated, characterize the post-cracking behaviour. F_j is the corresponding applied load for each CMOD (Fig 61).
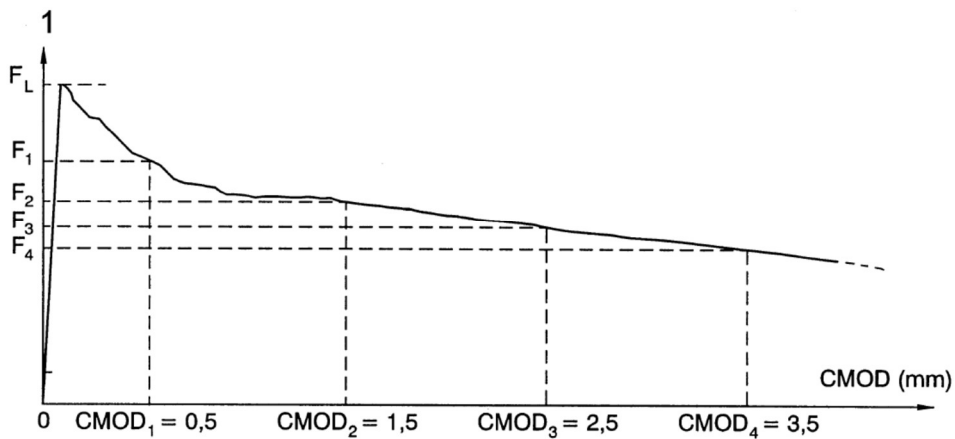
Figure 61 - CMOD values in which Fj should be registered

Then, the resulting stresses can be obtained similarly to f_L (Eq 10).

$$f_{r,j} = \frac{3*F_j*L}{2*b*h_{sp}^2}$$ (10)

4.2.2.2 Wedge Splitting Test (WST)

The Wedge Splitting Test (WST) was first proposed by Linsbauer and Tschegg (1986) and later developed by Brühwiler and Wittmann (1990). It's a simple test without sophisticated equipment, which determines the energy necessary to split the specimen while measuring the applied force and CMOD.

In figure 60, some types of used specimens are presented. The most commonly used is the cubic one (Fig 62a).
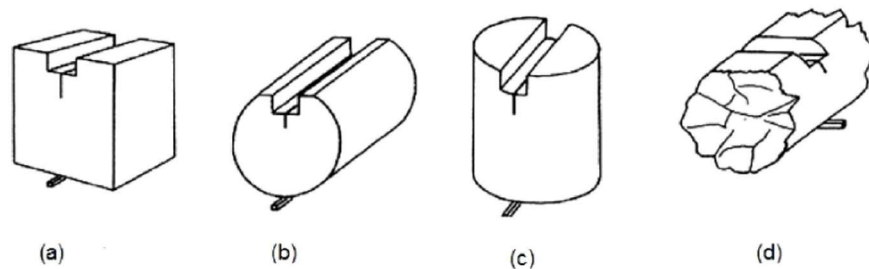
Figure 62 - Examples of specimens used in the WST: a) cubic; b) horizontal cylinder; c) vertical cylinder; d) irregular (Brühwiler and Wittmann, 1990)

According to Zandi Hanjari (2006), the main advantages of this test are:

- Light and compact specimens, as seen in Figure 63 where the WST specimen (full dash) is compared to the three-point bending test specimen (dashed);
- The ratio between the fracture area and the volume of the specimen is 5.2 times higher than in the three point bending test;
- The specimens can be easily cast during construction or extracted from the existing structures;
- The use of wedges to apply the loading enhances the stability and toughness of the test, allowing less rigid machines to be used;
- The self-weight of the specimen is negligible.
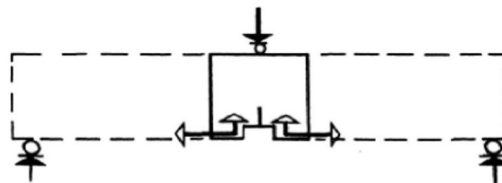
Figure 63 - Size of the WST specimen compared to the three point bending test specimen (Shah and Carpinteri, 1991)

On one hand, the specimens should have small dimensions in order to lower the load necessary to initiate and develop the fracture process (Chupanit, 2005). On the other hand, they should be big enough to not interfere with the cracking process. With that in mind, RILEM (1990) suggests that the specimen's dimensions in the cracking direction should be, at least, three times higher than the maximum aggregate

size. The outer dimensions of the specimen should be, at least, 3 times the fibre length and/or 5 times the maximum aggregate size in order to reduce the wall effect (Kooiman, 2000; Soroushian and Lee, 1990). Also, the length of the ligament should be at least 1.5 times the fibre length and/or 5 times the maximum aggregate size to obtain a large fracture surface which will reduce the scatter (Kooiman, 2000).

Although this method has proven to be successful in many applications with plain concrete (Löfgren, Stang and Olesen, 2008), its application with fibre reinforced concrete has much fewer references (Löfgren, 2004; Meda, Plizzari and Slowik, 2001; Nemegeer, Vanbrabant and Stang, 2003).

Löfgren, Stang and Olesen (2008) studied the application of the WST in determining the mechanical properties of FRC. A guide notch (Fig 64) was successfully used to prevent horizontal fractures, even though an increase of 5-15% of the fracture energy was registered.
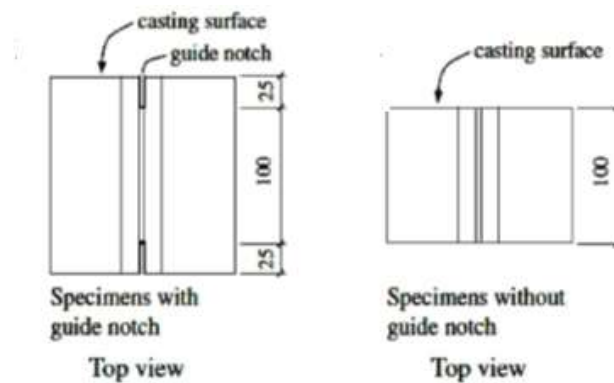
Figure 64 - Specimens a) with guide notch b) without guide notch (Löfgren, Stang and Olesen, 2008)

In Figure 65, the WST test set up adopted in the mentioned study is presented. A cubic specimen was used. It is equipped with a groove (where the load will be applied) and a notch (to localise the crack propagation). Two steel devices with roller bearings are placed partly on top of the specimen, partly into the groove, and through a wedging device the splitting force, F_{sp}, is applied. The specimen is equipped with two LVDT which measure the CMOD.
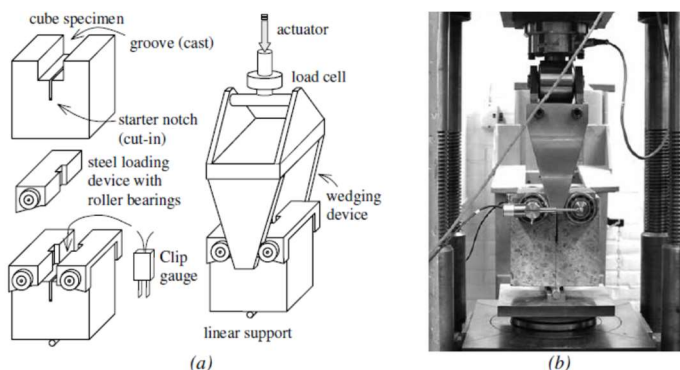
Figure 65 - Test set up: a) relevant parts; b) all parts assembled inside the testing machine (Löfgren, Stang and Olesen, 2008)

The applied vertical force, F_v, is also recorded and is transformed into horizontal force. The energy necessary to split the specimen is the area beneath the obtained F_v-CMOD curve. The horizontal splitting force can be calculated using the vertical force applied as seen in Equation 11 and illustrated in Figure 66 (Löfgren, 2005).

$$F_{sp} = \frac{F_v}{2*\tan(\alpha)} * \frac{1-\mu*\tan\alpha}{1+\mu*\cot\alpha}$$

(11)

Where α is the wedge angle (commonly α=15%) and μ is the coefficient of friction for the roller bearing. The coefficient of friction normally varies from 0.1% and 0.5%. If the friction is neglected, F_{sp}=1.866*F_v with an estimated error of 0.4 and 1.9% respectively.
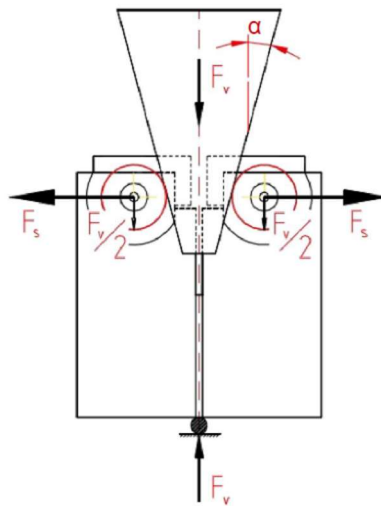
Figure 66 - Force transmission in WST (F_s=F_{sp}) (Löfgren, Stang and Olesen, 2008)

They compared the results of this test with the uniaxial tensile test and the three point bending test. The variation of results in the WST was non-significant and the scatter was smaller than in the other two tests. Also, compared to the three point bending test and the uniaxial tensile test, WST has the most fibres per unit area of the cracked cross-section (indicative of the fibre's efficiency). The specimen's size had no influence in this parameter.

4.3 From material to structural behaviour

Although many experimental studies have been carried out in the last 50 years, FRC's structural response only started to be deeply investigated 15 years ago. There is still a lack of international building codes for the structural design of FRC elements, just a few guidelines were recently introduced. This explains the limited use of FRC among designers (di Prisco, Colombo and Dozio, 2013).

In the United States, ACI (544, 1999) proposed some design considerations. RILEM TC162-TDF (2001) also introduced some guidelines for structural FRC elements (Vandewalle and Dupont, 2003;

Vandewalle et al., 2003) which were followed by other recommendations in several countries such as France, Sweden, Germany, Austria, Italy, Japan and Spain.

More recently, the fib Model Code 2010 added two new sections related to FRC – section 5.6 regarding the material behaviour and section 7.7 focusing on the structural behaviour - based on the recommendations mentioned in the previous paragraph. This chapter will analyse the fib Model Code 2010 and the work of di Prisco, Colombo and Dozio (2013).

The material classification of plain concrete is based on its compressive strength. However, since in FRC the compression strength is not significantly influenced (excluding those with high fibre volumes), the proposed classification is based on the post-cracking properties where the fibre has its most important contribution. These properties are determined through a standardized test according to the EN 14651, the three point bending test (already described in chapter 4.2.2.1). The classification is based on two post cracking residual strengths corresponding to two different CMOD values. For $CMOD_1=0{,}5mm$, its correspondent strength, f_{R1k}, is used for service limit state characterization while for ultimate limit state, characterization is based on f_{R3k} measured for $CMOD_3=2{,}5mm$. From these two values, two parameters are used: the first one is a number used for classifying the f_{R1k} class (1.0; 1.5; 2.0; 2.5; 3.0; 4.0; 5.0; 6.0; 7.0; 8.0 [MPa]) ; the second one is a parameter classifying the f_{R3k}/f_{R1k} ratio into five classes:

- a) if $0{,}5 < f_{R3k}/f_{R1k} < 0{,}7$;
- b) f $0{,}7 \leq f_{R3k}/f_{R1k} < 0{,}9$;
- c) if $0{,}9 \leq f_{R3k}/f_{R1k} < 1{,}1$;
- d) if $1{,}1 \leq f_{R3k}/f_{R1k} < 1{,}3$;
- e) if $1{,}3 \leq f_{R3k}/f_{R1k}$.

Fibres can only replace, even if partially, steel rebars at ULS if:

$$f_{R1k}/f_{Lk} \geq 0{,}4 \qquad\qquad (12)$$
$$f_{R3k}/f_{R1k} \geq 0{,}5 \qquad\qquad (13)$$

Where f_{Lk} is the stress correspondent to the load at limit of proportionality (4.2.2.1). This is to prevent a brittle failure.

In order to relate stress-strain law *(σ-ε)* and stress-crack opening *(σ-w)*, a new concept is introduced – the characteristic length, l_{cs}. The characteristic length is defined as the crack spacing when a multi-cracking process takes place or as the beam depth when a plane section approach is used (Fig 67)
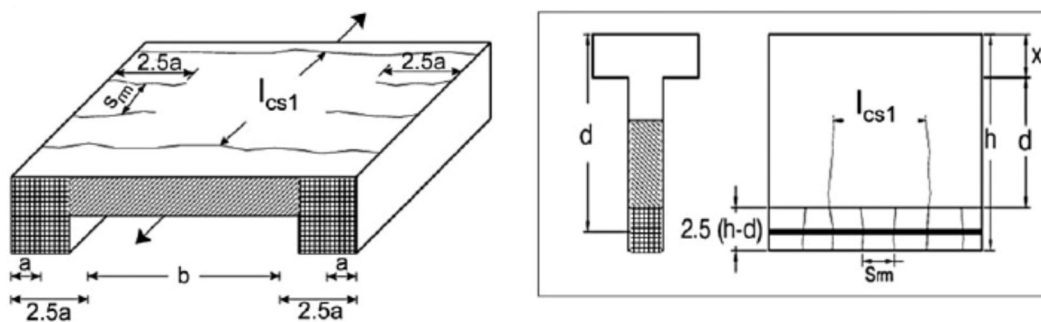
Figure 67- *l_{sc} (sm* in the figures) definition (di Prisco, Colombo and Dozio, 2013)

This parameter relates the strain, ε, and crack width, w, as seen in Equation 14:

$$\varepsilon = \frac{w}{l_{sc}} \tag{14}$$

The ultimate crack length, w_u, is then defined (see Eq 15)

$$w_u = \min(l_{sc} * \varepsilon_{Fu}; 2.5mm) \tag{15}$$

Where ε_{Fu} takes the value of 2% when the neutral axis is inside the cross-section and 1% when the neutral axis is external to the cross-section. 2.5mm is a limit value based on the market availability regarding the fibre length.

The need for this definition, independent from the tensile behaviour of FRC (strain-hardening or strain-softening), is justified because sometimes the same composite can show different responses depending on the direction (Ferrara, Ozyurt and Di Prisco, 2011).

In order to determine the σ-w relationship in uniaxial tensile tests, two basic models can be used, as shown in Figure 68.
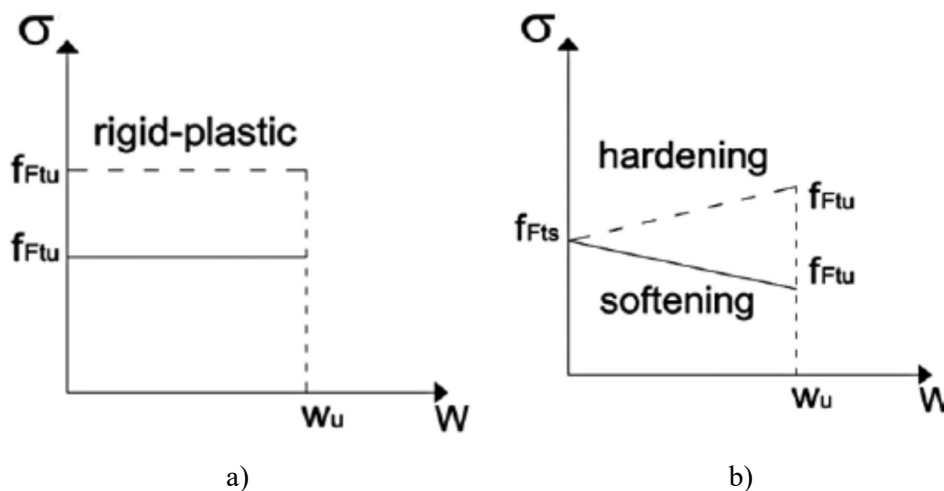
Figure 68 - σ-w relationship: a) rigid-plastic model; b) linear model (di Prisco, Colombo and Dozio, 2013)

The first one, the rigid-plastic model, only identifies one parameter, the f_{Ftu}. By assuming that the compressive stresses are concentrated in the top fibre (Fig 69), the equilibrium equation between the internal and external moment can be written (Eq 16)

$$M_{u,ext} = M_{u,int} \Leftrightarrow \frac{f_{R3}*b*h_{sp}^2}{6} = \frac{f_{Ftu}*b*h_{sp}^2}{2} \Leftrightarrow f_{Ftu} = \frac{f_{R3}}{3} \tag{16}$$

65
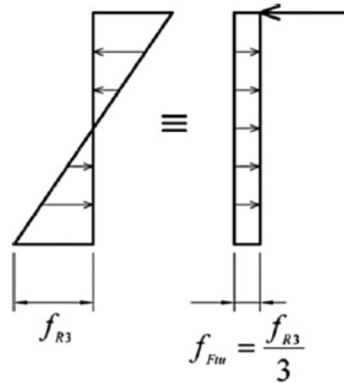
Figure 69 Stress distribution in bending of an FRC's cross-section (di Prisco, Colombo and Dozio, 2013)

The linear model uses two parameters, f_{Ftu} and f_{Fts} (Eq 17 and 18). More details on their calculation can be found in (di Prisco, Colombo and Dozio, 2013)

$$f_{Ftu} = f_{Fts} - \frac{\omega_u}{CMOD_3} * (f_{Fts} - 0,5 f_{R3} + 0,2 f_{R1}) \geq 0 \tag{17}$$

$$f_{Fts} = 0,45 f_{R1} \tag{18}$$

A more developed constitutive law, which takes into account the peak stress was then created (Fig 70). Up to point B where the peak strength, f_{ct}, is localized, the same constitutive relationship used for plain concrete can be adopted. In the post-cracking behaviour, a bilinear relationship is assumed. The pull-out mechanism can be translated by the second post-peak branch and is defined by two points, D and E. Also, in some situations, point C can be shifted to the first post-peak branch assuming a value of $k_a * f_{R1}$, where k_a is a factor depending on the Young Modulus, E, and the characteristic length, l_{sc} (Fig 71).
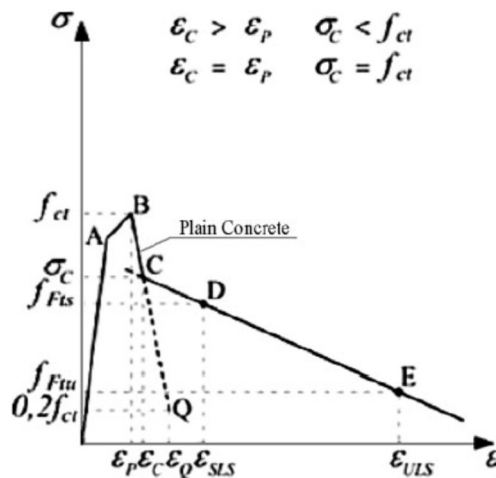
Figure 70 - Constitutive-law of FRC under uniaxial tension (di Prisco, Colombo and Dozio, 2013)
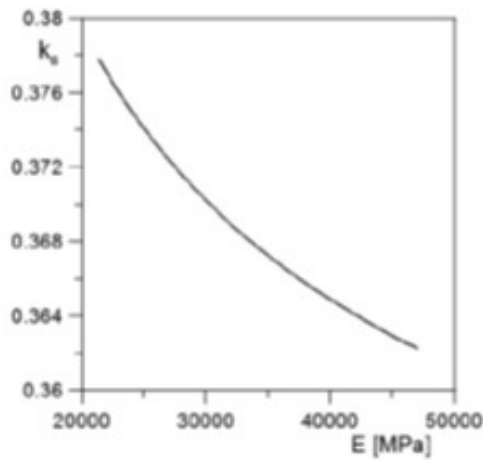
Figure 71 Relation between ka and E for $l_{sc}=h$ (di Prisco, Colombo and Dozio, 2013)

Experimental tests were made and compared this constitutive law and a finite elements method approach and the results were very encouraging (Figure 72).

a)

b)
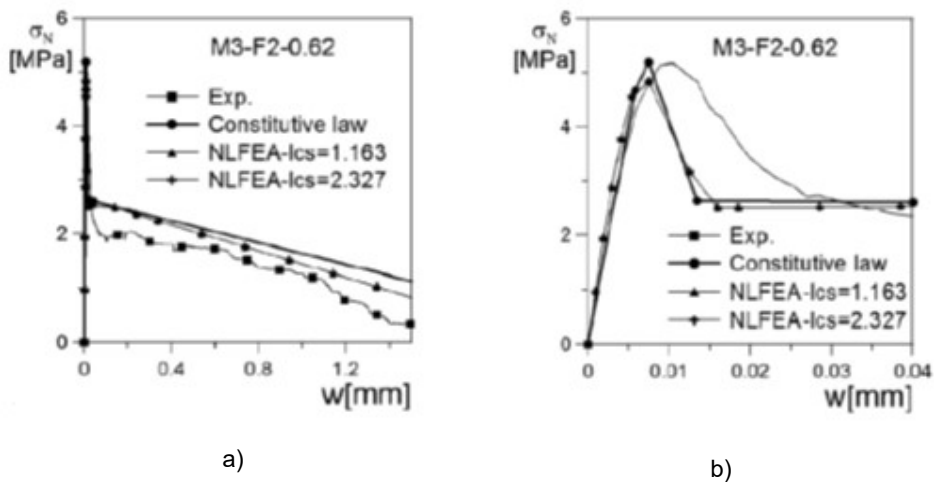
Figure 72 - Comparison between uniaxial tensile test results, the constitutive law and non-linear finite element analysis results: a) no zoom; b) with zoom in the smaller displacements (di Prisco, Colombo and Dozio, 2013)

Also, using finite element analysis and a plane section approach, a constitutive law σ-w obtained from bending tests was plotted and compared to many experimental results and the results were also very promising for both methods.

After comparison with many experimental tests, fib Model Code 2010 suggested that a value of the characteristic length, l_{sc}, equal to the height of the cross-section, h, is a reasonable choice.

As explained before in this work, fibre orientation and distribution have serious influence in the mechanical characteristics of FRC and are highly affected by casting procedures. The elements which are suggested to be employed in the standardized tests (150×150mm beams) have different casting

procedures compared the thin elements in which FRC are mainly used in construction. Also, the standardized specimens are notched which alters the cracking process. For these reasons, it is recommended to use unnotched specimens with the same casting procedures and thickness of the structural element. French and Italian guidelines first suggested to use these specimens and called them "structural specimens".

Chapter 7.7 of fib Model 2010 addresses the concrete's uniaxial tensile behaviour with the use of both fibres and traditional reinforcement.
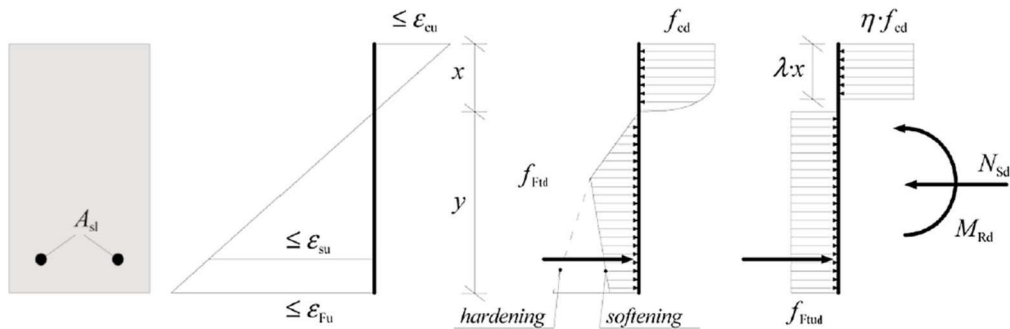
Figure 73 - ULS for bending moment and axial force: use of simplified stress-strain relationship (di Prisco, Colombo and Dozio, 2013)

The bending failure stage is supposed to be reached when one of the following conditions applies (Fig 73):

- ultimate compressive strain in the FRC, ε_{cu}, is reached;
- ultimate tensile strain in the steel (if present), ε_{su}, is reached;
- ultimate tensile strain in the FRC, ε_{Fu}, is reached.

The safety factors, γ_F, for designing FRC elements are shown in Table 13. For SLS, a safety factor of 1 should be used.

Table 13 - Safety factors for FRC design

Material	γ_F
FRC in compression	Same as plain concrete
FRC in tension (limit of linearity)	Same as plain concrete
FRC in tension	1,5

The choice of the safety factors is based on:

- the representativeness of the specimens used to characterize the mechanical response of the material, in relation to the structure considered;
- the number of specimens for mechanical characterization;
- the stress redistribution capacity of the structure under consideration;
- the fracture volume involved in the failure mechanism;

Another coefficient, K, is introduced. For isotropic fibre distribution, the fibre orientation factor, K, is equal to 1. In Equations 19 and 20, for favourable and unfavourable effects, K takes a value smaller than 1 and higher than 1, respectively,

$$f_{Ftsd, mod} = f_{Ftsd}/K \tag{19}$$

$$f_{Ftud, mod} = f_{Ftud}/K \tag{20}$$

FRC is more adequate for structures with diffused stresses applied, whether for structures with both localized and diffused stresses, a combination of rebars and fibres is suggested. A minimum degree of redundancy is required for structural elements using only fibres. Moreover, FRC with hardening behaviour in uniaxial tensile tests can use fibres as the only reinforcement.

Equations regarding shear, punching, torsion solicitations as well as suitable equations for slabs and walls as well as specific equations to compute crack distance and crack opening regarding fibre contribution, are also included in chapter 7.7. Designing FRC structures is then possible according to these principles.

4.4 Flexural behaviour of HPFRC developed at FEUP
4.4.1 Applied concrete mixture

WST testing campaign was carried out at FEUP. The applied mixture across all the specimens is the same mixture used in the specimens for the pull-out tests (Mix A).

Many different fibre combinations were tested, keeping the fibre content constant and equal to 1%. In this work three of them will be analysed. The details about the fibres can be seen in Table 14.

Table 14 - Fibres used in the WST

I	Short fibres 13/0,2	4D 65/35 BG	5D 65/60 BG
l_f (mm)	13	35	60
d_f (mm)	0,2	0,55	0,9
Fibre's aspect ratio	65	65	65
Fibre's tensile strength (N/mm^2)	2500	1500	2300
Fibre's hook	no hook	4D	5D

Also, the fibre volume of the different specimens is showed in Table 15.

Table 15 - Specimens produced for the wedge splitting tests

	Short fibres 13/0,2 (%)	4D 65 /35 BG (%)	5D 65/60 BG (%)	Specimens produced
WST1	1	0	0	6
WST4	0	1	0	6
WST6	0	0	1	6

4.4.2 WST testing procedure

The geometry of the specimens used in the wedge splitting tests performed in FEUP is presented in Figure 74. As the figure shows, specimens with a guided notch were chosen in order to obtain a more stable crack propagation. They were chosen based on other studies.
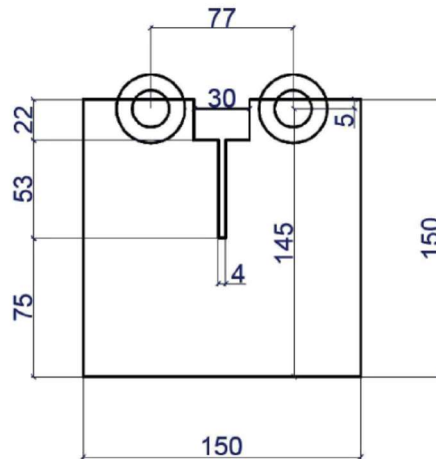
Figure 74 - Geometry of the specimens used in the wedge splitting tests in FEUP

The load is applied in a groove in the specimens. Also, there are two steel devices with roller bearings attached to the specimens and to the groove. The CMOD is measured by two LVDT devices installed in the specimen. The vertical force applied is measured by a load cell and is then transformed into a horizontal splitting force. The test set-up is illustrated in Figure 75.
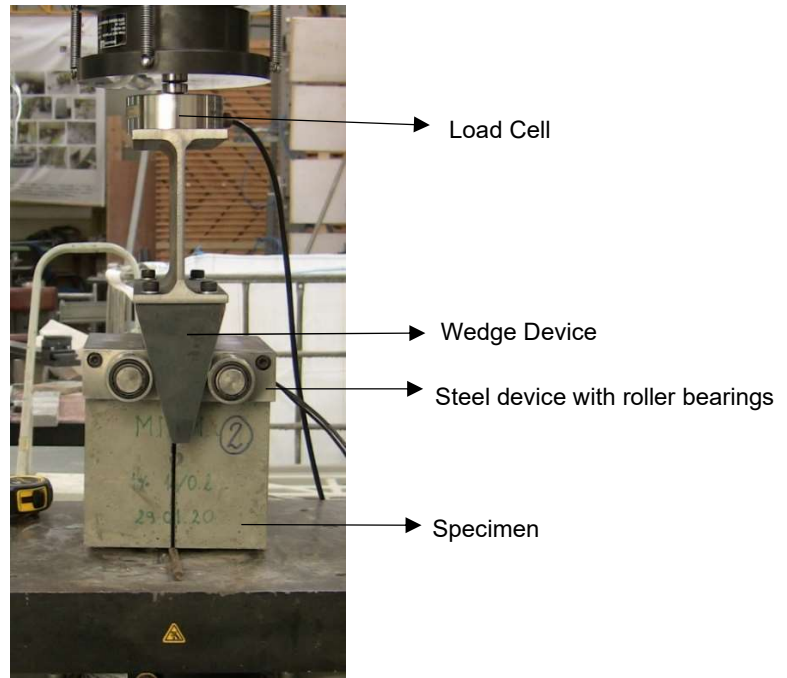
Figure 75 - Test set-up used at FEUP

4.4.3 Results of the WST

The average force-displacement curves of each type of specimen is presented in Figure 75 together with the respective maximum and minimum curves.
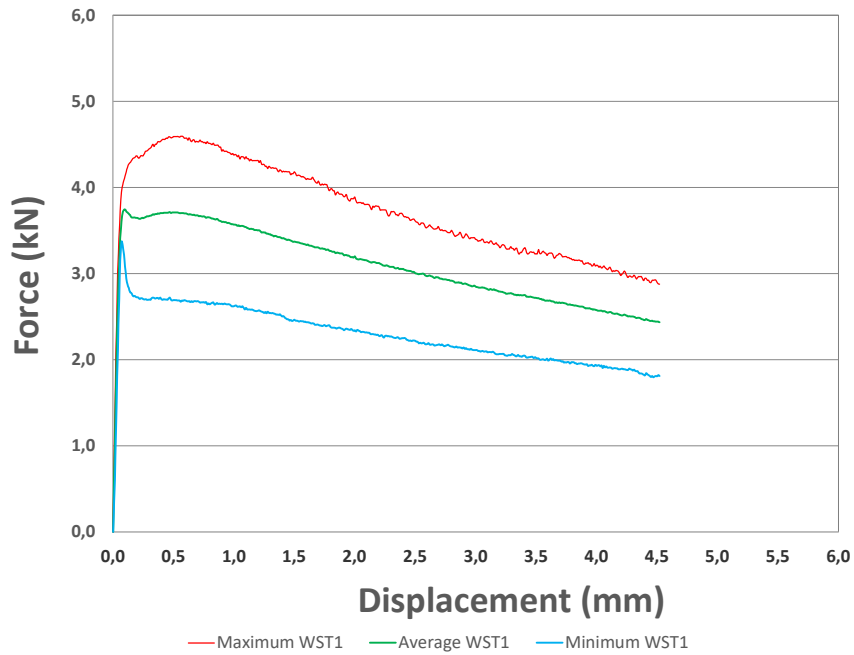
a)
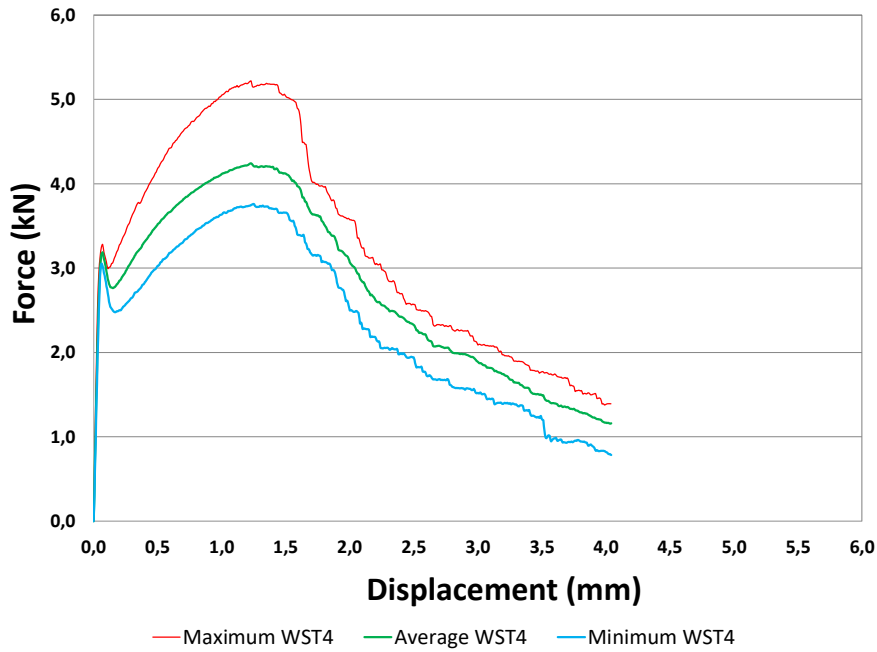
b)
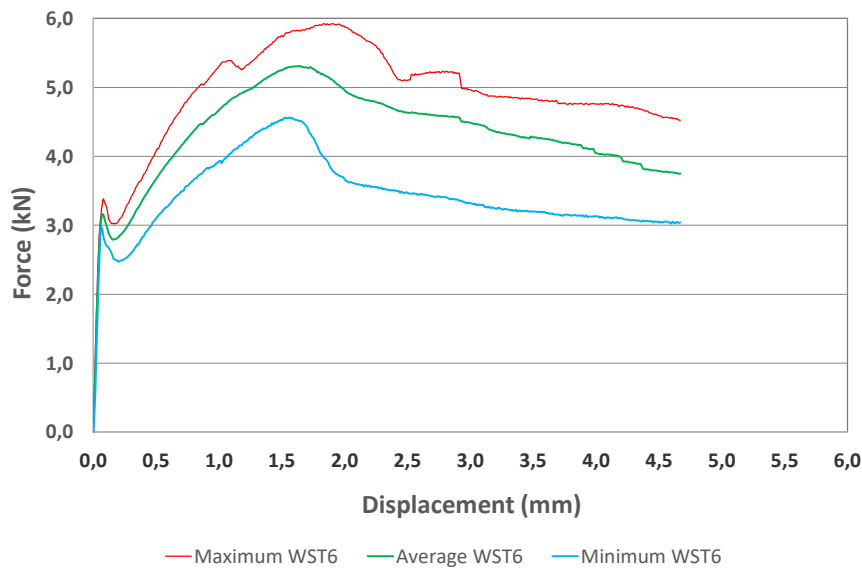
c)

Figure 76 - Average horizontal force (*Fs*)-displacement curves of a) WST1 b) WST2 c) WST3

In Figure 76a we can see that the specimens with short fibres presented a strain-softening post-peak behaviour: after the initial ascending linear branch, the concrete reaches its tensile strength and the first crack appears. This corresponds to the small descending branch after the peak. The fibres bridge this crack and allow a strain-softening branch with a smooth load reduction, instead of a brittle failure. In this phase, the fibres were mainly pulled-out from the concrete.

The use of 4D and 5D fibres (Fig 76b and 76c) did not change the elastic behaviour and matrix cracking strength, as expected. However, the post-cracking behaviour was different: the specimens showed a

strain-hardening response in the WST. After the matrix cracking, a small load decaying correspondent to the first crack was observed. Then the load starts to increase up to the peak value. In this stage, the specimens containing 5D fibres shows a higher peak value compare to the ones with 4D fibres. This is in accordance with the fibre pull-out test results discussed in previous chapter. This ascending branch ends with the localization of a critical crack. After that the fibres start to be pulled-out or to rupture and a smooth descent branch is observed. However, it is worth mentioning that, unlike specimen with 5D fibres, a sharper reduction of the load in the softening phase is observed in the specimen containing 4D fibres which means many fibres were ruptured. The specimens containing short and smooth fibres show higher residual forces than specimens containing 4D fibres.
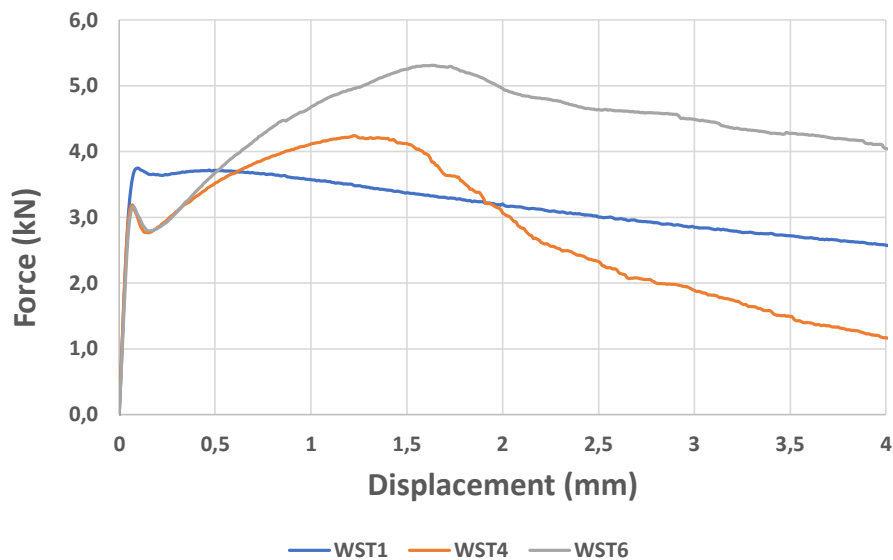
Figure 77 - Comparison of the average curves of the WST1, WST4 and WST6

From the analysis of Figure 77 one can see that the pre-peak branch is similar in the WST4 and the WST6. In the WST1, although the inclination is the same (it only depends on the Elastic Modulus of the matrix), the cracking strength is a bit higher.

The WST4 and WST6 present a strain-hardening behaviour in the WST test because of their hook-type shape which provides an additional mechanical bond between the fibre and the matrix that the smooth fibres of WST1 don't. The post-peak stress is higher and occurs for a higher displacement in the WST6 compared to the WST4 because the 5D fibres have an improved hook which provides a stronger anchorage and a more resistant and ductile steel which is able to endure more stresses.

The softening branch of the WST1 and WST6 have similar inclinations because the majority of the fibres are being pulled-out. In the WST4, the branch is much more inclined, compared to the previous two, because the fibres have a smaller tensile stress and the majority are rupturing instead of being pulled out.

4.4.4 Summary and concluding remarks

From the obtained results we can clearly see the influence of fibre type in the tensile response of the concrete, even though the tensile strength and the pre-peak branch is not influenced. The addition of a sufficient volume of strong fibres can solve the lack of ductility and the brittle failure, which are the main weaknesses of the concrete. Moreover, the strain-hardening behaviour can even add extra load capacity to the specimen. This property was not only obtained for the strongest 5D fibres but also for the 4D fibres due to their hook.

The scatter of the curves can be related to the fibres' random orientation and distribution which affects the effectiveness of the bridging effect, as already mentioned in this study.

5
INVERSE ANALYSIS

5.1 Introduction

One of the applications of the inverse analysis is to obtain the tensile constitutive law of the material indirectly from the results of wedge splitting test (Østergaard, 2003). The inverse analysis method used in this study was proposed by Østergaard (2003) and consists of three main stages: (1) obtaining the experimental results, (2) simulation of the test using the parameters to be determined , (3) a optimization process to minimize the differences between the experimental test data and the corresponding data obtained from the simulation (Skoček and Stang, 2008).

The inverse analysis can be performed in two ways: the first method consists of determining the curve point-by-point by the minimization of the discrepancy between the computed value at following point and the corresponding measured point on the load–displacement curve (Fig 78a); the second way uses an a priori defined relationship and the optimization is made for the entire curve (Fig 78b). The first one has the disadvantage of accumulating the errors from the previous points. However, it makes no assumptions, like the latter (Skoček and Stang, 2008).
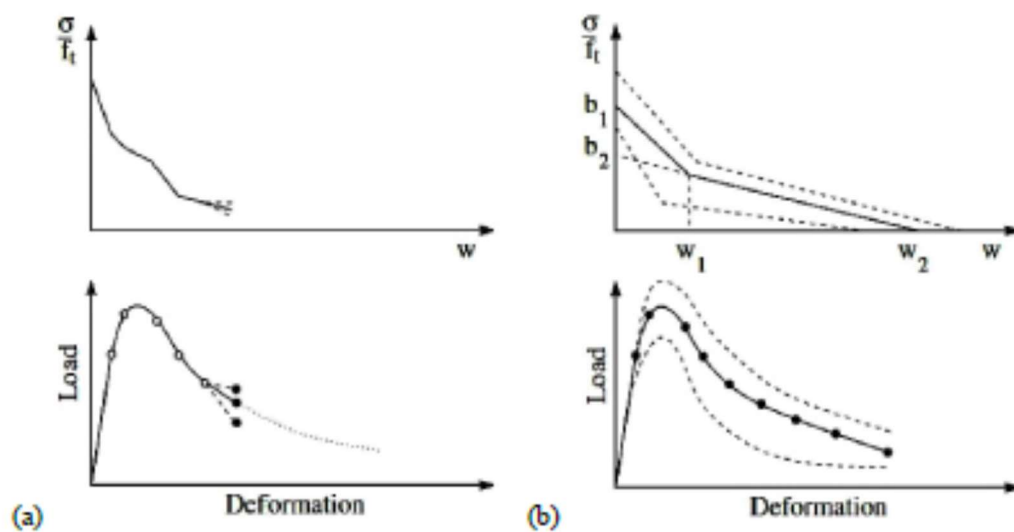
Figure 78 - General methods of the inverse analysis: a) determination point-by-point; b) use of an a priori relationship (Skoček and Stang, 2008)

In Figure 75b, the bi-linear curve is presented. Østergaard (2003) proposed that a bilinear curve can be used to simulate the tensile behaviour of cementitious materials. In this work, its suggestion will be applied and explained.

5.2 Relevant steps for inverse analysis

Østergaard (2003) distinguish three steps in this method: Step I consists in determining the modulus of elasticity, E, in the first phase of the cracking process, the non-cracked state; in Step II, the tensile strength, f_t, as well as a_1 are calculated; in Step III, a_2 and b_2 are determined. These values are represented in Figure 79. Each step is resolved by following an independent optimization process in three parts, as explained in Chapter 5.1. The final solution is an accurate approximation of the tensile behaviour of the material based on the five parameters already mentioned.

The author's approach is based on Hinge Model (Østergaard, 2003) solved by a Matlab® code. This model assumes that the crack changes the local stress and strain state of certain element with a certain width, s (see Figure 80). Outside this element no alterations occur. The hinge is modelled by a series of independent spring layers attached in the element's boundaries.

For each spring, the constitutive law is linear in the pre-cracking age, according to Equation 21.

$$\sigma = E * \varepsilon \tag{21}$$

Where E is the modulus of elasticity and ε is the strain.

In the cracked state, the spring assumes a bilinear relationship, as follows (Eq 22)

$$\sigma = b_i - a_i * w \tag{22}$$

where, for $0 \leq w \leq w_1$, (Eq 23)

$$\sigma = b_1 - a_1 * w \tag{23}$$

and for $w_1 \leq w \leq w_2$, (Eq 24)

$$\sigma = b_2 - a_2 * w \tag{24}$$

a_1 is the slope of the first branch b_1 is set to 1, a_2 is the slope of the second branch and b_2 is the value where the second branch intersects the y-axis. The four parameters are shown in Figure 79.
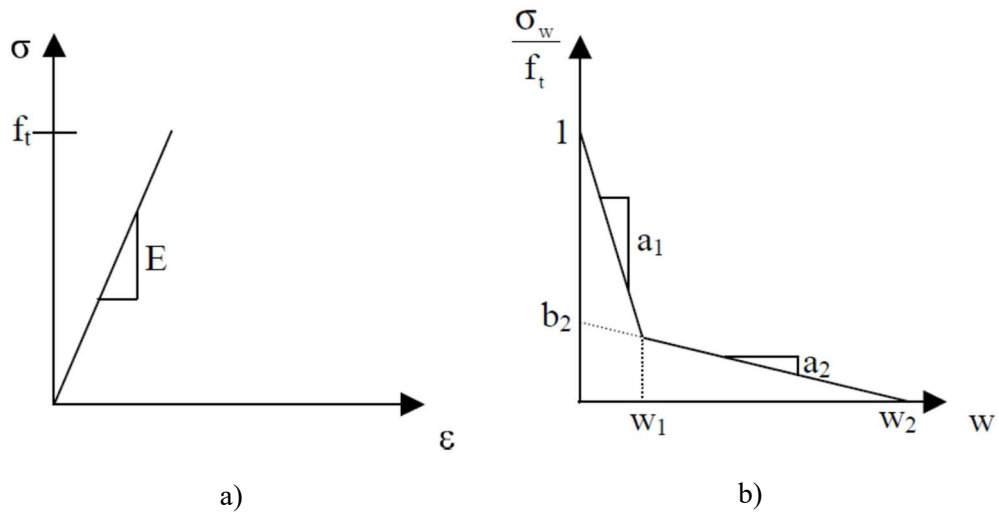
Figure 79 - Constitutive law of each spring: a) pre-crack state; b) cracked state (Østergaard, 2003)

The method can be used for both the three-point bending test and the WST. Its interest comes from its simplicity and short computation time. Figure 80 shows the hinge model adapted to the WST.
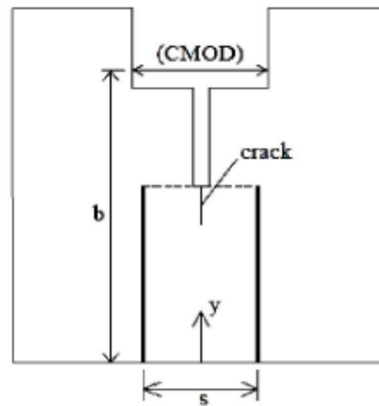
Figure 80 - Hinge model incorporated in the WST (Østergaard, 2003)

The model consists in balancing the external and internal stresses for different angular deformations in the different phases of the cracking process. The external loads are shown in Figure 81.
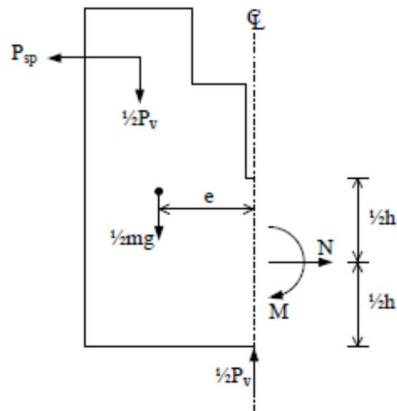
Figure 81 - External loads of the WST (Østergaard, 2003)

In Figure 81, P_{sp} is the splitting force, P_v is the applied vertical force, m is the specimen's mass, g is the gravity's acceleration and e is the eccentricity to the symmetric axis of the specimens. The normal force, N, and the moment, M, are obtained by Equations 25 and 26 respectively.

$$N = P_{sp} \tag{25}$$

$$M = P_{sp}\left(d_2 - \frac{h}{2}\right) + \frac{1}{2} * P_v * d_1 + \frac{1}{2} * m * g * e \tag{26}$$

where d_1 and d_2 are geometrical parameters of the specimen's test and are defined in Figure 82.
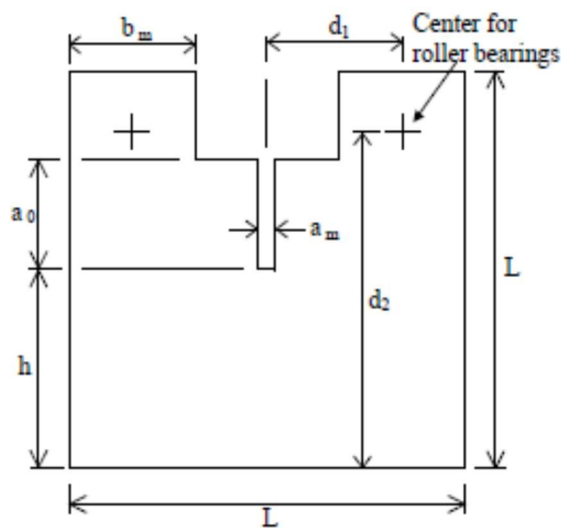
Figure 82 - Relevant dimensions of the WST

The Matlab® code needs the following geometrical characteristics of the specimen (geometry.dat, see Figure 81):

- m: Mass in [kg];
- a_0: Initial notch length;
- a_m: Mean width of groove;
- b: Distance from bottom of specimen to line of CMOD-measurements;
- b_m: Mean width of specimen on each side of groove;
- d_1: Horizontal coordinate of the load point measured from line of symmetry;
- d_2: Vertical coordinate of the load point measured from bottom of specimen;
- h: Height of ligament;
- L: Outer horizontal and vertical dimensions;
- t: Thickness of specimen;
- mu: Friction coefficient in roller bearings;
- $alpha\_w$: Wedge angle;
- v_2: Elastic deformation coefficient.

The internal stresses are explained, using the "hinge element", in Figure 83.
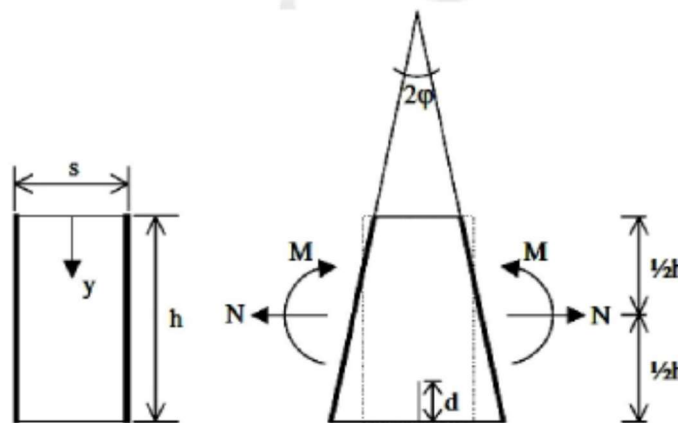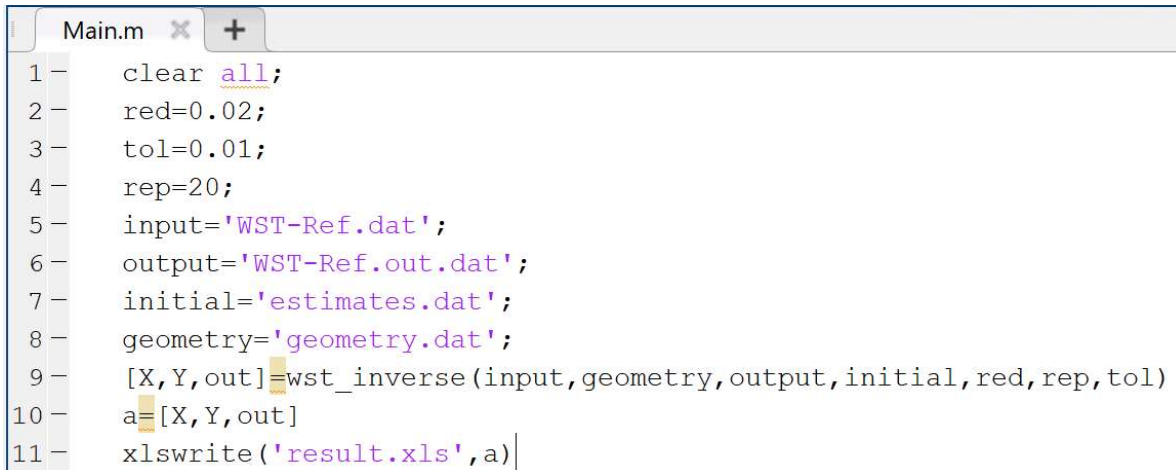
Figure 83 - Internal stresses of the hinge element (Østergaard, 2003)

More details can be found in Østergaard (2003) work.

5.3 Description of the Matlab® code

The inverse analysis procedure developed and implemented in Matlab® by Østergaard (2003) was used in the current thesis, which the main steps are showed in Figure 84.

```
Main.m  ×  +
1 —    clear all;
2 —    red=0.02;
3 —    tol=0.01;
4 —    rep=20;
5 —    input='WST-Ref.dat';
6 —    output='WST-Ref.out.dat';
7 —    initial='estimates.dat';
8 —    geometry='geometry.dat';
9 —    [X,Y,out]=wst_inverse(input,geometry,output,initial,red,rep,tol)
10 —   a=[X,Y,out]
11 —   xlswrite('result.xls',a)
```

Figure 84 - Main steps of the Matlab® code

In this code, the solution is obtained by an iterative procedure to minimize the error in each step. Prior to run the program, the following relationships and parameters should be inputted: experimental force-CMOD relationship, specimen´s geometry parameters (mentioned before) and initial parameters to define an estimated bilinear tensile curve and three scalars as described below:

- red: scalar specifying the wanted data reduction factor with a default value of 0.02;
- rep: scalar specifying the max. number of iterations for the inverse analysis algorithm with a default value 20;
- tol: scalar specifying the max. relative error for any of the constitutive parameters between two iterations with a default value 0.01.

In the end, the outputs of this code are five parameters - f_t, a_1, a_2, b_2, E - which are used to determine and re-produce a bilinear tensile constitutive law, explained in Figure 79, for the best fitted analytical to experimental force-CMOD relationship with minimum error.

- f_t: Tensile strength in Newtons;
- a_1: Slope of first part of *s(w)*;
- a_2: Slope of second part of *s(w)*;
- b_2: Intersection of second linear part with y-axis;
- E: Modulus of Elasticity;
- *Gf*: Area under stress-crack opening relationship;
- *Lch*: $Gf*E/f_t^2$;
- %error: error of the final estimated curve compared to the experimental curve.

The input file, "WST-Ref.dat" contains the experimental values of the CMOD-Split load obtained in the WST. The output data is provided in "WST-Ref.out.dat" file showed in Figure 84. All the inputted and outputted values are in Newtons and mm unless in some mentioned exceptions.

5.4 Results of the inverse analysis

The inverse analysis program was run for the experimental average curves of the three different series of specimens tested with the WST in FEUP. A comparison between the analytical curve obtained from the inverse analysis and the experimental curve from the laboratory tests are shown in Figure 85.

Moreover, the output parameters are presented in Table 16.

Table 16 - Results of the inverse analysis

Specimens	f_t (MPa)	a_1	a_2	b_2	E (MPa)	Gf	Lch	Error (%)
WST1	3,84	16,38	0,15	0,59	18940,00	4,48	5747,60	1,04
WST4	3,8114	31,863	0,46269	0,79556	19467	2,6094	3496,6	4,5426
WST6	4,91	28,20	0,04	0,56	16597,00	19,35	13313,00	7,87

a)

b)

c)
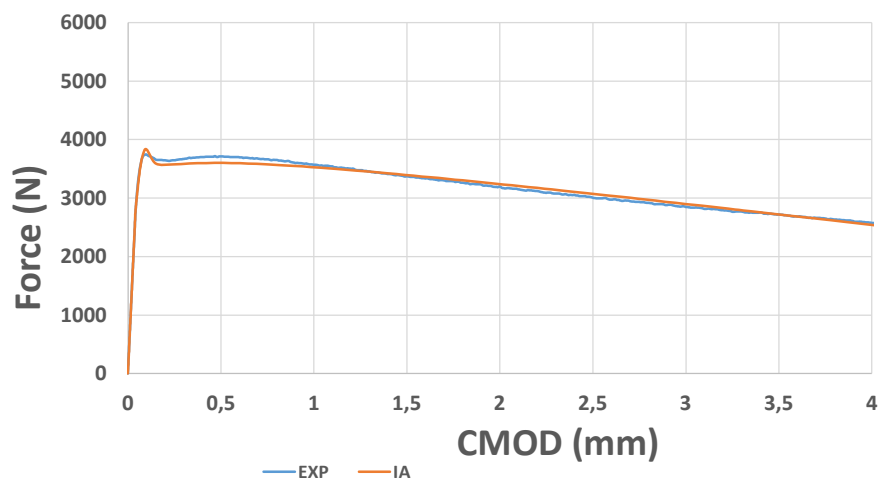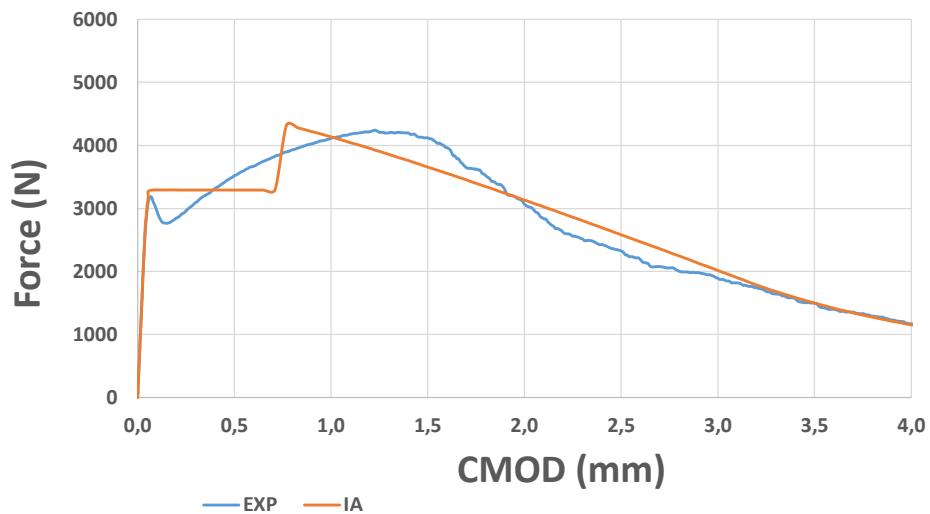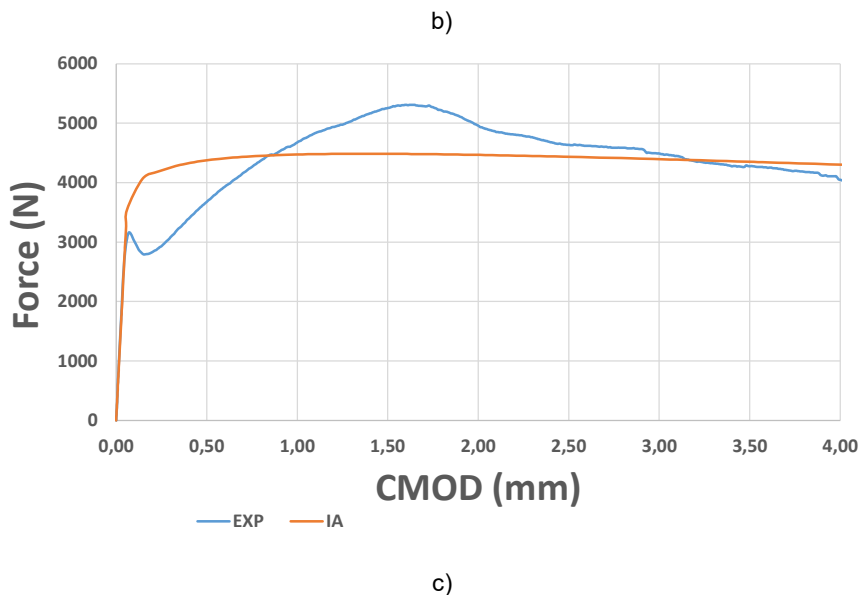
Figure 85 - Experimental curves vs theoretical curves a) WST1; b) WST4; c) WST6

The constitutive laws obtained from WST1, WST4 and WST6 using the parameters of Table 17, are shown in Figure 86, 87 and 88 respectively.

From the analysis of the approximated curve of the WST1 and Table 17, it's possible to understand the error percentage of the theoretical curve compared to the experimental curve is very small and the results are very accurate. In the case of WST4 and WST6, the analytical force-CMOD curve obtained by the inverse analysis did not follow the experimental curves closely and therefore a much higher error was obtained. This is expected since the input tensile constitutive law in inverse analysis is a bilinear curve. This type of curve is more suitable to simulate the tensile behaviour of plain concrete. However, in the case of the fibre reinforced concrete, at least a three linear curve should be implemented to simulate accurately the tensile response of this composite (Abrishambaf, 2015). WST1 and WST6 showed a strain softening behaviour in the analytical curve. This corresponds to the experimental behaviour of the WST1 but not to the WST6, that showed a strain-hardening behaviour. The model has more difficulties in adapting to this type of post-peak behaviour. However, in the theoretical curve of the WST4 the model was able to reproduce a strain-hardening behaviour.

The highest tensile stress and highest absorbed energy of the three approximate curves were both registered in the WST6, which is in accordance with the experimental results.
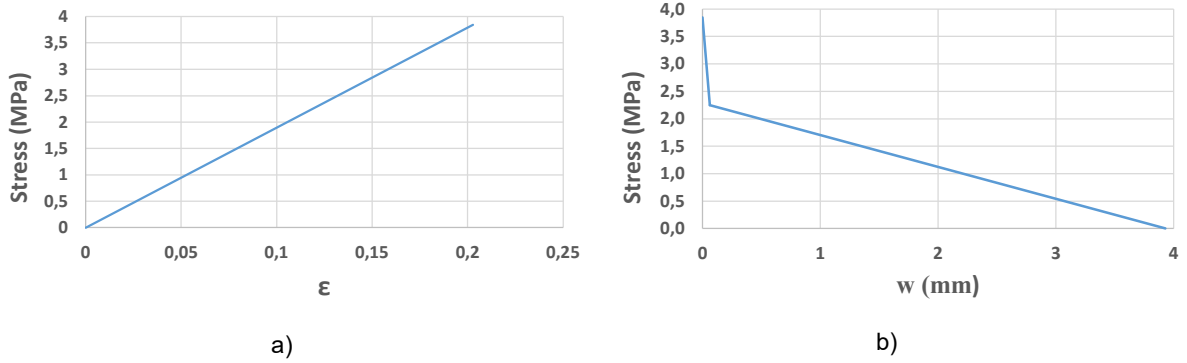
Figure 86 - Constitutive law of the material of the WST1: a) non-cracked stage; b) cracked state
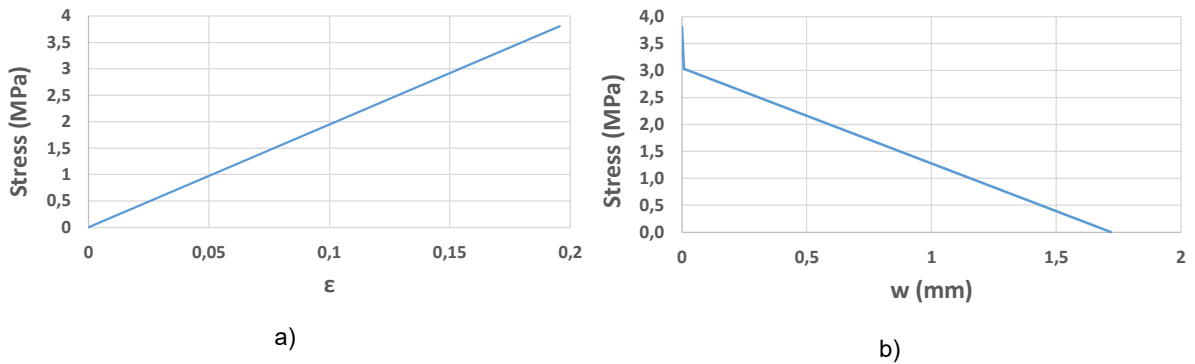
Figure 87 - Constitutive law of the material of the WST4: a) non-cracked stage; b) cracked state
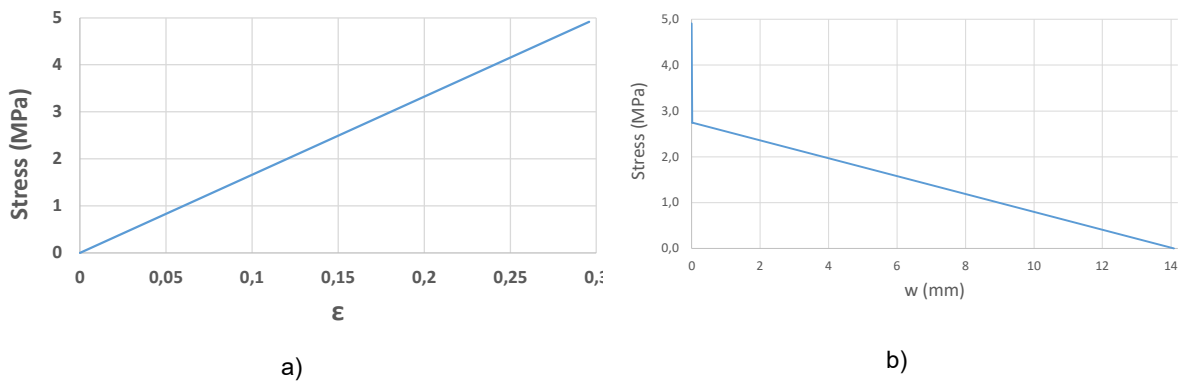
Figure 88 - Constitutive law of the material of the WST6: a) non-cracked stage; b) cracked state

We can see that the inclination of the three constitutive laws are according to the level of smoothness of their softening branches in the approximated force-CMOD curves: WST6 has the highest displacement because its softening branch is the smoothest and the WST4 has the smaller displacement because its post-peak branch was the more inclined.

In the pre-peak branch of each series, we can see that the displacement for the maximum stress is similar in the WST1 and in the WST4. In the WST6, its displacement is higher. This is related to the fact that, even though the inclination is similar, the model gives a higher tensile stress to this series because of its high post-peak stress.

6

CONCLUSIONS AND FUTURE DEVELOPMENTS

6.1 Final Remarks

From the experimental work it was possible to understand that:

- The maximum pull-out force of hooked-end fibres is not significantly influenced by the embedded length. The difference in maximum load is very small for all inclinations but, inversely of what was expected, the less embedded fibres showed a slight increment.
  The influence of the embedded length should be tested using smooth fibres in which the main contribution of the bond comes from the frictional stresses, which are dependent of the embedded length.
- Between the two embedded lengths, there was no significant difference in the slip at the maximum pull-out force of the aligned fibres. However, a slight increase regarding the more embedded fibres was registered in the inclined fibres because there was a larger difference in spalled concrete. The difference is more noted in the 60º inclined fibres because the difference in spalled concrete is also the highest
- The increase of the inclination has a negative effect on the maximum applied load of both embedded lengths. The snubbing effect and the concentrated stresses, which are proportional to the inclination, allows the fibres to rupture for smaller forces. This was expected for the 30º inclined fibres. In the 60º inclined fibres, previous studies showed that the fibres could be pulled out. In this work, this did not happen because the high resistance of the matrix didn't allow enough spalling of the concrete to overcome the snubbing effect;
- The slip at the maximum force increases with the inclination due to the more concrete spalling resultant of the bending of the fibre on its exit point. The increment in the slip was higher when the inclination raised from 30º to 60º compared to when it raised from 0º to 30º because the increment in spalled concrete was also higher. Also, with an inclination of 30º, the matrix, due to its high compressive strength, showed very little spalled concrete;
- The comparison between the results of this work and the work of Poças (2017), which used a lower strength matrix, showed that the bond between the fibre and concrete is influenced by the matrix strength. A matrix with higher strength can endure higher stresses caused by the fibre without debonding and without being crushed in the fibre's exit point. This caused higher pull-out loads in this work than in Poças's (2017) work. The difference was more noted in the aligned fibres because most inclined fibres ruptured;
- The high strength matrix used in this work showed a higher slip at the maximum force when compared to Poças's (2017) work. The resistance to the fibre's pressure in its bending point of

the more resistance matrix reduced the concrete spalling and did not allow the fibre to slip as the weaker matrix did;

- The improved hook of the 5D fibres created a tougher bond to the concrete which needed larger loads to be ruptured, compared to the 4D fibres. The steel with higher tensile strength also requested more energy to straighten the hook. Both these factors improved the pull-out energy of the aligned fibres. In the inclined fibres, for a 30º angle, the rupture stress was higher due to the more resistant steel and all the 60º inclined fibres were pulled out, unlike the 4D fibres, because the steel endured the concentrated stresses of the snubbing effect;
- The concrete spalling is not significantly influenced by the fibre type and so the slip at the maximum force is very close for both the 5D and 4D fibres. In the 5D fibres, the slip between the 30º and 60º did not change because there was less concrete spalling than expected regarding the second inclination;
- The 4D fibres are not adequate to matrixes with high strength such as the one used in this work. The requested stresses to break the very strong bond that the concrete created with the fibre were too high for the steel of the 4D fibres, causing the majority to rupture.
- In the WST tests, for the three curves, the pre-peak behaviour is practically the same and not influenced by the fibres, as expected. After the peak, it was only possible to achieve the strain hardening behaviour in the WST tests for the hooked-end fibres. The straight fibres were not able to support the multi-cracking process needed to create a post-peak stress higher than the cracking stress. However, the failure was more ductile when using the short fibres and the 5D fibres instead of the 4D fibres because the tensile stress of the second is lower and the fibres have mainly ruptured and were not pulled out. So, it is concluded that the 4D fibres are not a solution for this type of matrixes as their failure is more brittle.
- The inverse analysis method proposed by Østergaard (2003) and used in this work had high error percentages in the WST6 and WST4 while it was much more adequate for the WST1. The results have proven that the model is more adequate to a strain-softening behaviour (or to plain concrete) because it's uses a bi-linear model.

6.2 Future developments

It would be of interest to test fibres (pull-out tests) with more resistance steel, like the 5D fibres used in Poças's (2017) work, in the matrix used in this work. The 5D fibres, with a more resistance steel, would have been able to support the stresses and to be debonded. Also, unlike the matrix used in Poças's (2017) work, the matrix used in this work would have been able to fully straight the 5D fibre's hook and, because of that, to take full advantage of the mechanical bond.

With a 30º inclination angle, hooked end fibres mainly ruptured because the bond mechanism is too strong and requires very large loads in order to be ruptured. This happened in both matrixes. The creation of fibres with a more resistance steel, with a higher tensile stress that could endure the high concentrated stresses created by the bending of the fibre would allow to take full-advantage of the strong adhesion of both constituents.

A desirable characteristic of HPFRC is the strain-hardening behaviour when subjected to tension. This model as an extra ascending branch that plain concrete or FRC with strain-softening behaviour do not show. The development of a tri-linear model is important in order to obtain a better constitutive law of this material.

The potential regarding HPFRC is clear. It can be a great structural solution for many situations combined with traditional reinforcement allowing lighter and slender structures There is a general lack of sufficient knowledge because FRC is a relatively new composite in structural engineering. In order to start using fibres as a principal reinforcement of concrete structures, more studies need to be done so more guidelines and standards can be produced.

BIBLIOGRAPHY

544, ACI Committee (1999) - Design considerations for steel fiber reinforced concrete. 1999. American Concrete Institute.

ABBASS, W.; KHAN, M. I.; MOURAD, S. (2018) - Evaluation of mechanical properties of steel fiber reinforced concrete with different strengths of concrete. Construction and Building Materials [Em linha]. 168: 556-569. Disponível em WWW: <URL: https://www.scopus.com/inward/record.uri?eid=2-s2.085042870959&doi=10.1016%2fj.conbuildmat.2018.02.164&partnerID=40&md5=1b341ee9bce7c0f42d49c9d3b3b8b0fa>.

ABDALLAH, S.; FAN, M. (2017) - Anchorage mechanisms of novel geometrical hooked-end steel fibres. Materials and Structures/Materiaux et Constructions. 50:2. Disponível em WWW: <URL: https://www.scopus.com/inward/record.uri?eid=2-s2.0-85013277174&doi=10.1617%2fs11527-016-0991-5&partnerID=40&md5=8bcc57806a7ee6e37c6d7b9a9a8aeb>.

ABRISHAMBAF, Amin (2015) - Creep behaviour of cracked steel fibre reinforced self-compacting concrete laminar structures.

ALMEIDA, J.; NEVES, R. (2005) - Compressive behaviour of steel fibre reinforced concrete. Structural Concrete. 6: 1-8.

BANTHIA, Nemkumar; TROTTIER, Jean-Fancois (1994) - Concrete reinforced with deformed steel fibers, part I: bond-slip mechanisms. Materials Journal. 91:5. 435-446. ISSN 0889-325X.

BARNETT, Stephanie J [et al.] (2010) - Assessment of fibre orientation in ultra high performance fibre reinforced concrete and its effect on flexural strength. Materials and Structures. 43:7. 1009-1023. ISSN 1359-5997.

BARRAGÁN, Bryan E [et al.] (2000) - Study of the distribution and orientation of fibers in cast cylinders. Structural Technology Laboratory, Universitat Politècnica de Catalunya.

BARRAGÁN, Bryan Erick (2002) - Failure and toughness of steel fiber reinforced concrete under tension and shear. Universitat Politècnica de Catalunya. ISBN 8468807362.

BARROS, Joaquim AO [et al.] (2005) - Post-cracking behaviour of steel fibre reinforced concrete. Materials and Structures. 38:1. 47-56. ISSN 1359-5997.

BENTUR, Arnon; MINDESS, Sidney (2006) - Fibre reinforced cementitious composites. Crc Press. ISBN 1482267748.

BRÜHWILER, E; WITTMANN, FH (1990) - The wedge splitting test, a new method of performing stable fracture mechanics tests. Engineering fracture mechanics. 35:1-3. 117-125. ISSN 0013-7944.

CARPINTERI, Alberto; CHIAIA, Bernardino; CORNETTI, Pietro (2002) - A scale-invariant cohesive crack model for quasi-brittle materials. Engineering Fracture Mechanics. 69:2. 207-217. ISSN 0013-7944.

CHUPANIT, Punya (2005) - Characterization of concrete pavement joint surfaces. University of Illinois at Urbana-Champaign. ISBN 0542229013.

COUTINHO, J (2011) - Betões eco-eficientes com resíduos. Porto: 1as Jornadas de Materiais na Construção. 171-214.

CUNHA, Vitor MCF (2010) - Steel fibre reinforced self-compacting concrete (from micromechanics to composite behavior).

CUNHA, Vítor MCF; BARROS, Joaquim AO; SENA-CRUZ, José (2007) - Pullout behaviour of hooked-end steel fibres in self-compacting concrete

DARWIN, David [et al.] (2001) - Fracture energy of high-strength concrete. 2001. American Concrete Institute.

DEEB, R.; KARIHALOO, B. L.; KULASEGARAM, S. (2014) - Reorientation of short steel fibres during the flow of self-compacting concrete mix and determination of the fibre orientation factor. Cement and Concrete Research. 56: 112-120. Disponível em WWW: <URL: https://www.scopus.com/inward/record.uri?eid=2-s2.0-84890302889&doi=10.1016%2fj.cemconres.2013.10.002&partnerID=40&md5=98665b8cdb7425b85 96a2e76e3377537>.

DI PRISCO, Marco; COLOMBO, Matteo; DOZIO, Daniele (2013) - Fibre-reinforced concrete in fib Model Code 2010: principles, models and test validation. Structural Concrete. 14:4. 342-361. Disponível em WWW: <URL: https://onlinelibrary.wiley.com/doi/abs/10.1002/suco.201300021>. ISSN 1464-4177.

DI PRISCO, Marco; IORIO, Francesco; PLIZZARI, Giovanni (2003) - HPSFRC prestressed roof elements. 2003.

DUPONT, D (2003) - Modelling and experimental validation of the constitutive law (σ-ε) and cracking behaviour of steel fibre reinforced concrete. KU Leuven: Leuven, Belgium.

DUPONT, D.; VANDEWALLE, L. (2005) - Distribution of steel fibres in rectangular sections. Cement and Concrete Composites. 27:3. 391-398. Disponível em WWW: <URL: https://www.scopus.com/inward/record.uri?eid=2-s2.0-12244267734&doi=10.1016%2fj.cemconcomp.2004.03.005&partnerID=40&md5=43d3ad4f4f86b162 16f209e55fe6d76d>.

FAIFER, Marco [et al.] (2010) - Nondestructive testing of steel-fiber-reinforced concrete using a magnetic approach. IEEE Transactions on Instrumentation and Measurement [Em linha]. 60:5. 1709-1717. ISSN 0018-9456.

FERRARA, Liberato; OZYURT, Nilufer; DI PRISCO, Marco (2011) - High mechanical performance of fibre reinforced cementitious composites: the role of "casting-flow induced" fibre orientation. Materials and Structures. 44:1. 109-128. ISSN 1359-5997.

FIGUEIREDO, Antonio; CECCATO, Marcos (2015) - Workability Analysis of Steel Fiber Reinforced Concrete Using Slump and Ve-Be Test. Materials Research .

GHOLAMPOUR, Aliakbar; OZBAKKALOGLU, Togay (2018) - Fiber-reinforced concrete containing ultra high-strength micro steel fibers under active confinement. Construction and Building Materials. 187: 299-306. ISSN 0950-0618.

GLAVIND, Mette (1992) - Evaluation of the compressive behaviour of fiber reinforced high strength concrete. Lyngby. ISBN 8777401263.

GRÜNEWALD, S; WALRAVEN, JC (2000) - Self-compacting fiber reinforced concrete: Test methods and properties in the fresh state. 2000.

GRÜNEWALD, S.; WALRAVEN, J. C (2002) - High strength self-compacting fibre reinforced concrete: behaviour in the fresh and hardened state. 2002.

GUERRERO, Patricia; NAAMAN, Antoine E (2000) - Effect of mortar fineness and adhesive agents on pullout response of steel fibers. Materials Journal [Em linha]. 97:1. 12-20. ISSN 0889-325X.

HAMIRUDDIN, N. A. [et al.] (2018) - Effect of steel fibre content with high strength fibre reinforced concrete on compressive behaviour. USA, 2018. AIP Publishing. Disponível em WWW: <URL: http://dx.doi.org/10.1063/1.5066690>. ISBN 0094-243X.

HILLERBORG, Arne (1980) - Analysis of fracture by means of the fictitious crack model, particularly for fibre reinforced concrete.

HILLERBORG, Arne (1989) - Stability problems in fracture mechanics testing in fracture of concrete and rock. 1989. Elsevier. ISBN 1851664149.

HOMRICH, Joseph R; NAAMAN, Antoine E (1987) - Stress-strain properties of SIFCON in compression. Special Publication. 105: 283-304.

HTUT, Trevor Nyan Soe (2010) - Fracture processes in steel fibre reinforced concrete. The University of New South Wales Sydney, Australia.

JANG, S. J.; JEONG, G. Y.; YUN, H. D. (2018) - Use of steel fibers as transverse reinforcement in diagonally reinforced coupling beams with normal- and high-strength concrete. Construction and Building Material. 187: 1020-1030. Disponível em WWW: <URL: https://www.scopus.com/inward/record.uri?eid=2-s2.0-85051624036&doi=10.1016%2fj.conbuildmat.2018.08.063&partnerID=40&md5=11ed58e14a53d599fc10f1c84452ba03>.

JOHNSTON, CD (2004) - 14 proportioning, mixing and placement of fibre-reinforced cements and concretes. Production Methods and Workability of Concrete. 32: 155. ISSN 0203627377.

KAZEMI, M. T. [et al.] (2017) - Fracture properties of steel fiber reinforced high strength concrete using work of fracture and size effect methods. Construction and Building Materials. 142: 482-489. Disponível em WWW: <URL: https://www.scopus.com/inward/record.uri?eid=2-s2.0-85015622931&doi=10.1016%2fj.conbuildmat.2017.03.089&partnerID=40&md5=789e97933a6c00cee9436b8777d66d21>.

KIRBY, Richard Shelton; LAURSON, Philip Gustave (1932) - The early years of modern civil engineering. Yale University Press.

KOBAYASHI, K; CHO, R (1976) - Mechanics of concrete with randomly oriented discontinuous fibres. 1976.

KOOIMAN, Alain Geoffré (2000) - Modelling steel fibre reinforced concrete for structural design.

KRENCHEL, Herbert (1975) - Fibre spacing and specific fibre surface.

LEE, Seong-Cheol; OH, Joung-Hwan; CHO, Jae-Yeol (2015) - Compressive behavior of fiber-reinforced concrete with end-hooked steel fibers. Materials. 8:4. 1442-1458.

LI, P. P.; YU, Q. L.; BROUWERS, H. J. H. (2018) - Effect of coarse basalt aggregates on the properties of Ultra-high Performance Concrete (UHPC). Construction and Building Materials. 170: 649-659. Disponível em WWW: <URL: https://www.scopus.com/inward/record.uri?eid=2-s2.0-85044150769&doi=10.1016%2fj.conbuildmat.2018.03.109&partnerID=40&md5=ded1fe38cc666528 bf0147a49bf9a4f4>.

LI, V. C.; WU, H. C. (1992) - Conditions for pseudo strain-hardening in fiber reinforced brittle matrix composites. Applied Mechanics Reviews. 45:8. 390-394. Disponível em WWW: <URL: https://www.scopus.com/inward/record.uri?eid=2-s2.0-0000887803&doi=10.1115%2f1.3119767&partnerID=40&md5=d9158759e846b97699307d33481374 db>.

LI, Victor C; STANG, Henrik (1997) - Interface property characterization and strengthening mechanisms in fiber reinforced cement based composites. Advanced cement based materials. 6:1. 1-20. ISSN 1065-7355.

LI, Victor C; WANG, Youjiang; BACKER, Stanley (1991) - A micromechanical model of tension-softening and bridging toughening of short random fiber reinforced brittle matrix composites.

LINSBAUER, HN; TSCHEGG, EK (1986) - Fracture energy determination of concrete with cube-shaped specimens. Zement und Beton. 31:1. 38-40. ISSN 0514-2946.

LÖFGREN, Ingemar (2004) - The wedge splitting test a test method for assessment of fracture parameters of FRC? 2004. ISBN 0870311352.

LÖFGREN, Ingemar (2005) - Fibre-reinforced Concrete for Industrial Construction - a fracture mechanics approach to material testing and structural analysis.

LÖFGREN, Ingemar; STANG, Henrik; OLESEN, John Forbes (2008) - The WST method, a fracture mechanics test method for FRC. Materials and Structures. 41:1. 197-211. ISSN 1359-5997.

MANSUR, MA; CHIN, MS; WEE, TH (1999) - Stress-strain relationship of high-strength fiber concrete in compression. Journal of materials in civil engineering. 11:1. 21-29. ISSN 0899-1561.

MARKOVIĆ, Ivan (2006) - High-performance hybrid-fibre concrete: development and utilisation. IOS Press. ISBN 9040726213.

MCKEE, Dean Clive (1969) - The properties of an expansive cement mortar reinforced with random wire fibers. University of Illinois at Urbana-Champaign.

MEDA, A; PLIZZARI, GA; SLOWIK, V (2001) - Fracture of fiber reinforced concrete slabs on grade. Fracture Mechanics of Concrete Structures. 1013-1020.

MOUSAVI, S. M.; RANJBAR, M. M.; MADANDOUST, R. (2019) - Combined effects of steel fibers and water to cementitious materials ratio on the fracture behavior and brittleness of high strength concrete. Engineering Fracture Mechanics. 216: Disponível em WWW: <URL: https://www.scopus.com/inward/record.uri?eid=2s2.085067646089&doi=10.1016%2fj.engfracmech.2 019.106517&partnerID=40&md5=087ed506bbd0d25a2fdcb44e752c4538>.

NAAMAN, A. E. [et al.] (1991) - Fiber pullout and bond slip. I: Analytical study. Journal of Structural Engineering (United States). 117:9. 2769-2790. Disponível em WWW: <URL: https://www.scopus.com/inward/record.uri?eid=2-

s2.00026220401&doi=10.1061%2f%28ASCE%290733-9445%281991%29117%3a9%282769%29&partnerID=40&md5=a46fba6825cc4fc4a1521af01e1d8cb3>.

NAAMAN, A. E.; REINHARDT, H. W. (2006) - Proposed classification of HPFRC composites based on their tensile response. Materials and Structures. 39:5. 547-555. Disponível em WWW: <URL: https://doi.org/10.1617/s11527-006-9103-2>. ISSN 1871-6873.

NAAMAN, Antoine E; REINHARDT, H.W. (2003) - High performance fiber reinforced cement composites (HPFRCC4). E&Fn Spon.

NAAMAN, Antoine E (2000) - Fiber reinforcements for concrete: looking back, looking ahead. 2000. ISBN 2912143187.

NAAMAN, Antoine E (2007a) - Fiber reinforced concrete: State of progress at the edge of the new millennium. Design and Sustainability

NAAMAN, Antoine E (2007b) - High performance fiber reinforced cement composites: classification and applications. 2007b. Citeseer.

NAAMAN, Antoine E (2008) - High performance fiber reinforced cement composites. Naaman AE. High-performance construction materials: science and applications. Singapore: World Scientific Publishing. 91-153.

NAAMAN, Antoine E; NAJM, Husamuddin (1991) - Bond-slip mechanisms of steel fibers in concrete. Materials Journal. 88:2. 135-145. ISSN 0889-325X.

NAAMAN, Antoine E; SHAR, SR (1976) - Pull-out mechanism in steel fibre-reinforced concrete. Journal of the Structural Division. 102:

NAAMAN, Antoine E. (2003) - Engineered Steel Fibers with Optimal Properties for Reinforcement of Cement Composites. Journal of Advanced Concrete Technology. 1:3. 241-252.

NEMEGEER, Dirk; VANBRABANT, Johan; STANG, H (2003) - Brite Euram program on steel fibre concrete subtask: durability: corrosion resistance of cracked fibre reinforced concrete. 2003. RILEM Publications SARL.

NOUSHINI, Amin; VESSALAS, Kirk; SAMALI, B. (2014) - Static Mechanical Properties of Polyvinyl Alcohol Fibre Reinforced Concrete (PVA-FRC). Magazine of Concrete Research. 66: 1-19.

NUNES, S. [et al.] (2015) - PTDC/ECM/122446/2010 - Non-destructive monitoring of fibre dispersion and orientation in a field application of UHPFRC on the Chillon viaduct, Switzerland

NUNES, Sandra; PIMENTEL, Mário; CARVALHO, Adriano (2016) - Non-destructive assessment of fibre content and orientation in UHPFRC layers based on a magnetic method. Cement and Concrete Composites. 72: 66-79. ISSN 0958-9465.

OKEH, C. A. O. [et al.] (2019) - Behaviour of hybrid steel fibre reinforced self compacting concrete using innovative hooked-end steel fibres under tensile stress. Construction and Building Materials. 202: 753-761. Disponível em WWW: <URL: https://www.scopus.com/inward/record.uri?eid=2-s2.0-85060247739&doi=10.1016%2fj.conbuildmat.2018.12.067&partnerID=40&md5=44517be0b610669b2408617433094e62>.

ØSTERGAARD, Lennart (2003) - Early age fracture mechanics and cracking of concrete: Experiments and Modelling. Technical University of Denmark. ISBN 8778771331.

PIÉRARD, Julie; DOOMS, Bram; CAUBERG, Niki (2013) - Durability evaluation of different types of UHPC. 2013.

PIMENTEL, M. [et al.] (2015) - Non-destructive measurements to evaluate fiber dispersion and orientation in UHPFRC reinforcement layers. In International Conference on Multi-Span Large Bridges. 2015. p. 1001-1008.

POÇAS, H. (2017) - Previsão do comportamento do BRFA em tração direta pelo recurso a ensaios de flexão e arrancamento.

REINHARDT, H-W; GROSSE, C; WEILER, B (2001) - Material characterization of steel fibre reinforced concrete using neutron CT, ultrasound and quantitative acoustic emission techniques. NDT. net–The electronic Journal on Non-Destructive Testing. 6:5.

ROBINS, P; AUSTIN, S; JONES, P (2002) - Pull-out behaviour of hooked steel fibres. Materials and structures. 35:7. 434-442. ISSN 1359-5997.

ROMUALDI, James P; MANDEL, James A (1964) - Tensile strength of concrete affected by uniformly distributed and closely spaced short lengths of wire reinforcement. 1964. ISBN 0002-8061.

ROSSI, P; HARROUCHE, N (1990) - Mix design and mechanical behaviour of some steel-fibre-reinforced concretes used in reinforced concrete structures. Materials and Structures. 23:4. 256. ISSN 1359-5997.

ROSSI, P.; ACKER, P.; MALIER, Y. (1987) - Effect of steel fibres at two different stages: The material and the structure. Materials and Structures. 20:6. 436-439. Disponível em WWW: <URL: https://doi.org/10.1007/BF02472494>. ISSN 1871-6873.

RUANO, G. [et al.] (2014) - Shear retrofitting of reinforced concrete beams with steel fiber reinforced concrete. Construction and Building Materials. 54: 646-658. Disponível em WWW: <URL: https://www.scopus.com/inward/record.uri?eid=2-s2.0-84893493710&doi=10.1016%2fj.conbuildmat.2013.12.092&partnerID=40&md5=9453edaf451df316316fc19ab2dd7e69>.

SAHMARAN, M.; YURTSEVEN, A.; OZGUR YAMAN, I. (2005) - Workability of hybrid fiber reinforced self-compacting concrete. Building and Environment. 40:12. 1672-1677. Disponível em WWW: <URL: https://www.scopus.com/inward/record.uri?eid=2-s2.0-23144445273&doi=10.1016%2fj.buildenv.2004.12.014&partnerID=40&md5=e896d4f63a2be79577d519d902c7c1a1>.

SHAH, Surendra; CARPINTERI, Alberto (1991) - Fracture Mechanics Test Methods For Concrete. CRC Press. ISBN 0412411008.

SKAZLIĆ, Marijan; SERDAR, Marijana; BJEGOVIĆ, Dubravka (2008) - Influence of test specimen geometry on compressive strength of ultra high performance concrete. 2008.

SKOČEK, Jan; STANG, Henrik (2008) - Inverse analysis of the wedge-splitting test. Engineering Fracture Mechanics 75:10. 3173-3188. ISSN 0013-7944.

SOROUSHIAN, Parviz; LEE, Cha-Don (1990) - Distribution and orientation of fibers in steel fiber reinforced concrete. Materials Journal. 87:5. 433-439. ISSN 0889-325X.

STÄHLI, Patrick; CUSTER, Rocco; VAN MIER, Jan GM (2008) - On flow properties, fibre distribution, fibre orientation and flexural behaviour of FRC. Materials and structures. 41:1. 189-196. ISSN 1359-5997.

STANG, Henrik; LI, Zongjin; SHAH, SP (1990) - Pullout problem: stress versus fracture mechanical approach. Journal of Engineering Mechanics. 116:10. 2136-2150. ISSN 0733-9399.

SUKSAWANG, Nakin; WTAIFE, Salam; ALSABBAGH, Ahmed (2018) - Evaluation of elastic modulus of fiber-reinforced concrete.

VAN GYSEL, Ann (2000) - Studie van het uittrekgedrag van staalvezels ingebed in een cementgebonden matrix met toepassing op staalvezelbeton onderworpen aan buiging.

VAN MIER, Jan GM (1996) - Fracture processes of concrete. CRC press. ISBN 0849391237.

VAN MIER, JGM; VAN VLIET, MRA (2002) - Uniaxial tension test for the determination of fracture parameters of concrete: state of the art. Engineering Fracture Mechanics. 69:2. 235-247. ISSN 0013-7944.

VAN VLIET, Marcel René Antoine (2000) - Size effect in tensile fracture of concrete and rock. TU Delft, Delft University of Technology.

VANDEWALLE, Lucie; DUPONT, David (2003) - Test and design methods for steel fibre reinforced concrete: Bending test and interpretation. Rilem Proceeding 31. 1-14.

VANDEWALLE, Lucie [et al.] (2003) - RILEM TC 162-TDF: Test and design methods for steel fibre reinforced concrete'-sigma-epsilon-design method-Final Recommendation. Materials and Structures. 36:262. 560-567. ISSN 1359-5997.

VONK, Rene Alfred (1992) - Softening of concrete loaded in compression.

WEI, Sun; MANDEL, James A; SAID, Samir (1986) - Study of the interface strength in steel fiber-reinforced cement-based composites. 1986. ISBN 0002-8061.

WILLE, Kay; EL-TAWIL, Sherif; NAAMAN, Antoine E (2014) - Properties of strain hardening ultra high performance fiber reinforced concrete (UHP-FRC) under direct tensile loading. Cement and Concrete Composites. 48: 53-66. ISSN 0958-9465.

YOO, D. Y.; YOON, Y. S.; BANTHIA, N. (2015) - Predicting the post-cracking behavior of normal- and high-strength steel-fiber-reinforced concrete beams. Construction and Building Materials. 93: 477-485. Disponível em WWW: <URL: https://www.scopus.com/inward/record.uri?eid=2-s2.0-84934983751&doi=10.1016%2fj.conbuildmat.2015.06.006&partnerID=40&md5=43c6483da2f35f6da7e13130c01f0102>.

YOO, Doo-Yeol; SHIN, Hyun-Oh (2018) - Bond performance of steel rebar embedded in 80–180 MPa ultra-high-strength concrete. Cement and Concrete Composites. 93: 206-217. ISSN 0958-9465.

ZANDI HANJARI, Kamyab (2006) - Evaluation of WST Method as a Fatigue Test for Plain and Fiber-reinforced Concrete-experimental and numerical investigation.

ZHOU, Fan Ping (1988) - Some aspects of tensile fracture behaviour and structural response of cementitious materials.